JOSÉ EDUARDO ALVES GRACIANO

Real Time Optimization in chemical processes: evaluation of strategies, improvements and industrial application

São Paulo
2016

JOSÉ EDUARDO ALVES GRACIANO

Real Time Optimization in chemical processes: evaluation of strategies, improvements and industrial application

Tese apresentada à Escola Politécnica da Universidade de São Paulo para obtenção do título de Doutor em Engenharia

São Paulo
2016

JOSÉ EDUARDO ALVES GRACIANO

Real Time Optimization in chemical processes: evaluation of strategies, improvements and industrial application

Tese apresentada à Escola Politécnica da Universidade de São Paulo para obtenção do título de Doutor em Engenharia

Área de concentração: Engenharia Química

Orientador: Prof. Dr. Galo Antonio Carrillo Le Roux

São Paulo

2016

Este exemplar foi revisado e corrigido em relação à versão original, sob responsabilidade única do autor e com a anuência de seu orientador.

São Paulo, de de

Assinatura do autor: _____

Assinatura do orientador: _____

Catalogação-na-publicação

Graciano, José Eduardo Aves

Real Time Optimization in chemical processes: evaluation of strategies, improvements and industrial application / J. E. A. Graciano -- versão corr. -- São Paulo, 2016.

160 p.

Tese (Doutorado) - Escola Politécnica da Universidade de São Paulo. Departamento de Engenharia Química.

1.Otimização em tempo real 2.Controle de processos 3.Estimação de parâmetros 4.self-optimizing control I.Universidade de São Paulo. Escola Politécnica. Departamento de Engenharia Química II.t.

AGRADECIMENTOS

Ao professor Galo Antonio Carrillo Le Roux, pela oportunidade, orientação e constante estímulo transmitido durante todo o trabalho.

I would like to express my special gratitude to Professor Lorenz T. Biegler for receiving me in his research group, contributing to my professional and personal development.

I sincerely thank Professor Johannes Jäschke for helping me in the development of new ideas, which improved the quality of the present work.

Aos meus pais, Silvana e José, por todo carinho, dedicação e apoio incondicional às minhas escolhas.

Às minhas irmãs Simone e Juliana, que sempre me inspiraram na busca pelo conhecimento.

Às minhas sobrinhas Heloísa e Manuela, pelos ótimos fins de semana que passamos juntos.

À minha companheira Flávia, por todo amor, paciência, incentivo e risadas, que sempre me ajudaram a esquecer os pequenos problemas do dia-a-dia.

Ao amigo Lucas, por sempre afirmar que tudo daria certo, discordando dos meus argumentos contrários.

Ao amigo Diego que contribuiu imensamente na elaboração deste trabalho, tornando-se um modelo para meu desenvolvimento profissional.

Aos amigos Bruno, André e Zé pelas correções e sugestões de melhoria deste trabalho, bem como pelo apoio na organização dos churrascos que animaram nosso departamento.

Aos meus colegas de laboratório, pelo apoio e auxílio durante a execução do trabalho, bem como nos momentos de descontração nos nossos cafés de fim de tarde.

Ao CNPq e à Petrobras, pelo apoio financeiro.

E a todos que colaboraram direta ou indiretamente, na execução deste trabalho.

E mesmo que pareça tolo
E sem sentido
Eu ainda brigo por sonhos
Eu ainda brigo

(Herbert Vianna)

RESUMO

O aumento da concorrência motiva a indústria a implementar ferramentas que melhorem a eficiência de seus processos. A automação é uma dessas ferramentas, e o *Real Time Optimization* (RTO) ou Otimização em Tempo Real, é uma metodologia de automação que considera aspectos econômicos e restrições de processos e equipamentos para atualizar o controle do processo, de acordo com preços de mercado e distúrbios. Basicamente, o RTO usa um modelo fenomenológico em estado estacionário para predizer o comportamento do processo, em seguida, otimiza uma função objetivo econômica sujeita a esse modelo. Embora amplamente utilizado na indústria, não há ainda um consenso geral sobre os benefícios da implementação do RTO, devido a algumas limitações discutidas no presente trabalho: incompatibilidade estrutural entre planta e modelo, problemas de identificabilidade e baixa frequência de atualização dos *set points*. Algumas metodologias de RTO foram propostas na literatura para lidar com o problema da incompatibilidade entre planta e modelo. No entanto, não há uma comparação que avalie a abrangência e as limitações destas diversas abordagens de RTO, sob diferentes aspectos. Por esta razão, o método clássico de RTO é comparado com metodologias mais recentes, baseadas em derivadas (*Modifier Adaptation, Integrated System Optimization and Parameter estimation, and Sufficient Conditions of Feasibility and Optimality*), utilizando-se o método de Monte Carlo. Os resultados desta comparação mostram que o método clássico de RTO é coerente, desde que seja proporcionado um modelo suficientemente flexível para se representar a topologia do processo, um método de estimação de parâmetros apropriado para lidar com características de ruído de medição e um método para melhorar a qualidade da informação da amostra. Já os problemas de identificabilidade podem ser observados a cada iteração de RTO, quando o método atualiza alguns parâmetros-chave do modelo, o que é causado principalmente pela ausência de medidas e ruídos. Por esse motivo, quatro abordagens de estimação de parâmetros (Discriminação Rotacional, Seleção Automática e Estimação de Parâmetros, Reparametrização via Geometria Diferencial e o clássico Mínimos Quadrados não-lineares) são avaliados em relação à sua capacidade de predição,

robustez e velocidade. Os resultados revelam que o método de Discriminação Rotacional é o mais adequado para ser implementado em um ciclo de RTO, já que requer menos informação *a priori*, é simples de ser implementado e evita o sobreajuste observado no método de Mínimos Quadrados. A terceira desvantagem associada ao RTO é a baixa frequência de atualização dos *set points*, o que aumenta o período em que o processo opera em condições subotimas. Uma alternativa para lidar com este problema é proposta no presente trabalho, integrando-se o RTO e o *Self-Optimizing Control* (SOC) através de um novo algoritmo de *Model Predictive Control* (MPC). Os resultados obtidos com a nova abordagem demonstram que é possível reduzir o problema da baixa frequência de atualização dos *set points*, melhorando o desempenho econômico do processo. Por fim, os aspectos práticos da implementação do RTO são discutidos em um estudo de caso industrial, que trata de um processo de destilação com bomba de calor, localizado na Refinaria de Paulínia (REPLAN - Petrobras). Os resultados deste estudo sugerem que os parâmetros do modelo são estimados com sucesso pelo método de Discriminação Rotacional; que o RTO é capaz de aumentar o lucro do processo em cerca de 3%, o equivalente a 2 milhões de dólares por ano; e que a integração entre SOC e RTO pode ser uma alternativa interessante para o controle deste processo de destilação.

Palavras-chave: Otimização em Tempo Real. Controle de Processos. Estimação de Parâmetros. *Self-optimizing control*.

ABSTRACT

The increasing economic competition drives the industry to implement tools that improve their processes efficiencies. The process automation is one of these tools, and the Real Time Optimization (RTO) is an automation methodology that considers economic aspects to update the process control in accordance with market prices and disturbances. Basically, RTO uses a steady-state phenomenological model to predict the process behavior, and then, optimizes an economic objective function subject to this model. Although largely implemented in industry, there is not a general agreement about the benefits of implementing RTO due to some limitations discussed in the present work: structural plant/model mismatch, identifiability issues and low frequency of set points update. Some alternative RTO approaches have been proposed in literature to handle the problem of structural plant/model mismatch. However, there is not a sensible comparison evaluating the scope and limitations of these RTO approaches under different aspects. For this reason, the classical two-step method is compared to more recently derivative-based methods (Modifier Adaptation, Integrated System Optimization and Parameter estimation, and Sufficient Conditions of Feasibility and Optimality) using a Monte Carlo methodology. The results of this comparison show that the classical RTO method is consistent, providing a model flexible enough to represent the process topology, a parameter estimation method appropriate to handle measurement noise characteristics and a method to improve the sample information quality. At each iteration, the RTO methodology updates some key parameter of the model, where it is possible to observe identifiability issues caused by lack of measurements and measurement noise, resulting in bad prediction ability. Therefore, four different parameter estimation approaches (Rotational Discrimination, Automatic Selection and Parameter estimation, Reparametrization via Differential Geometry and classical nonlinear Least Square) are evaluated with respect to their prediction accuracy, robustness and speed. The results show that the Rotational Discrimination method is the most suitable to be implemented in a RTO framework, since it requires less *a priori* information, it is simple to be implemented and avoid the overfitting caused by the Least Square method. The third RTO drawback discussed in the present thesis is

the low frequency of set points update, this problem increases the period in which the process operates at suboptimum conditions. An alternative to handle this problem is proposed in this thesis, by integrating the classic RTO and Self-Optimizing control (SOC) using a new Model Predictive Control strategy. The new approach demonstrates that it is possible to reduce the problem of low frequency of set points updates, improving the economic performance. Finally, the practical aspects of the RTO implementation are carried out in an industrial case study, a Vapor Recompression Distillation (VRD) process located in Paulínea refinery from Petrobras. The conclusions of this study suggest that the model parameters are successfully estimated by the Rotational Discrimination method; the RTO is able to improve the process profit in about 3%, equivalent to 2 million dollars per year; and the integration of SOC and RTO may be an interesting control alternative for the VRD process.

Keywords: Real Time Optimization. Process Control. Parameter Estimation, Self-Optimizing Control.

LIST OF ILLUSTRATIONS

LIST OF TABLES

NOMENCLATURE

Chapter 2

B	matrix of estimated derivatives
F	mathematical model
F_c	corrected model
F_p	plant map
g	process constrains
M	scaling (diagonal) matrix
s	slack variable
u	are the decision variables
y	plant output
θ	parameters vector
ρ	regularization parameter
v	auxiliary variables
ε	gap between the plant and predicted function values
ξ	Lagrange multipliers
μ	Lagrange multipliers
λ	modifiers
ϕ	process (economic) performance index
$\delta_{g,j}$	deviation from the active constraints
δ_{φ}	Minimum improvement in the objective function
$\nabla\varphi$	plant derivative of the economic objective function
∇g_j	plant derivative of the constraints
$\frac{\partial \underline{g}}{\partial u_i}$	lower bounds of the constraint derivatives
$\frac{\partial \overline{g}}{\partial u_i}$	upper bounds of the constraint derivatives
$\frac{\partial \underline{\varphi}}{\partial u_i}$	lower bounds of the objective function derivatives
$\frac{\partial \overline{\varphi}}{\partial u_i}$	upper bounds of the objective function derivatives

Chapter 3

D_k	eigenvalues matrices in APS method

E	overall parameter effect index
FIM	Fischer Information Matrix
H^{rec}	reconditioned Hessian matrix
H_{red}	reduced Hessian matrix
k_{opt}	optimum step length
$k_{\max}$	maximum step size
P	reconditioning matrix
r	residual vector
S	sensitivity matrix
V	variance matrix
V_k	eigenvectors matrices in APS method
Λ	eigenvalues matrix
R	eigenvectors matrix
Λ_{red}	reduced eigenvalues matrix
R_{red}	reduced eigenvectors matrix
$\delta_{1,q}$	Kronecker delta
ξ	vector of residues
ε	minimal condition number of FIM
ϕ^{+}	estimable parameter space
ϕ^{-}	inestimable parameter space
θ	parameters vector
$\rho_{\max}$	maximum allowed parameter correlation
$\overline{\rho}_y$	covariance matrices of the predicted outputs
$\overline{\rho}_\theta$	covariance matrices of the parameters
τ_q	predictability degradation index
η_q	parameter correlation degradation index
Ω_q	set of estimated parameters
Φ	parameter space

Chapter 4

$b_{\min}$	lower bound of constrained variables
$b_{\max}$	upper bound of constrained variables
c	vector of self-optimizing controlled variables

$\bar{c}$	vectors of predicted controlled variables
$\bar{c}^{sp}$	controlled variable set points
d	analyzed disturbances
D	optimum NLP sensitivity matrix of outputs with respect to the vector of analyzed disturbances
F	mathematical model
g	process constraint
H	selected matrix in the left null space of D
L_1	linear penalty function
nu	number of inputs
ny	number of outputs
Q	diagonal weighting matrix for controlled variable
r	vector of constrained variables
$\bar{r}$	vectors of predicted constrained variables
R	diagonal weighting matrix on the input variable movements
s	slack variables
u	manipulated variables
y	output variables
$\hat{y}$	predicted output variables
W	diagonal matrix of zeros and ones
θ	model parameters
ϕ	economic objective function

Chapter 5

R	reflux stream
D	overhead stream
F_{boil}	Reboiler outlet stream
F_{cool}	Cooler outlet stream
Q_{CP}	compressor mass flow rate
R_i	stationary index R_i
R_{cr}	critical value
X_i	measured state
$X_{f,i}$	filtered state
$\upsilon_{f,i}^2$	first variance estimate
$\delta_{f,i}^2$	second variance estimate
λ_1	smoothing factor for the states
λ_2	smoothing factor for the first variance
λ_3	smoothing factor for the second variance
η_{CP}	isentropic efficiency
ΔP_{CP}	Pressure variation between the inlet and outlet stream of the compressor

CONTENTS

1. INTRODUCTION

The chemical industry is a mature business that has two main reasons for innovation: economical (due to increasing competition) and environmental (due to new and stricter laws). Considering the former reason, the reduction of energy used per pound of product is the most relevant driving force (REN, 2009). Therefore, process automation is a key factor to help the petrochemical industry to meet new requirements in energy efficiency and economic performance.

The hierarchical structure of the control framework in a chemical industry may be characterized either by a functional or a temporal decomposition. Functional decomposition sorts the control objectives in an order of decreasing importance (i.e. to ensure safe operation, to meet product quality and yield demands, and to maximize the plant profit). Temporal decomposition is applied when the control framework should be formulated as a dynamic optimization due to a significant difference between fast and slow state variables or dynamics disturbances (BRDYS; TATJEWSKI, 2005).

This work is focused on the functional hierarchical decomposition control (Figure 1.1), mainly in the optimization and control layers that are represented by RTO (Real Time Optimization) and MPC (Model Predictive Control) blocks respectively. The RTO module is inserted into the functional hierarchical control structure, in order to provide ideal economic targets for the MPC layer, which is responsible to control the process around this optimum steady-state.

Figure 1.1 – Functional process control hierarchy

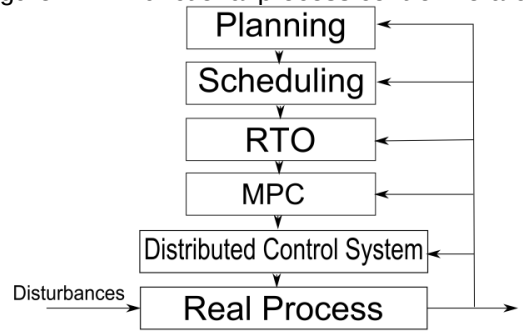

source: DARBY et al. (2011)

The classical way RTO layer design uses a first principles steady-state model to describe the plant behavior and to optimize an economic objective function subject to this phenomenological model. This strategy gained prominence in the late 1980's when new developments allowed for the application of this kind of RTO, namely: equation oriented modeling environments, computational processing capability and large scale sparse matrix solvers (DARBY et al., 2011a).

The basic idea behind the "classical RTO method" (also called Model Parameter Adaptation, MPA) is to rely on plant measurements to update some key parameters of a phenomenological steady-state model, in order to reduce the plant/model mismatch (MILETIC; MARLIN, 1998), and then to optimize the plant operation using the updated model. A flow chart describing the basic implementation of this technique can be observed in Figure 1.2, which depicts the most important processes demanded by the RTO algorithm: Steady State Detection, Data Reconciliation and Gross Error Detection, Parameter Estimation, and Economic Optimization.

Figure 1.2 – "Classical RTO" or Model Parameter Adaptation (MPA)

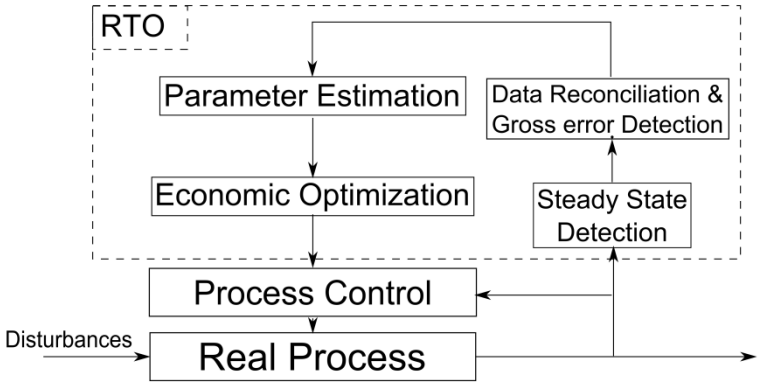

1.1. Motivation

Although the RTO methodology is one of the most applied optimization methods for continuous processes in industry (DARBY et al., 2011a), MPA has several well-known shortcomings that have been pointed out in the literature, reducing its applicability. For instance, one may cite the following limitations inherent in practical

implementation of model based methodologies: lack of process measurements, measurement noise, structural plant/model mismatch, numerical optimization (QUELHAS; DE JESUS; PINTO, 2013) and low frequency of set points update.

The first RTO drawback discussed in the present thesis is the structural plant/model mismatch. Despite the use of high-fidelity mathematical models in the RTO layer (see Figure 1.1), the absence of structural plant/model mismatch is not ensured. In 1985, Biegler and coauthors discussed the use of simplified models to optimize complex processes (which is the main idea behind the classical RTO method). They found out that plant/model mismatch derived from the simplified model may cause problems, since its mathematical optimum is likely to disagree with the real plant optimum. Furthermore, they showed that an adequate model must share the same Karush-Kuhn-Tucker (KKT) point with the real plant.

Forbes; Marlin and Macgregor (1994) introduced the concept of “model adequacy” for the classical RTO method. They developed a procedure to determine if a model is sufficiently flexible to represent a more complex model by a suitable choice of adjustable parameters. In other words, the question is if there is at least one set of parameters, for the simple model, able to yield the same economic optimum of the complex one. Nonetheless, this adequacy criterion does not take into account the model outputs (which should also be equal at the optimal point), causing problems in the classical RTO algorithm, since it relies on the parameter estimation method to reduce the plant/model mismatch (MARCHETTI, 2009). Consequently, the classical RTO method cannot guarantee the convergence to the true process optimum under structural plant/model mismatch.

Several methods have been developed in the literature to supposedly make the RTO algorithm able to converge to the plant "true" optimum in spite of uncertainties. However, they are based on plant derivatives (from process), which are quantities difficult to obtain in the real world.

Due to uncertainties of each RTO approach, there is not a general consensus about the reliability of different RTO methods to increase the profit of an industrial plant (DARBY et al., 2011a). Lack of experimental and theoretical works focused on

evaluating the scope and limitations of different RTO approaches makes it even harder to reach a sensible opinion about this topic. Most works available in the literature about different RTO approaches use a few (often one) operating conditions to draw general conclusions about the adequacy of a particular methodology.

Figure 1.3 gives an example to explain why it is necessary to consider different process conditions to evaluate the overall performance of an RTO algorithm. In this case, three RTO sequences (sharing the same process model) are simulated, departing from the same starting point and trying to converge to the “optimum” operational point, but with different uncertainty values (measurement noise and parameters' initial guesses). For comparison, the experiments are defined as:

- Blue and Red paths use the same parameter initial guesses but different measurements noise;
- Black and Red paths use different parameter initial guesses but the same measurement noises.

Figure 1.3 – Illustrative example of an RTO implementation under uncertainties; (A) economic objective function value with respect to RTO iterations; (B) economic objective function profile with respect to controlled variables (Temperature and flow rate Fb).

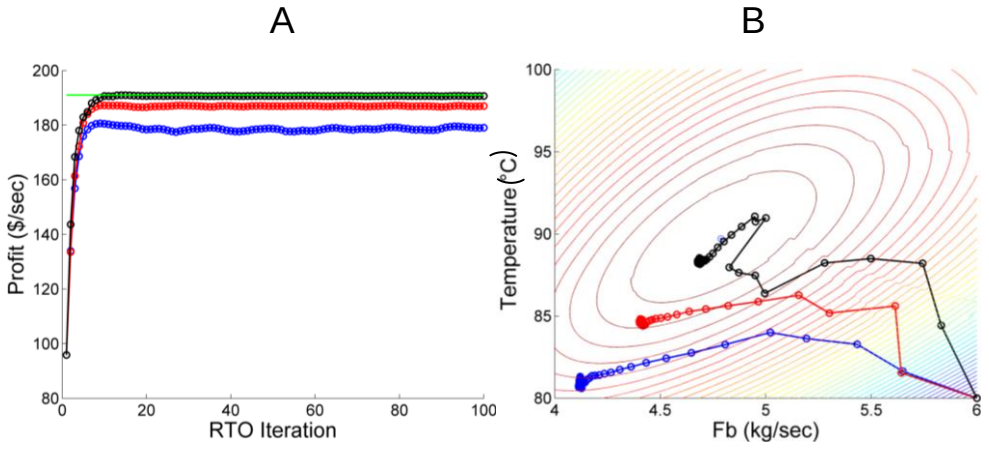

As can be observed in Figure 1.3, the uncertainties involved in the simulations could lead to different conclusions about the RTO performance, which requires an approach such as Monte Carlo to draw general conclusions about the performance of a determined method.

In the first part of the present work, the performance of the classic RTO method (MPA) and derivative-based methods (Modifier Adaptation, MA; Integrated System

Optimization Parameter Estimation, ISOPE; and an algorithm based on the Sufficient Conditions of Feasibility and Optimality, SCFO) are compared under different levels of measurement noise, model mismatch and process disturbances, using a Monte Carlo methodology.

The second RTO problem addressed in the present work is related to the parameter estimation module. Theoretically, while a model becomes mathematically more complex, and more mechanistic, it would potentially allow a broader representation and prediction of the system behavior (which is generally expected from a RTO model). However, the main disadvantage associated with complex models is the amount of information (both theoretical and experimental) required to describe the internal mechanisms, which are hindered by the noise of the available measurements, increasing possible sources of uncertainties. In this situation, identifiability problems are prone to take place.

Basically, the identifiability problem may result in ill-conditioning of the Hessian matrix in the parameter estimation problem, and/or model overfitting (MCLEAN; MCAULEY, 2012), with subsequent poor predictions by the process model and, consequently, suboptimal targets obtained by the RTO cycle. Some parameter estimation methods are proposed in the literature to tackle the identifiability problem; however, there is not a comprehensive review and performance comparison targeting these main techniques. For this reason, the second part of the present work aims to provide this review, building sufficient background to choose the most suitable parameter estimation method for RTO implementations.

The third RTO shortcoming explored in the present work is the low frequency of set point update. Since RTO is only performed under steady-state conditions, the plant operates suboptimally in presence of disturbances until the detection of the next steady-state. This is a clear disadvantage over other economic optimization methodologies, such as Economic MPC or Dynamic Real Time Optimization, where a dynamic model is used and it is not necessary to wait for a new steady-state before updating the set points.

Considering this disadvantage, it is important for the control layer to be more tightly coordinated with the RTO layer. In particular, the control layer must be robust regarding common disturbances affecting the plant profit. In other words, it should “obtain acceptable profit loss with constant set point values”. That is the definition of Self-Optimizing Control (SOC, Skogestad, 2000), in which the main idea is to choose a set of controlled variables that have set point values insensitive to disturbances, for instance, state variables that are kept at active constraints despite the presence of disturbances.

In this setting, the SOC methodology is complementary to the RTO method, and it can be an alternative to mitigate the problem of low frequency of set point updates in the RTO implementation (JÄSCHKE; SKOGESTAD, 2011; MANUM; SKOGESTAD, 2012). However, the practical implementation of the SOC in the MPC layer requires the solution of some problems, such as the active set changes due to disturbances. This limitation is also addressed in this work.

The analysis and results obtained addressing each current shortcoming of the RTO method are combined into a prototype software for RTO implementation. Its application is illustrated by an industrial case study of a vapor recompression distillation process for propylene production (a particular process of the REPLAN refinery, Petrobras). The practical implementation aspects of the RTO are detailed in Chapter 5, considering the background information developed in previous Chapters.

1.2. Objectives

The present thesis aims to develop a more robust RTO algorithm for industrial application. For this reason, the main weaknesses of RTO algorithms are addressed, in order to find alternatives and overcome the most significant implementation problems of this methodology. Each Chapter has its own objective:

1. Evaluate the performance of each RTO method to establish sensible opinion about the advantages and disadvantages of each RTO approach;

2. Find the best choice for parameter estimation methodology to be implemented in the RTO algorithm ;
3. Develop an MPC based on SOC concepts to reduce the intrinsic problem of the low frequency of set point updates of RTO approach;
4. Discuss the practical implementation of a RTO algorithm in an industrial case study (a vapor recompression distillation process) of the refinery REPLAN, Petrobras.

1.3. Outline of thesis

This thesis is structured as follows: In Chapter 2, the structural plant/model mismatch is discussed, comparing four different RTO methodologies. In Chapter 3, the identifiability problem is addressed through comparison of four parameter estimation techniques. Chapter 4 brings the development of a new MPC formulation with concepts of SOC, which aims to reduce the problem of low frequency of set point updates. Then, Chapter 5 discusses the practical implementation of the RTO methodology in an industrial case study. Finally, general conclusions are given in Chapter 6.

2. STRUCTURAL MODEL MISMATCH

One instrument used by the RTO method is the prediction of a process future behavior through a mathematical representation, for this reason, it commonly requires the use of high-fidelity models. However, there are many phenomenological behaviors that are hard to be described by equation systems (e.g.: hydraulic effects or reaction kinetics), and in these cases, simplifying hypothesis are employed in the process modeling. Such assumptions are a source of mismatch between the process behavior and the model prediction, resulting in inaccurate predictions and consequently, poor performance of the RTO method.

Biegler; Grossmann and Westerberg (1985) exposed that the RTO model must have the same Karush-Kuhn-Tucker (KKT) point than the real plant, in order to obtain the optimum solution. Forbes and Marlin (1994) suggested that the process model must have at least one set of model parameters resulting in the same KKT point of the real plant to be considered "adequate". Nonetheless, the existence of this parameter set does not guarantee that the optimum will be obtained by the closed-loop RTO. For instance, the measured outputs could be different, as showed in a numerical example given by Marchetti (2009). For this reason, several theoretical methods have been developed to make the RTO algorithm able to converge to the true optimum of the plant in spite of structural plant-model mismatch.

The first one, proposed by Roberts (1979), is a modification of the classical RTO method called Integrated System Optimization and Parameter Estimation (ISOPE). In this methodology the parameter estimation and the optimization steps are integrated, resulting in a modified economic objective function for the optimization step that is able to handle the structural mismatch problem, in cases when plant derivative can be calculated accurately.

The second method, called Modifier Adaptation method (MA) (MARCHETTI; CHACHUAT; BONVIN, 2009), differs from the classical RTO method in the way the plant information is used, since the measurements are employed to fulfill the necessary first-order optimality conditions (NOC) of the plant (using the so-called modifiers) without updating the model parameters. The MA scheme is able to

calculate the plant optimum in the presence of plant-model mismatch, provided that an accurate plant gradient is available, which, until now, is its main limitation for industrial applications.

Bunin; François and Bovin (2013a) proposed a method to tackle the plant-model mismatch problem, called Sufficient Conditions for Feasibility and Optimality (SCFO). This method combines the concepts of descent half-space and quadratic upper bound to derive sufficient conditions to guarantee the improvement of the plant objective function at each iteration; and concepts of approximately active constraints and Lipschitz continuity to ensure constraint feasibility at each step. Although this method has a solid mathematical background to carry out what it claims (BUNIN; FRANÇOIS; BONVIN, 2013b), some of its assumptions are very difficult to meet in practice, such as the knowledge of global Lipschitz constants, global quadratic upper bounds and the exact value of the unmeasured restrictions at the current iteration.

For this reason, Bunin; François and Bonvin (2013b) extended the SCFO method for practical implementation. They proposed to use a feasible region for the plant gradient to guarantee a descent region. In other words, the algorithm works within a region where the worst case ensures a decrease in the plant objective function without violating process constraints. However, Bunin and coworkers (2013b) state that it is unclear if the application of SCFO is benefical, since the SCFO algorithm may affect the convergence speed, especially when the RTO target is accurate (provided by the MPA for instance).

Due to the limitations of each RTO approach, there is not a general consensus about the reliability of the different RTO methods to increase the profit of a process plant (DARBY et al., 2011b). Therefore, in the present work, a Monte Carlo methodology is applied to evaluate the performance of each strategy under the same process uncertainties, namely: parameter plant-model mismatch, measurement noise and disturbances in the unmeasured variables. The Williams-Otto reactor benchmark problem is considered as case study.

This Chapter is organized as follows: first, the particularities of four RTO methods are presented in Section 2.1. Then, the Williams-Otto reactor case study is shown with

the experimental design for the Monte Carlo analysis in Section 2.2 and 2.3. The main results are displayed in Section 2.4. and discussed in Section 2.5. Finally, the conclusions are given in Section 2.6.

2.1. Materials and methods

2.1.1. MPA method

The structure of the classical RTO algorithm is presented in Figure 2.1. The RTO cycle starts with the steady-state detection module, responsible to analyze the process measurements and to decide, based on statistical criteria, if the plant has reached steady state. Then, the stationary point goes through the data reconciliation and gross error detection stage. Further, the screened information is used in the parameter estimation module to update the model parameters. Then, the updated model is employed to find a new operating point that hopefully maximizes the plant profit. Finally, this new condition is passed to the process control layer as set points for the controlled variables.

Figure 2.1 – Classical RTO structure

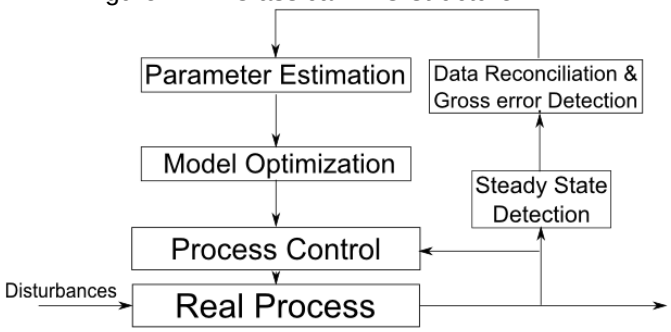

The basic statement of the optimization module can be written as:

$$\begin{aligned} u^* &= \min_u \varphi(u,y) \\ \text{s.}t.\ \ & y = F_p(u) \\ & g(u,y) \le 0 \end{aligned} \tag{2.1}$$

where φ is the process (economic) performance index, y is the plant output, u are the decision variables, $F_p(u)$ is the plant map, and $g(u,y)$ are the process constrains. In the model-based RTO (MPA) the plant outputs are estimated from a mathematical model, $F(u,\theta)$, locally fitted by the estimated parameters θ.

$$\begin{aligned} u = \min_{u} \quad & \varphi(u,\hat{y}) \\ \text{s.t.} \quad & \hat{y} = F(u,\theta) \\ & g(u,\hat{y}) \le 0 \end{aligned} \tag{2.2}$$

The MPA method has common vulnerabilities, namely: lack of process information (discussed in Chapter 3), plant-model mismatch and numerical optimization issues. (QUELHAS; DE JESUS; PINTO, 2013) However, it is the most used online optimization method by the industry (DARBY et al., 2011b).

2.1.2. ISOPE method

One of the difficulties with the optimization problem stated in eq.(2.2) is the mismatch between the model and the real plant. The Integrated System Optimization and Parameter Estimation (ISOPE) method was developed to handle the structural plant-model mismatch (BRDYS; TATJEWSKI, 2005), complementing the measurements used in the MPA method with plant derivative information, to reduce the offset created by the structural mismatch. ISOPE still retains the parameter estimation and economic optimization steps as in the MPA. However, ISOPE optimizes a modified economic function, adding a term coming from the parameter estimation step that allows a first-order correction.

ISOPE derivation starts by reformulating the RTO problem (eq.(2.2)), and adding a penalty term (the so-called regularization term) to the economic performance index,

$$\begin{aligned} \min_{u,\theta} \quad & \phi(u,F(u,\theta)) + \rho\|u-v\|^2 \\ \text{s.t.} \quad & F(u,\theta) = F_p(u) \\ & g(v) \le 0 \\ & u = v \end{aligned} \tag{2.3}$$

where ρ is the regularization parameter and v are additional variables that allow eq.(2.3) to have essentially the same solution than the problem stated in eq.(2.1). The Lagrange function of the optimization problem, given in eq.(2.3), is:

$$L(u,\theta,v,\xi,\mu,\lambda) = \phi(v,\theta) + \rho\|u-v\|^2 + \xi^T(F(u,\theta) - F_p(u)) + \mu^T g(v) + \lambda^T(u-v) \tag{2.4}$$

where ξ, μ and λ are Lagrange multipliers (or "modifiers"). The first order optimality conditions applied to Lagrange's function are:

$$2\rho(u-v) + \lambda + [\nabla_u F(u,\theta) - \nabla_u F_p(u)]^T \xi = 0 \tag{2.5a}$$
$$\nabla_v \phi(v,\theta) - 2\rho(u-v) - \lambda + \nabla_v g(v)^T \mu = 0 \tag{2.5b}$$
$$\nabla_\theta \varphi(v,\theta) + \nabla_\theta F_p(u,\theta)^T \xi = 0 \tag{2.5c}$$
$$u - v = 0 \tag{2.5d}$$
$$F(u,\theta) - F_p(u) = 0 \tag{2.5e}$$
$$g(v) \le 0,\ \mu \ge 0,\ \mu^T g(v) = 0 \tag{2.5f}$$

The multipliers ξ and λ, can be calculated from eq. (2.5a), (2.5c) and (2.5d)

$$\xi = -[\nabla_\theta F(u,\theta)\nabla_\theta F(u,\theta)^T]^{-1}\nabla_\theta F(u,\theta)\nabla_\theta \phi(v,\theta) \tag{2.6}$$

$$\lambda = [\nabla_u F(u,\theta) - \nabla_u F_p(u)]^T \nabla_y \phi(u, F(u,\theta)) \tag{2.7}$$

Finally, the optimization problem solved by the ISOPE method is the modified model-based optimization problem

$$\begin{aligned} \min_{v} \quad & \phi(u,\theta) - \lambda(u,\theta)^T v + \rho\|u-v\|^2 \\ \text{s.t.} \quad & y = F(u,\theta) \\ & g(v) \le 0 \end{aligned} \tag{2.8}$$

where $\lambda(u, \theta)$ is the multiplier given in eq.(2.7). This new optimization problem has the same optimality conditions as eq.(2.3). A comprehensive description of this formulation is given by Brdys and Tatjewski (2005). The basic ISOPE algorithm is shown in Figure 2.2.

Figure 2.2 - ISOPE structure

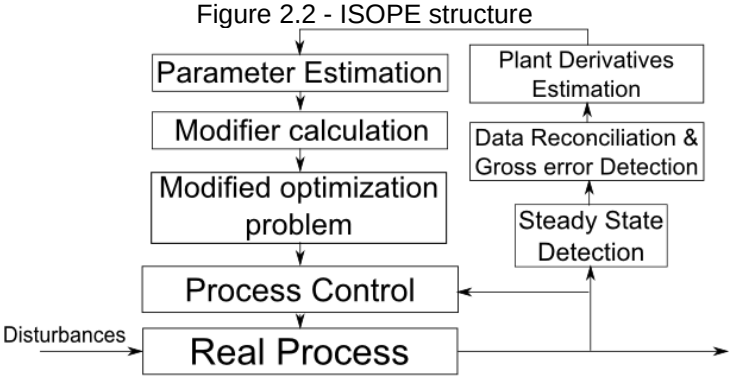

ISOPE has been derived assuming that the model is able to perfectly match the plant outputs by updating model parameters (point parametric condition (ROBERTS, 1979)) and that accurate plant derivative is available. These crucial assumptions ensure that the solution obtained by the modified model-based optimization problem converges to the true plant optimum (MANSOUR; ELLIS, 2003). The challenges faced by this method are the lack of process information, numerical optimization issues, and also, the requirement of plant derivatives (the most significant problem), which are used to compute the modifier values, since the estimation of these quantities is considerably affected by measurement noise.(LUBANSKY et al., 2006)

2.1.3. MA method

The idea behind modifier adaptation (MA) method is to use measurements to correct the cost and constraint predictions between successive RTO iterations in such a way that the KKT point for the model coincides with the plant optimum (MARCHETTI, 2009).

Given the real process model $F_p(u)$ and the RTO model $F(u)$, it is possible to construct a corrected model $F_c(u)$ similar to the real process model, eq.(2.9). The correction term, proposed in eq.(2.10), comes from a first-order Taylor series expansion of the discrepancy term around the current operating point, eq.(2.10). The final corrected model is presented in eq.(2.11).

$$F_c(u) = F(u) + [F_p(u) - F(u)] \tag{2.9}$$

$$F_p(u) - F(u) = \underbrace{F_p(u^0) - F(u^0)}_{\varepsilon} + \underbrace{\left(\nabla_u F_p\left(u^0\right) - \nabla_u F\left(u^0\right)\right)}_{\lambda}(u - u^0) \tag{2.10}$$

$$F_c(u) = F(u) + \varepsilon + \lambda^T (u - u^0) \tag{2.11}$$

where ε and λ^T are the so called modifiers, ε corresponds to the gap between the plant and predicted function values, and λ^T represents the difference between the slopes, which are calculated as the difference between model and plant derivatives (see eq.(2.10)). A very useful graphical interpretation of these features is presented by Marchetti; Chachuat and Bonvin (2009).

The objective function and the constraints of the RTO problem are reformulated using this methodology. The problem is restated as:

$$\begin{aligned} &\min \varphi_c(u,\theta) = \varphi_m(u,\theta) + \lambda_\varphi^T (u - u_k) \\ &s.t. g_c(u,\theta) = g_m(u,\theta) + \varepsilon + \lambda_g^T (u - u_k) \le 0 \end{aligned} \tag{2.12}$$

where the subscripts c and m indicate the corrected and the original RTO model, respectively; ϕ is the economic objective function and g is the set of inequality constraints.

Figure 2.3 - MA structure

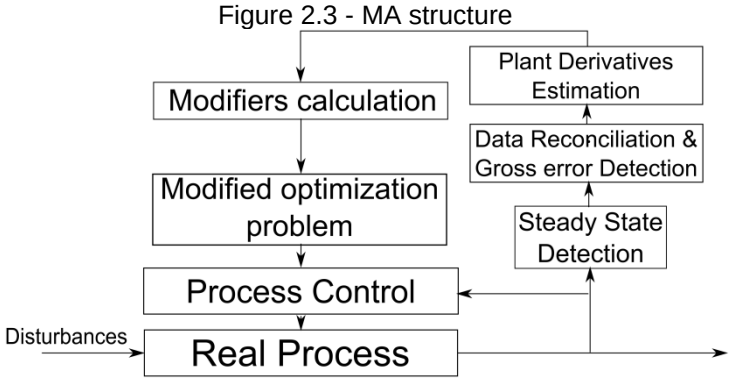

The fundamental differences between the MA and ISOPE frameworks are how the modifiers are calculated and the parameters updated. In MA, the modifier is calculated from the derivatives of economic objective function with respect to inputs (u), while the ISOPE method uses the derivatives of outputs (y) with respect to the inputs (u). Moreover, the parameters are updated during ISOPE iterations whereas

MA uses a fixed parameter set during optimization, i.e., there is no parameter updating. With this configuration, MA method also suffers from some problems as numerical optimization issues and lack of accurate plant derivative information.

2.1.4. SCFO method

The SCFO, initially proposed by Bunin; François and Bovin (2013a) and modified for practical implementation by Bunin; François and Bovin (2013b), adapts the nonlinear optimization theory to RTO problems. The method is devised to calculate the plant optimum without violating any hard constraint and improving the plant profit at each RTO iteration, executing a projection problem based on information of plant derivatives and topology. In other words, given a target (a possible future RTO point predicted by any RTO algorithm, MPA for instance) the SCFO method implements a correction to this target, based on plant derivative information. The projection problem, given by eq.(2.13), minimizes the distance between the target (u_{k+1}^{*}) and the feasible point (u), subject to a bounded deviation ($\delta_{g,j}$) from the active constraints ($g_j(u_k) \geq -\varepsilon_j$) and an improvement in the objective function (δ_{φ}). These two restrictions try to maintain the solution of the projection problem ($\bar{u}_{k+1}^{*}$) at the interior of the hard constraints region, given by $g_j(u_k) \geq -\varepsilon_j$, and to grant a profit improvement $\nabla\varphi(u_k)^T(u-u_k) \leq -\delta_{\varphi}$. This behavior is achieved within the region where the problem nonlinearities are well approximated by the first order local information (gradient information).

$$
\begin{aligned}
&\bar{u}_{k+1}^{*} = \arg\min_{u} \left(\left\| u - u_{k+1}^{*} \right\| \right)_2^2 \\
&s.t. \quad \nabla g_j(u_k)^T(u-u_k) \leq -\delta_{g,j} \;\; \forall j : g_j(u_k) \geq -\varepsilon_j \\
&\qquad \nabla\varphi(u_k)^T(u-u_k) \leq -\delta_{\varphi} \\
&\qquad u^L \leq u \leq u^U
\end{aligned}
\tag{2.13}
$$

where the subscript k indicates the RTO iteration, the point u_{k+1}^{*} is the input target (calculated from classical RTO approach in this work), $\bar{u}_{k+1}^{*}$ is the target projected

into a feasible descent space, $\nabla\varphi$ and ∇g_j are, respectively, the plant derivative of the economic objective function and constraints with respect to the input variables, δ are minimal changes required in the projected direction, and the superscripts U and L indicate the upper and lower bound vectors.

The need for accurate real process derivatives limits the practical implementation of this algorithm. For this reason the authors modified the projection problem to work within a feasible region given by the derivative of the real process. These regions can be obtained assuming a certain local structure for the economic objective function (BUNIN; FRANÇOIS; BONVIN, 2013e), or in a less rigorous way, they may be calculated from the estimated gradient, adding an uncertainty region around it (as implemented in the present work). This modified projection problem is given by eq.(2.14).

$$
\begin{aligned}
\bar{u}_{k+1}^{*} = & \min_{u,S,s_\phi} \left(\left\| u - u_{k+1}^{*} \right\| \right)_2^2 \\
s.t. \quad & \sum_{i=1}^{nu} s_{ji} \le -\delta_{g,j} \\
& \frac{\partial \underline{g}_j}{\partial u_i} \Big|_{uk} \left(u_i - u_{k,i} \right) \le s_{ji} \;\; \forall j : g_j(u_k) \ge -\varepsilon_j \\
& \frac{\partial \bar{g}_j}{\partial u_i} \Big|_{uk} \left(u_i - u_{k,i} \right) \le s_{ji} \;\; \forall j : g_j(u_k) \ge -\varepsilon_j \\
& \sum_{i=1}^{nu} s_{\varphi,i} \le -\delta_{\varphi} \\
& \frac{\partial \underline{\varphi}}{\partial u_i} \Big|_{uk} \left(u_i - u_{k,i} \right) \le s_{\varphi,i} \\
& \frac{\partial \bar{\varphi}}{\partial u_i} \Big|_{uk} \left(u_i - u_{k,i} \right) \le s_{\varphi,i}
\end{aligned}
\tag{2.14}
$$

where s are slack variables responsible for ensuring the choice of direction for the worst case (for objective function s_φ and constraints S); $\frac{\partial \underline{g}}{\partial u_i}$ and $\frac{\partial \bar{g}}{\partial u_i}$ are the lower and upper bounds of the constraint derivatives; $\frac{\partial \underline{\varphi}}{\partial u_i}$ and $\frac{\partial \bar{\varphi}}{\partial u_i}$ are the lower and upper bounds of the objective function derivatives. The main structure of the algorithm is

presented in figure 2.4, where the target calculation corresponds to the MPA solution and the projection problem is performed by the solution of eq.(2.14).

Figure 2.4 - SCFO structure

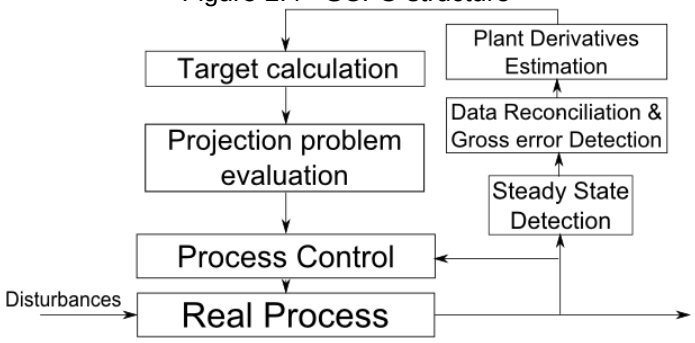

2.2. Plant derivative estimation

The plant derivative is estimated from process measurements using Broyden's approximation formula:

$$B_k = B_{k-1} + \left[(y_k - y_{k-1}) - (B_{k-1}(u_k - u_{k-1})^T)\right] \cdot \frac{(u_k - u_{k-1})M}{((u_k - u_{k-1})M(u_k - u_{k-1})^T)} \qquad (2.15)$$

where B is the matrix of estimated derivatives, u is the vector of input variables, y is the vector of outputs and M is a scaling (diagonal) matrix (RODGER, 2010). The indices k and $k-1$ indicate the current and previous steady-state points, respectively. In this work, Broyden is preferred to methods such as finite differences (FD) or dynamic model identification (DMI) on the basis of practical applicability, since FD and DMI require large numbers of upsets and/or depend on the availability of dynamic plant information, which are difficult and costly to achieve in a real process plant (MANSOUR; ELLIS, 2003)

The Dual approach, proposed by Rodger and Chachuat (2011), is implemented in MA and ISOPE algorithms to improve the plant derivatives estimated by Broyden's method, enforcing minimal perturbation in different directions (to get better information at each step), and maximum step length (to avoid the "peak phenomenon", as discussed by Rodger (2010)). This approach is implemented by a

set of constraints (eq.(2.16) and (2.17)), which determine two possible regions for solution search.

$$\begin{aligned} -w_k(u-u_k)+\sqrt{w_k{}^T \mathrm{B}^{-1} w_k} \;&\leq\; 0 \\ (u-u_k)^T \Gamma (u-u_k) \;&\leq\; 1 \end{aligned} \tag{2.16}$$

$$\begin{aligned} +w_k(u-u_k)-\sqrt{w_k{}^T \mathrm{B}^{-1} w_k} \;&\leq\; 0 \\ (u-u_k)^T \Gamma (u-u_k) \;&\leq\; 1 \end{aligned} \tag{2.17}$$

where u_k and u are the current and future RTO points, respectively, w_k is an unitary vector orthogonal to the last two RTO points, B is the parameter matrix for the minimum upset and Γ is the parameter matrix of maximum step length. In this work the values of B and Γ are $diag([50\ 0.4])$ and $diag([40\ 0.15])$ respectively.

In the Dual approach, the economic optimization problem is divided in two problems, one defined by eq.(2.16) and other by eq.(2.17). Then, these problems are simultaneously solved and the best result is implemented. A graphical interpretation can be found in Rodger and Chachuat (2011).

2.3. Case study: Williams Otto reactor

The Williams Otto CSTR (continuous-stirred tank reactor) is a well-known case study that has been used for the development and comparison of RTO strategies by several authors (MARCHETTI; CHACHUAT and BONVIN, 2009; PFAFF, 2001; ZHANG; NADLER and FORBES, 2001). This process is illustrated in Figure 2.5. The reactor is fed with Fa and Fb (pure streams of components A and B, respectively), these components react producing an intermediate component C, which reacts with another B molecule to produce the desired products P and E. There is a side reaction between components C and P, producing a waste byproduct G that has zero commercial value. The reactions and their kinetics are given in eq.(2.18).

Figure 2.5. - Williams Otto reactor

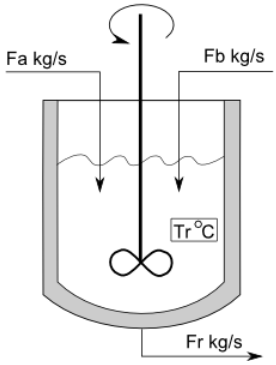

$$\begin{aligned} A+B &\rightarrow C & k1 &= \eta p1 \exp(-Ea1/(T_R+273.15)) \\ B+C &\rightarrow P+E & k2 &= \eta p2 \exp(-Ea2/(T_R+273.15)) \\ P+C &\rightarrow G & k3 &= \eta p3 \exp(-Ea3/(T_R+273.15)) \end{aligned} \quad (2.18)$$

where Ea, the activation energy and ηp, the pre-exponential factor, are given in Table 2.1.

The process is modeled at steady-state by the mass balances, using the reactor temperature (T_R) and flow rate of B (Fb) as controlled variables, and keeping the flow rate of reactant A (Fa) and the mass holdup (W) at 1.8275 kg/s and 2105 kg, respectively. The economic objective is to maximize the profit USD/s given by eq.(2.19).

$$\phi = 1143.38 X_P F_R + 25.92 X_E F_R - 76.23 F_A - 114.34 F_B \quad (2.19)$$

where X_P and X_E are the mass fractions of P and E, respectively, in the reactor outlet stream (F_R).

To analyze the performance of each RTO methodology under structural plant-model mismatch, a simpler kinetic (approximated model) is proposed to describe the original system (FORBES; MARLIN and MACGREGOR, 1994) (eq.(2.20)).

$$\begin{aligned} A+2B &\rightarrow P+E & k1 &= \eta 1 \exp(-\nu 1/(T_R+273.15)) \\ P+C &\rightarrow G & k2 &= \eta 2 \exp(-\nu 2/(T_R+273.15)) \end{aligned} \quad (2.20)$$

where v is the activation energy and η is the pre-exponential factor, both estimated by the parameter estimation module.

2.3.1.1. Parameter estimation module

In our analysis we consider a perfect and an approximate model, eq.(2.18) and (2.20) respectively. In both cases, all kinetic parameters (pre-exponential factors and activation energies) are estimated using the product compositions Xp, Xe and the flow rate, Fa, as measurements. This is due to the fact that it is very unlikely that a real plant has online measurements of all products compositions (online composition measurements are very expensive). The objective function corresponds to an unweighted least squares problem. Furthermore, the last three historical points in the RTO path are used by the parameter estimation module, as suggested and implemented by Pfaff (2001), to increase the amount of information.

2.3.1.2. Experimental Design

The present section aims to design a comprehensive experiment to evaluate the algorithms performance over a wide range of different situations. For this reason, we consider five process characteristics that can modify the evaluation of a RTO algorithm. The first two problems are related to the parameter estimation module: measurement noise and the initial values of parameters. Both may deteriorate the parameter estimation and change the RTO path, resulting in different performances for the same RTO algorithm. The influence of these random variables is assessed through Monte Carlo simulations, where 500 RTO trials are carried out using different initial values of the parameters and measurement noise sampled following uniform and normal distributions, respectively (see Appendix A).

The third and fourth problems are disturbances presented in measured and unmeasured variables. These process characteristics are simulated in the plant by changing the parameter listed in Table 2.1, which results in four regions depicted in Figure 2.6 The first and second disturbance steps correspond to changes in the

values of the kinetic constants (unmeasured disturbances), which may be associated for example to a decrease in the catalyst performance, while the last one is due to a sudden increase in the feed flow rate Fa (measured disturbance).

Table 2.1 - Experimental design

Parameters	Region 1	Region 2	Region 3	Region 4
$\eta p1$	1.6599e6	1.6599e6	1.6599e6	1.6599e6
$\eta p2$	7.2117e8	7.2117e8	7.2117e8	7.2117e8
$\eta p3$	2.6745e12	2.6745e12	2.6745e12	2.6745e12
$Ea1$	6666.7	6666.7	6666.7	6666.7
$Ea2$	8333.3	8444.3	8333.3	8333.3
$Ea3$	11111	11101	11111	11111
Fa [kg/s]	1.8275	1.8275	1.8275	2.2000

Figure 2.6 – Optimum profile with respect to disturbances

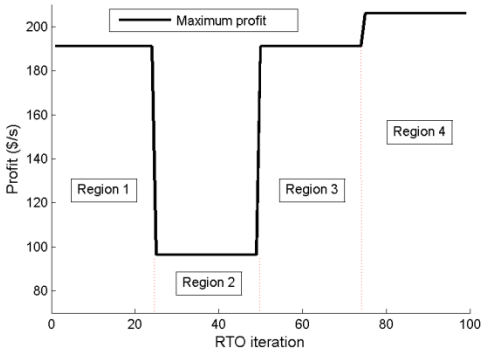

The fifth problem that modifies the RTO performance is the structural mismatch between plant and model. Two cases are considered in the experimental design: perfect model when both plant and model are represented by eq.(2.18) and approximate model when plant is given by eq.(2.18) and the model by eq.(2.20). In both cases the plant is simulated according to the parameters described in Table 2.1, while the model parameters are estimated by the parameter estimation module.

In short, the Monte Carlo (MC) simulations are performed for each RTO algorithm using measurement noise of 0% and 0.5%, with perfect and approximated models (summing up to a total of 16 experiments). In each MC experiment, 500 RTO trials are conducted (with 100 iterations in each RTO) starting from the same nominal point. Three disturbance scenarios are assumed along the path at iterations: 25, 50 and 75, creating four different regions (see Figure 2.6).

The performance of the RTO methodologies are compared using three statistics computed from the profit error, namely: root mean square error, average profit loss (absolute value) and frequency to obtain profit loss less than 1% in the last 5 RTO iterations of each region (%). In this work the profit loss is defined as the difference between the instantaneous profit using the set points calculated by the RTO and the true optimum in each region defined in Figure 2.6.

Appendix B shows the performance of each RTO method under perfect conditions. These experiments are important to illustrate that the algorithms work well under ideal conditions and their implementation was done correctly.

2.4. Results

2.4.1. Results for perfect model

Figure 2.7 presents the results of the four RTO methods using noise-free measurements and perfect model. In this figure the frequency distribution of the economic objective function is denoted by the color scale.

The behavior shown in Figure 2.7 and the dispersion metric presented in Table 2.2 indicate that the MPA method presents the lowest scattering profile, since this method is not influenced by the errors in the derivative caused by the Broyden's approximation that affects all the derivative-based methods tested. Among these strategies, the SCFO exhibits the lowest dispersion.

The frequency of attaining the optimum profit (within 1 %) in the last 5 RTO iterations is shown in Table 2.3. It can be appreciated that the MPA methodology follows the optimum plant operation path along the different plant upsets. In this case, the information quality as well as the model structure allow the parameter estimation routine to identify a topology converging to the "true" optimum in few RTO cycles (around 15 cycles on average), even after plant disturbances.

Regarding the profit loss during the RTO, the path followed by MPA is the most cost effective (on average 3.04 USD/s), since it presents lower profit loss than any derivative based method tested. SCFO shows the best result for the first region (see Table 2.4), basically because it has the largest first step among the methods; however its average profit loss is 4.64 USD/s.

Figure 2.7 – MC experiments using noise free measurements and perfect model: (A) MPA, (B) MA, (C) ISOPE and (D) SCFO

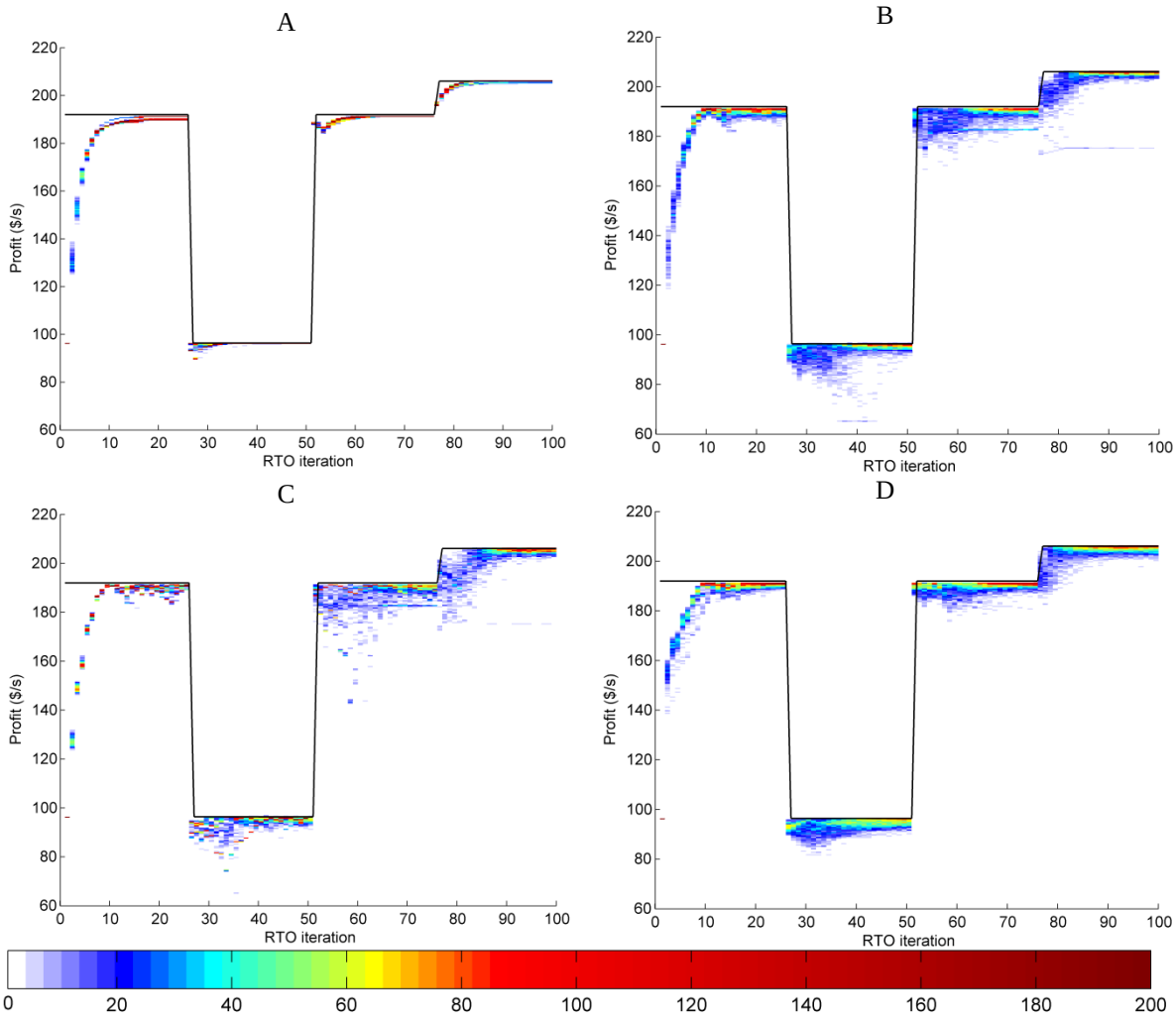

Table 2.2. - Root mean square error for MC experiments using noise free measurements and perfect model

Method	Region 1	Region 2	Region 3	Region 4
MPA	8.15	4.59	8.36	9.13
MA	8.44	7.35	10.61	11.58
ISOPE	8.15	6.31	10.89	12.24
SCFO	8.68	5.07	8.81	9.83

Table 2.3. - Frequency of achieving less than 1% profit loss in the last 5 RTO iterations of each region. MC experiments using noise free measurements and perfect model.

Method	Region 1	Region 2	Region 3	Region 4
MPA	100	100	100	100
MA	72.16	43.36	60.48	84.80
ISOPE	55.00	39.24	56.16	79.24
SCFO	86.48	28.72	76.84	67.08

Table 2.4. - Average profit loss for MC experiments using noise free measurements and perfect model

Method	Region 1 [USD/s]	Region 2 [USD/s]	Region 3 [USD/s]	Region 4 [USD/s]
MPA	8.50	0.78	1.33	1.56
MA	8.90	5.44	6.30	5.57
ISOPE	9.33	4.23	6.88	7.88
SCFO	7.59	3.78	3.06	4.13

The results for the MC simulations with perfect model and measurement noise are shown in Figure 2.8. A comparison of the statistics of the RTO performance using noisy measurements (Tables 2.5 to 2.7) with previous noise free measurements (Tables 2.2, 2.3 and 2.4) indicates a lower performance of the RTO methodologies due to corrupted information.

The comparison of the RTO methods with and without measurement noise shows that , as expected, noise always increases profit loss (cf. Tables 2.4 and 2.7). As in the noise-free case, the MPA is the one with the lowest profit loss on average, this loss is even lower than the ones achieved by the derivative based methods using perfect measurements.

Table 2.5. - Root mean square error for MC experiments using noisy measurements (0.5%) and perfect model

Method	Region 1	Region 2	Region 3	Region 4
MPA	9.95	5.19	8.59	9.34
MA	9.40	8.61	10.81	12.54
ISOPE	8.95	9.11	11.14	13.33
SCFO	9.97	5.09	6.36	9.91

Table 2.6. - Frequency of achieving less than 1% of profit loss in the last 5 RTO iterations of each region. MC experiments using noisy measurements (0.5%) and perfect model

Method	Region 1	Region 2	Region 3	Region 4
MPA	75.44	44.96	79.08	80.84
MA	28.08	11.20	23.36	32.12
ISOPE	25.72	12.20	22.08	28.56
SCFO	25.32	18.60	28.96	17.96

Table 2.7. - Average profit loss for MC experiments using noisy measurements (0.5%) and perfect model

Method	Region 1 [USD/s]	Region 2 [USD/s]	Region 3 [USD/s]	Region 4 [USD/s]
MPA	9.72	2.96	1.98	2.87
MA	11.72	8.42	8.14	10.14
ISOPE	11.60	8.08	8.63	11.41
SCFO	9.97	5.09	6.36	9.91

Figure 2.8 – MC experiments using noisy measurements (0.5%) and perfect model: (A) MPA (B) MA (C) ISOPE and (D) SCFO

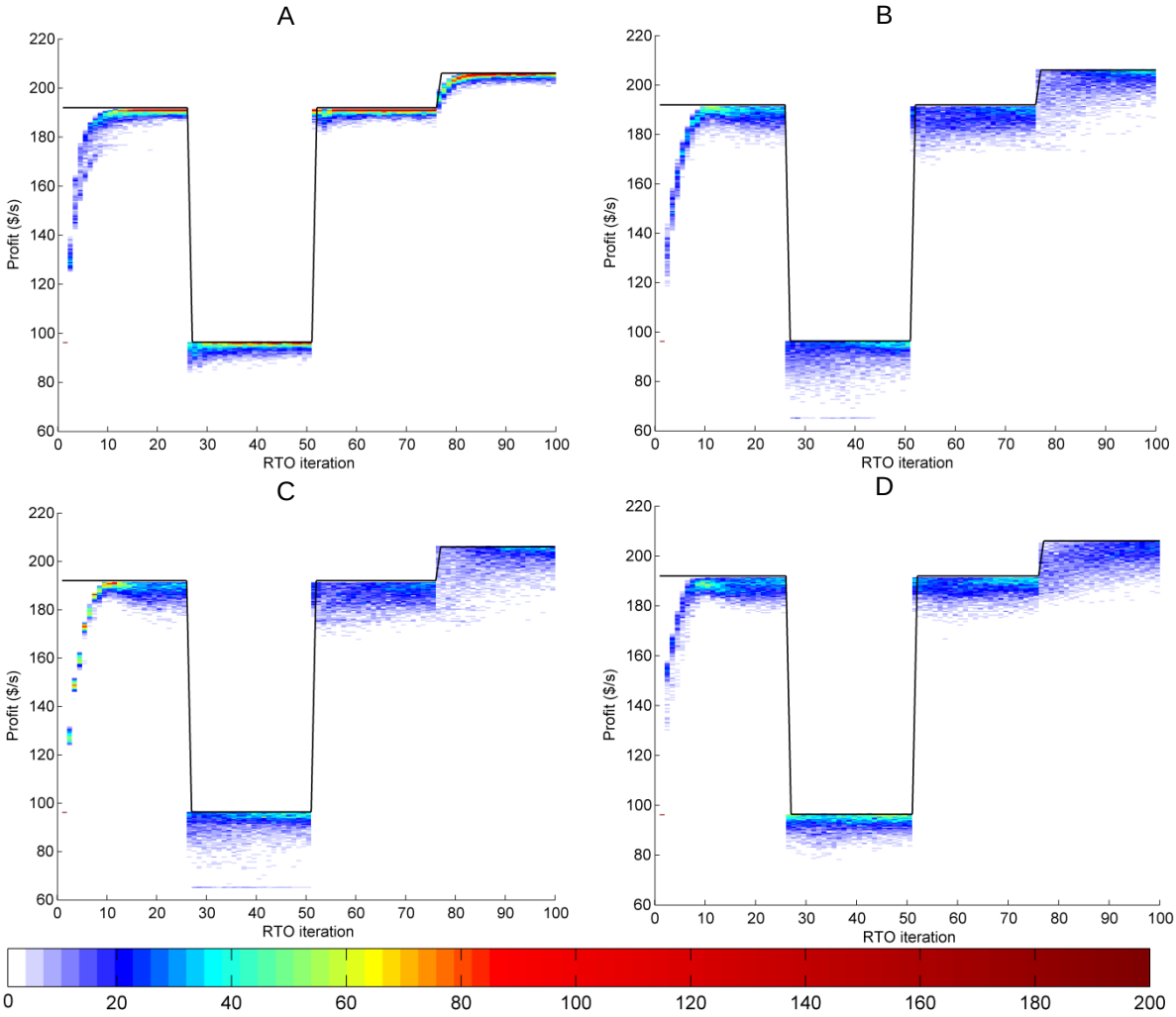

2.4.2. Results for the approximated model

These experiments assess the behavior of the RTO methodologies under structural plant-model mismatch. The results obtained in the Monte Carlo simulations using the approximate model and noise free measurements are depicted in Figure 2.9. The structural mismatch does not allow the convergence of the MPA method to the true

optimum in all regions, which is confirmed by low frequency of obtaining profit losses less than 1% (see Table 2.9). In contrast, the derivative based methods are able to handle the structural mismatch in all tested regions, as can be observed in Figure 2.9 and Table 2.9.

The scattering presented by MPA and SCFO tend to be alike in every region, this dispersion is lower than the obtained by the MA and ISOPE under similar conditions (see Table 2.8). However, the lower average profit loss corresponds to the path followed by MA in the first region, MPA in the second region and by SCFO in the third and fourth regions (see Table 2.10). On average SCFO presents the best economic results.

Figure 2.9 – MC experiments using noise free measurements and approximate model: (A) MPA (B) MA (C) ISOPE and (D) SCFO

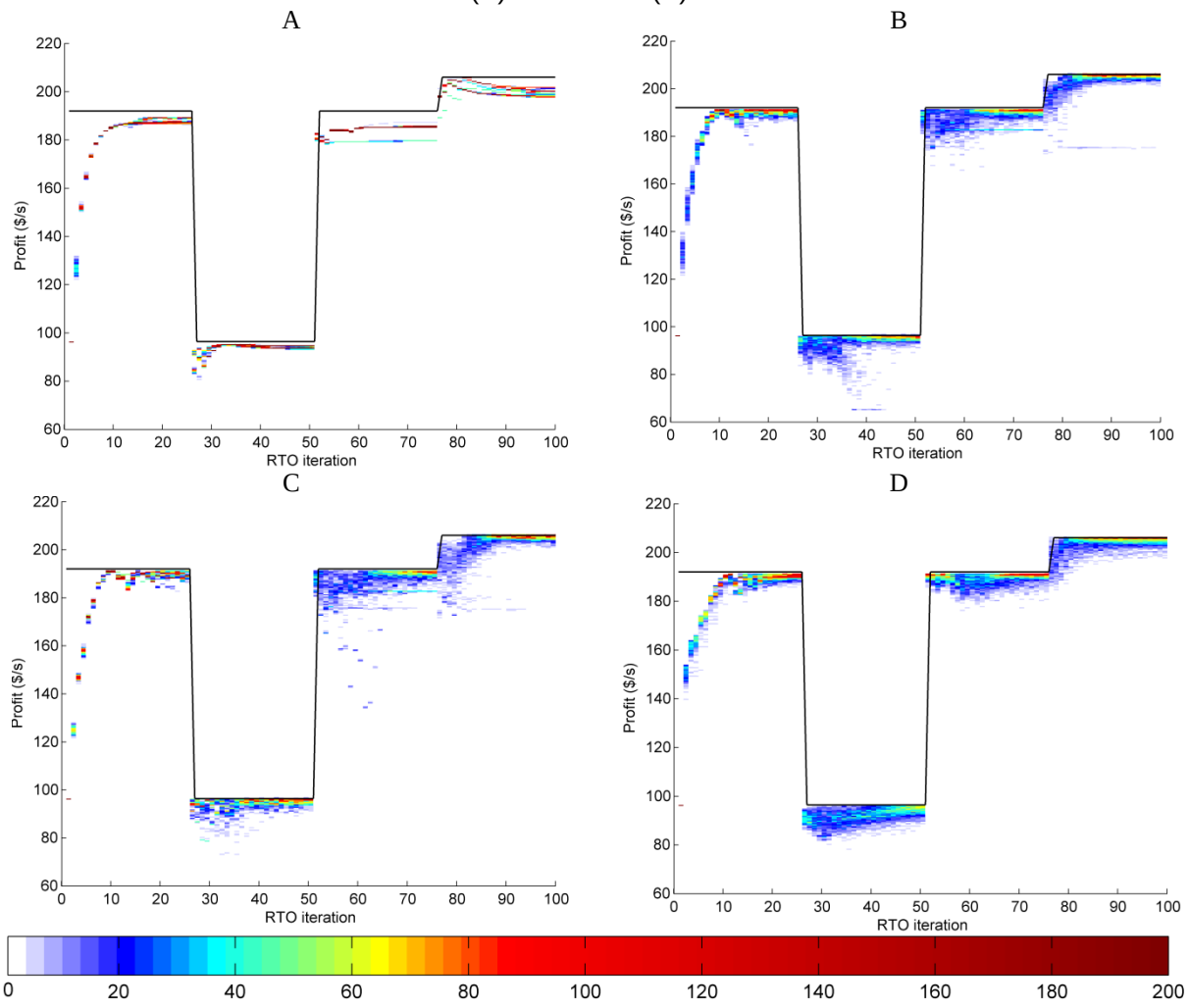

Table 2.8. - Root mean square error for MC experiments using noise free measurements and approximate model

Method	Region 1	Region 2	Region 3	Region 4
MPA	8.00	4.58	8.22	9.22
MA	8.32	7.61	10.74	11.47
ISOPE	8.09	5.90	11.25	12.22
SCFO	8.45	5.51	8.99	9.66

Table 2.9. - Frequency of achieving less than 1% profit loss in the last 5 RTO iterations of each region. MC experiments using noise free measurements and approximate model

Method	Region 1	Region 2	Region 3	Region 4
MPA	1.12	0.00	0.00	0.00
MA	73.40	42.28	62.72	81.44
ISOPE	57.80	37.76	54.28	74.56
SCFO	73.52	13.04	64.28	65.24

Table 2.10. - Average profit loss for MC experiments using noise free measurements and approximate model

Method	Region 1 [USD/s]	Region 2 [USD/s]	Region 3 [USD/s]	Region 4 [USD/s]
MPA	10.90	3.15	7.64	5.97
MA	8.92	5.61	6.44	5.31
ISOPE	9.84	3.77	7.55	7.72
SCFO	9.28	5.77	3.74	3.94

Figure 2.10 shows the outcome of the MC simulations for the case using the approximate model and measurement noise of 0.5%. The results point out increasing scattering of the RTO path compared to the case with same structural model mismatch and noise-free measurements (Tables 2.8 and 2.11). Another fact observed is that the derivative-based methods are more sensitive to noise than the MPA method. Indeed, the profit loss increases around 45% for MA and 36% for ISOPE and SCFO methods, in comparison with an approximate decrease of 18% presented by MPA under the same conditions (Tables 2.10 and 2.13).

The MPA, as observed in the MC simulations using an approximate model and noise free measurements, presents offset between the predicted optimum and the real one in the first three regions, this behavior reduces the frequency of obtaining profit losses less than 1% in these regions using MPA rather than the derivative-based methods (Table 2.12). However, this method outperforms the derivative-based approaches in region 4 where the offset is not present.

A comparison of the approximate model with its noise-free counterpart reveals a constant increase in the scattering in each region, similar to the one observed in the perfect model simulation with and without noise.

Figure 2.10 – MC experiments using noisy measurements (0.5%) and approximate model: (A) MPA (B) MA (C) ISOPE and (D) SCFO

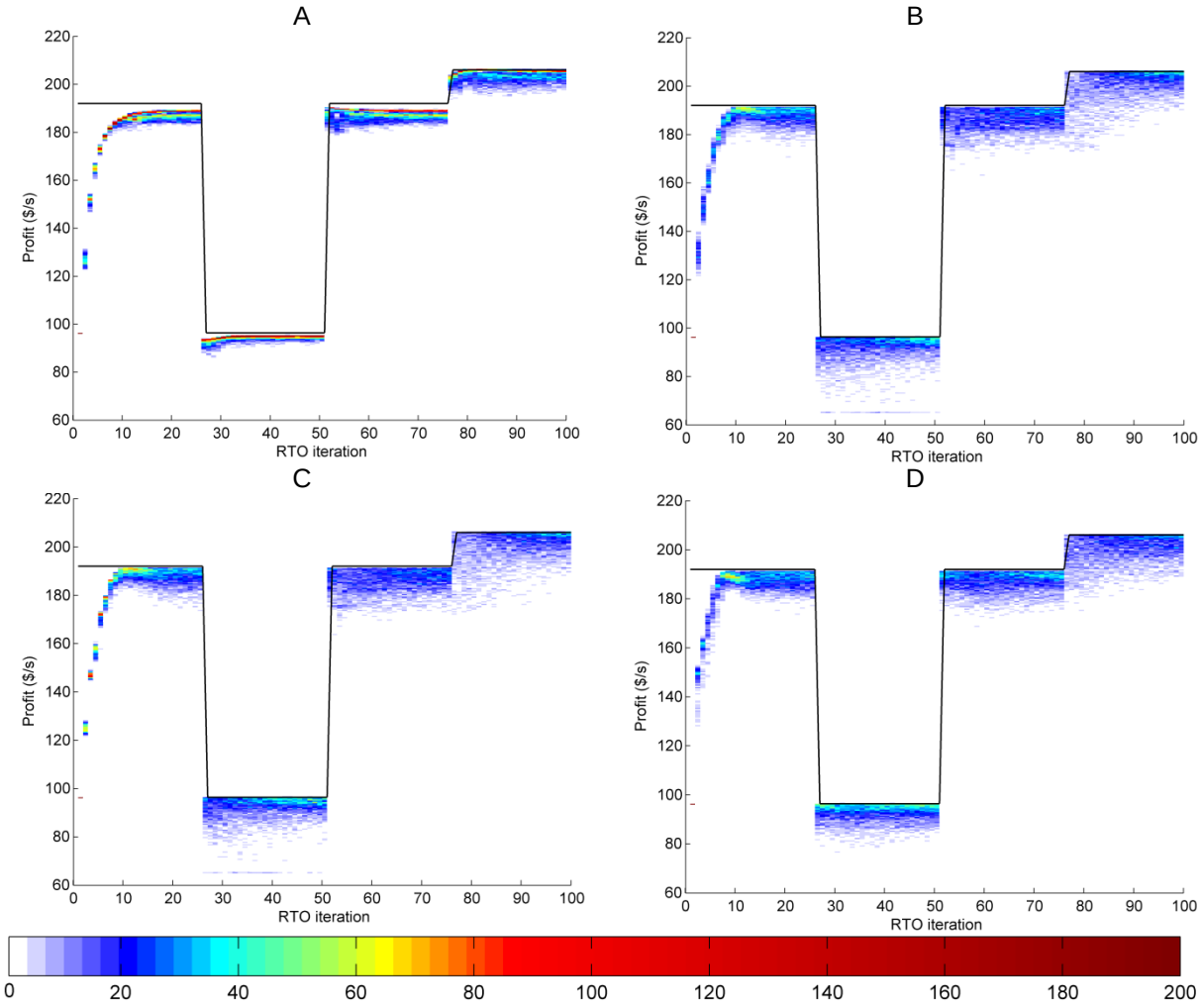

Table 2.11. - Root mean square error for MC experiments using noisy measurements (0.5%) and approximate model

Method	Region 1	Region 2	Region 3	Region 4
MPA	8.10	4.63	8.53	9.45
MA	9.25	8.79	10.77	12.46
ISOPE	8.88	8.43	11.27	13.40
SCFO	9.36	6.60	9.88	11.18

Table 2.12. - Frequency of achieving less than 1% profit loss in the last 5 RTO iterations of each region. MC experiments using noisy measurements (0.5%) and approximate model

Method	Region 1	Region 2	Region 3	Region 4
MPA	1.44	0.00	1.92	49.44
MA	27.48	13.72	23.60	31.28
ISOPE	27.32	11.84	20.44	28.96
SCFO	25.20	15.96	26.56	25.16

Table 2.13. - Average profit loss for MC experiments using noisy measurements (0.5%) and approximate model

Method	Region 1 [USD/s]	Region 2 [USD/s]	Region 3 [USD/s]	Region 4 [USD/s]
MPA	11.47	2.67	4.84	3.75
MA	11.66	8.11	8.15	10.25
ISOPE	11.98	7.49	8.74	11.10
SCFO	9.88	5.51	6.64	8.95

2.5. Discussion

The Monte Carlo simulations using a structural perfect model points out that MPA performs better than derivative-based methods in the presence of disturbances and measurement noise. This result is partially due to the fact that the experimental conditions fulfill the assumptions made for the parameter estimation method, since the least squares estimator is able to handle noisy data composed of independent, normally distributed zero-mean measurements (PFAFF, 2001). On the other hand, it would be expected a poor performance of the Least Squares estimator, and in the overall performance of the MPA method, in cases where measurements are corrupted with gross errors or correlated noise. In these cases, redescending or appropriate likelihood estimators should be used (ARORA; BIEGLER, 2001).

The approximate model used in the second analysis fulfills the adequacy criterion of Forbes; Marlin and Macgregor (1994), since there is at least one set of parameters that predicts the same optimal point than the plant (at least for regions 1 and 3). However, Marchetti (2009) pointed out that for this set of parameters the model outputs differ from the plant output, becoming unlikely to converge to the “ideal” set of parameters through a parameter estimation and optimization approach (MPA method).

The results obtained in the MC simulations using the approximate model and noise free measurements suggest that MPA is unable to converge to the true optimum, in consequence, the derivative-based RTO methods (SCFO and MA) have better economic performance. On the other hand, MPA shows better economic performance than derivative-based methods in cases where optimization runs under measurement noise and plant-model mismatch. Also in this case, in the fourth region, MPA does not present offset, since the model is able to simulate the process topology.

The improvement observed in the MPA method is related to the parameter estimation module, since the upsets introduced by the measurement noise are sufficient to increase the sample distribution quality, obtaining better information. Similar results could be achieved by introducing the Dual methodology to the MPA approach. Figure 2.11 shows a comparison between MPA with and without the Dual methodology. One can note that Dual approach decreases the bias observed in the RTO path calculated by the MPA method, consequently decreasing the profit loss by approximately 28% with respect to MPA without Dual approach.

Figure 2.11. - Comparison between MPA with approximate model and free measurement noise. (A) MPA without Dual approach; (B) MPA with Dual approach.

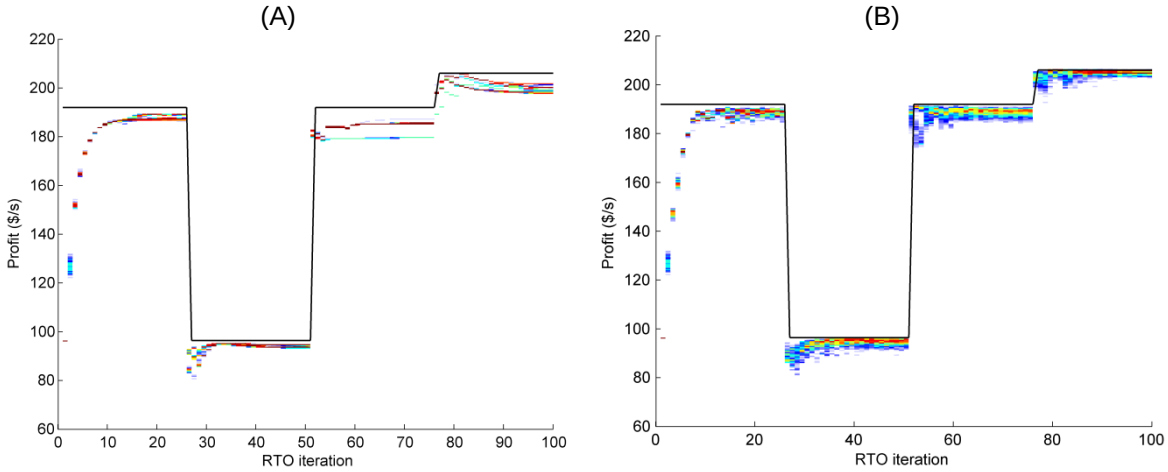

The derivative-based methods present better results than the MPA only in the case of model mismatch and noise free measurements. In particular, the SCFO method presents the best economic performance among the derivative-based methods, followed by the MA and then ISOPE. This fact indicates that SCFO is better designed to handle the uncertainty introduced by the Broyden's estimation. In comparison with

ISOPE, MA shows a slightly better performance, indicating that the parameter estimation module is not necessary for this approach type.

In general, the results show that derivative-based methods are more sensitive to measurement noise than the classical MPA method. In fact, the conditions used in the numerical experiments are especially difficult for the derivative-based methods, since the random sampling of parameters (in the first iteration - Appendix A) is likely to produce significant plant-model mismatch from the first RTO iteration, therefore the approximation given by Broyden is prone to produce a misleading search direction from the beginning of the RTO iterations. Another factor affecting Broyden's methods performance are the "drastic" changes in process topology induced by the sudden disturbances added in the experiments during the RTO iterations. For instance, see that the dispersions obtained by MA and ISOPE in regions 1 and 3 are notoriously different even though the plant parameters are the same in both regions (Figure. 2.7 and 2.9). In the first region, the algorithm starts from a unique point where the derivatives are estimated by the model, at a corner point where the derivative module is large and points approximately to the optimum solution while region 3 may start at several different points (end points of second region). In comparison to this region 1, the starting points of region 3 are placed in a flatter area, which decrease the quality of Broyden's derivative prediction.

The influence of measurement noise on the gradient prediction is analyzed through a simple experiment and consists in calculating a sequence of gradient approximations using Broyden's method, under different levels of noise. The quality of the gradient estimate is evaluated using the angle and the norm ratio between the predicted and the true gradient. Figure 2.12 shows the influence of the measurement noise over these two characteristics, for a sequence of four RTO iterations, starting from the same point and converging to the optimum (#1 blue, #2 green, #3 red and #4 black), using noises of 0 (Figure 2.12 A and B), 0.05% (Figure 1.12 C and D), 0.5% (Figure 1.12 E and F) and 1% (Figure 1.12 G and H).

Figure 2.12. - Derivative analysis: (A – C – E - G) angle distribution between true and predicted gradient; (B – D – F - H) Norm ratio distribution between true and predicted gradient

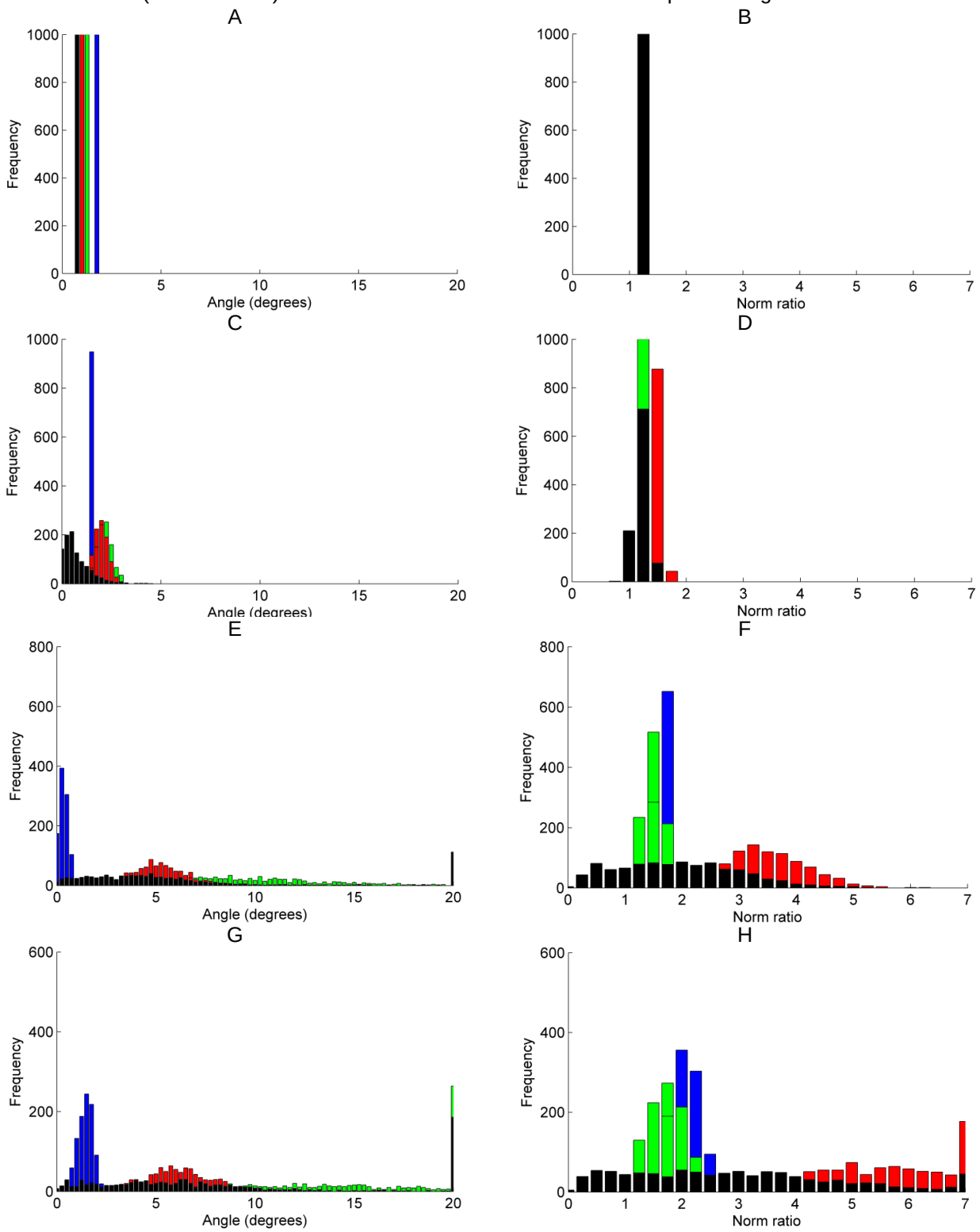

For the noise free case, the maximum average angle between the predicted plant gradient using Broyden and the true is less than 2 degrees, meaning that Broyden approximation is close to the true local direction of maximum function increase. Moreover, for this case the predicted derivative norms are similar to the true one,

indicated by a norm ratio close to 1 in Figure 2.12 B. Under these conditions, viz. noise free and good initial guess, Broyden's approximation shows a reasonable estimation of the plant gradient.

The increment in the angle between the true and the estimated gradient confirms the high sensitivity of Broyden's method to measurement noise (Figure 1.12 A, C, E and G). Also the increase of the scattering at each RTO step indicates high sensitivity to information degradation (i.e. measurement noise); this behavior can be better appreciated in cases with 0.5% and 1% of noise, where the norm ratios between the derivatives are highly scattered, affecting the step length taken toward the optimum by the derivative-based RTO routine.

The high sensitivity to measurement noise of Broyden's gradient estimation (even for measurement noises as low as 0.5%) is a serious pitfall for its implementation in practical situations, and is the reason why several alternative approaches have been devised to improve the plant gradient estimation (BUNIN; FRANÇOIS and BONVIN, 2013c; MANSOUR; ELLIS, 2003). An interesting alternative is to take advantage of the transient periods to get more information from the plant (GRACIANO; MENDOZA and LE ROUX, 2014). Some techniques are known to use this information as identification of linear or nonlinear dynamic models used to predict plant gradients (BAMBERGER and ISERMANN, 1978), which can be implemented without affecting the basic (derivative-based) steady-state RTO scheme, probably improving the performance of this method.

2.6. Partial Conclusions

The main findings of this chapter can be summarized as:

i) The MPA presents the best performance among the methods compared, for the perfect model case. This method shows the lowest profit loss in the studied scenarios. The key point in this method, provided a flexible enough model to generate the local process topology, lies on using a parameter estimation method capable to minimize the overfitting caused by the lack of practical identifiability

(BARD, 1974). On the other hand, for the approximate model experiments, MPA presents better results than the derivative-based method in cases with measurement noise or when a specific method (e.g., Dual methodology) is used to improve the sample information quality.

ii) The plant derivative predicted by Broyden's method is highly sensitive to measurement noise and to initial estimates of the derivatives. The SCFO is the most suitable method to handle this kind of uncertainty, presenting the best economic results. The comparison between MA and ISOPE shows that the parameter estimation module is less important than the derivative quality, for this kind of approach.

In conclusion, the results show that classical RTO method can be reasonably reliable provided a model flexible enough to mimic process topology, a parameter estimation method suitable to handle process noise characteristics (better discussed in next chapter), gross errors and lack of model identifiability and a method to generate process upsets to improve the sample information quality (Dual methodology).

The implementation of a derivative-based RTO method, in cases of evident model mismatch, should be considered only if the gap between the predicted and the real optimum is large enough (which is impossible to know *a priori*) and the level of measurement noise is low. Furthermore, other aspect to be considered is the need for implementing better techniques to estimate the plant gradient using transient information.

Considering these outcomes, only the MPA method is considered for implementation in the industrial case study, which is carried out in Chapter 5 of the present thesis.

The paper "Assessing the Reliability of Different Real-Time Optimization Methodologies", which was accepted for publication in Canadian Journal of Chemical Engineering, presents the main findings shown in Chapter 2.

3. PARAMETER ESTIMATION

The success of an RTO implementation is directly correlated with the accuracy of the mathematical model used to represent the plant behavior; therefore detailed models are commonly employed in this approach.

Mathematical models can be classified with regard to the relative amount of knowledge of the internal mechanisms used to describe a specific process, ranging from empirical (black box), to semi-empirical (grey box) and mechanistic (white box) models (HANGOS and CAMERON, 2001). Empirical models are entirely based on experimental input/output information without taking into consideration any information about the internal mechanisms of the system, while mechanistic models are derived from the knowledge of the basic principles governing a specific process. Semi-empirical models are in between, since they include both basic principles and experimental information (used to fit purely mathematical correlations). The degree of complexity of a model increases as it includes more basic principles, i.e., as it incorporates more mechanistic description.

Theoretically, while a model becomes mathematically more complex and more mechanistic, it would potentially allow a broader representation and prediction of the system behavior, becoming more interesting from the point of view of RTO. However, the main disadvantage associated with complex models is the amount of information (both theoretical and experimental) on the internal mechanism. Available measurements noise hinders the reliability of such information, which widens the possible sources of uncertainties and may result in identifiability problems.

A model is said locally (globally) identifiable when the objective function of the parameter estimation problem, e.g. least squares, has a local (global) minimum at an isolated point (NGUYEN and WOOD, 1982). The model identifiability can be analyzed from structural and practical points of view. The first one assesses if the functional form of the model (model structure) permits the determination of a unique parameter set from noise-free measurements whereas the second evaluates if the quality (e.g., measurement noise) and quantity (statistical degrees of freedom e.g.,

few measured states in a bio/chemical reactor) of the available measurements allow such a determination in practice (BELLMAN; ÅSTRÖM, 1970; RAUE et al., 2009).

The lack of structural identifiability implies lack of practical identifiability, but the converse is not true (MIAO et al., 2011), since structurally identifiable models might not be identifiable in practice due to the limitations imposed by the quality and quantity of the available measurements and by the numerical difficulty to find the local minimum.

Even if a model is structurally identifiable, model predictions can be extremely insensitive to some individual parameters and their combination. One of the main consequences of this is the ill-conditioning of the Hessian matrix in the optimization problem used to find the estimate. The ill-conditioning can make the solution of the optimization problem impossible to obtain (MCLEAN; MCAULEY, 2012).

However, even if the solution could be calculated accurately (in a numerical sense, i.e., if the computational precision could be increased adequately in order to obtain precise results in spite of severe ill-conditioning) the solution is contaminated by overfitting. As a consequence, the regression coefficient vector estimated by the least squares is expected to be far from the real parameter vector, and negligible changes in data can cause the least squares solution coefficients to assume very large absolute values and even to reverse signs (MARQUARDT, 1970).

In order to tackle the practical identifiability problem, two approaches can be conceived, simply stated as follows: obtaining more experimental information by generating more data points spanning different operating conditions or modifying the model estimation procedure, and applying mathematical strategies without neither adding new experimental data nor modifying the experimental procedure. The first approach tends to be costly, time consuming and sometimes physically infeasible, therefore a great deal of effort has been devoted to find methods to tackle the practical identifiability problem using the least amount of experimental data.

An approach to successfully reduce uncertainty in parameters can be obtained by providing a priori information about the physical process, model parameters or the

estimator. This information can be used to modify the model structure (e.g. model reduction, reparameterization) or to identify a subset of identifiable parameters (for instance, via sensitivity analysis) (MIAO et al., 2011).

Model reduction methods aim to reduce the model complexity using simplifying assumptions to decrease the number of equations, and consequently, the number of parameters that should be estimated (KEESMAN; SPANJERS; STRATEN, 1998; NIKEREL et al., 2009; TJÄRNSTRÖM; LJUNG, 2002). It can be shown that this approach can be equivalent to introducing false a priori information, but it is a common practice (LE ROUX, 1995). A consequence of using model simplifications is that the reduced model might not represent a wide range of conditions as the original one would.

In the reparameterization approach, the original model is rearranged grouping some parameters in order to reduce its number. It is said that this approach, as well as the model reduction, requires expertise to obtain a suitable transformation (BIEGLER; DAMIANO; BLAU, 1986; SURISETTY et al., 2010). However, this problem has major analogies with the problem of finding what vectors to select as a basis in a rank deficient linear algebra problem.

Benzvi (2008) proposed a reparameterization method for unidentifiable models via differential geometry, in which the reparameterization is implemented by developing a transformation that divides the parameter space into an estimable and an inestimable part. The estimable part of the parameter space is chosen based on a priori information about the system. This method does not require sensitivity calculations and is applicable over a wide variety of experimental conditions.

Sensitivity-based methods tackle the identifiability problem by determining the influence of the model parameters in the model outputs. In this way, it is possible to select which parameters should be fitted from the available information. These sensitivities can be classified as global and local; the former serve to quantify the parameter influence over the whole search space, whereas local sensitivities show parametric influence locally (CHU; HUANG; HAHN, 2011; HAAKER; VERHEIJEN, 2004). The main drawback using local sensitivities is that they may change from

point to point in the search space, therefore there is no certitude about the real importance of a parameter in the model. This issue becomes critical when sensitivities are the only criterion to decide which parameter subset should be adjusted by the available information. On the other hand, global sensitivities provide an unambiguous picture of the importance of a parameter in the model, at the expense of a higher computational cost, thus, global sensitivities are employed to study the general behavior of mathematical models rather than to determine a specific solution (SOBOL, 2001), which is not relevant in the present work.

Miao and coworkers (2011) reported four typical local-sensitivity-based methods: correlation method, principal component analysis (PCA) method, eigenvalue method and orthogonal method. They point out that the last two methods outperform the first two, because they are better designed to evaluate and compare the influence of the parameter values in the system outputs (QUAISER; MÖNNIGMANN, 2009).

A simple and useful eigenvalue-based method is the rotational discrimination algorithm (FARISS; LAW, 1979). This method performs a decomposition of the search space, such that it projects the least-squares direction onto a reduced space, where the objective function decreases the most. The issue of near-singular Hessian matrix, typical of unidentifiable systems, is addressed by spectral decomposition. Thus, the search direction restricted to a principal-component projection helps to reduce model overfitting, compared to an unbiased parameter estimator.

The combination between orthogonality and eigenvalue analyses gives rise to a family of methods that automatically adjust a subset of model parameters, while keeping the others at arbitrary nominal values. The challenge in this approach is to choose a parameter subset to fit the model, since the available data must be used to adjust the most relevant parameters. The objective of these methods is to determine how many and which parameters should be chosen to compose the subset of adjustable parameters.

Estimation methods based on automatic selection of parameters have been an intensive research field. Initially, Weijers and Vanrolleghem (1997) suggested a method to evaluate all possible permutations of model parameters, using the

determinant and condition number of the Fisher Information Matrix (FIM) to choose the best parameter subset to fit the model. Li and coworkers (2004) presented a parameter ranking methodology based on eigenvalue and orthogonality criteria.This algorithm starts with a PCA of FIM to find the most sensitive parameters, then, it continues choosing the parameters with lower linearity index in relation to the parameters already chosen (using an orthogonality analysis), until completing the parameter subset to adjust the model. The number of elements in this subset was heuristically selected. Later, Lund and Foss (2008) proposed a method to determine the ideal number of elements in the parameter subset employing variance contribution analysis. Secchi and coworkers (2006), on the other hand, improved the algorithm created by Li et al. (2004) employing predictability degradation and parameter correlation indexes, that gave rise to an algorithm for automatic selection of the parameter subset used to adjust the model.

In this work, the performance of four methods representing different parameter estimation approaches (Rotational discrimination, RD (FARISS; LAW, 1979), Automatic parameter selection, APS (SECCHI et al., 2006), reparameterization via differential geometry, RDG (BEN-ZVI, 2008) and the classic nonlinear least squares, LSq) are assessed in terms of quality of the parameters obtained (understood as the prediction capacity of the model on a validation set), robustness and speed, using a Monte Carlo (MC) strategy. The outcome of this study is useful to evaluate the suitability of these methods to handle unidentifiable models, commonly encountered in real time optimization problems and in online state identification, where parameters are constantly updated from limited and noisy measurements.

The present Chapter is ordered as follows: the selected estimation methods are described in Section 3.1, Section 3.2 discusses the local parametric sensitivity method, Section 3.3 and 3.4 are devoted to explain the case studies. The main findings are presented and discussed in Sections 3.5 and 3.6, respectively. Final considerations and conclusions drawn from this study are given in Section 3.7.

3.1. Practical identifiability improvement approaches

This section is aimed to present fundamental aspects of the methods employed in this work to improve practical identifiability. An in depth treatment of each method can be found in the original works.

3.1.1. Reparameterization via differential geometry (RDG)

Ben-zvi's method (BEN-ZVI, 2008) is used for reparameterizing non-linear systems by identifying *a priori* process quantities that have strong impact on model predictions. These process quantities will be accurately estimated even if specific model parameters are not.

The pseudo-outputs are used to partition the parameter space Φ, into estimable ϕ^+, and inestimable ϕ^-, subspaces. The parameters belonging to the estimable subspace are likely to be estimated from available measurements, while parameters in the inestimable subspace are not. Optimizing in the ϕ^+ coordinates has the following properties (BEN-ZVI, 2008): i) the parameters ϕ^+ are estimable, ii) the parameters ϕ^- are inestimable and iii) parameters ϕ^+ and ϕ^- are independent. This condition is given by the orthogonality criterion $\left\langle d\phi_j^+, d\phi_i^- \right\rangle = 0$, where $\langle . \rangle$ denotes the scalar product between the derivatives of the j^{th} pseudo output of the estimable ($d\phi_j^+$) and the i^{th} pseudo output of the inestimable subspaces ($d\phi_i^-$). Pseudo output derivatives are calculated from the partial derivatives with respect to the parameters θ, i.e. $d\phi_j^+ = \frac{\partial \phi_j^+}{\partial \theta}$ and $d\phi_i^- = \frac{\partial \phi_i^-}{\partial \theta}$.

The nonlinear transformation employed by Ben-zvi to reparameterize the original model is insensitive to the choice of experimental conditions and parameter estimates. Furthermore, it does not require the cause or mechanisms of inestimability to be identified. The main features of the method are summarized in the following algorithm (see Figure 3.1).

Figure 3.1 - Main steps of the RDG method.

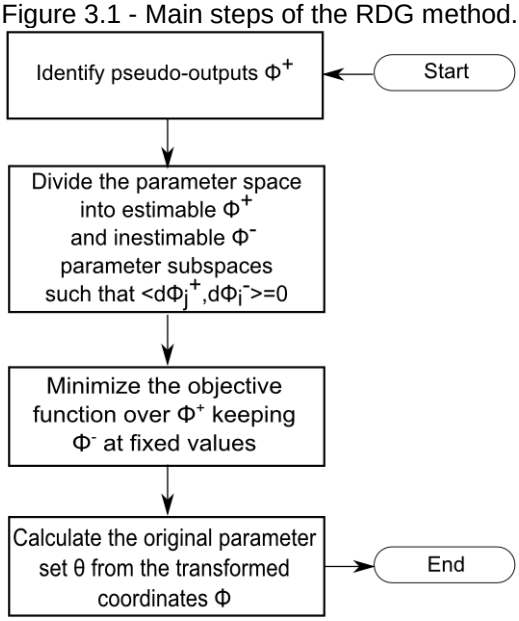

Ben-zvi's Algorithm

1. Given a model with a parameter set θ.
2. Identify pseudo-outputs (ϕ^+): Pseudo-outputs are process quantities (non-linear combinations of parameters and/or states) that have strong impact on model predictions. Pseudo-outputs will be, in the general case, functions of both parameters and state variables; in this case pseudo-outputs should be evaluated using nominal values of the states.
3. Use pseudo-outputs and coordinate transformation to partition the parameter space into an estimable, ϕ^+, and inestimable, ϕ^-, subspace so that the space $\Phi = \left[\phi^+, \phi^-\right]^T$ is a local diffeomorphism and $\left\langle d\phi_j^+, d\phi_i^- \right\rangle = 0$. This condition implies that optimizing over all parameters is approximately equivalent to optimizing over ϕ^+ while holding ϕ^- at fixed values.
4. Optimize over ϕ^+ while holding ϕ^- at fixed values. The optimization problem in the ϕ^+ coordinates is well posed, computationally efficient, and the estimates obtained for ϕ^+ are independent of the fixed nominal values used for ϕ^-.
5. Obtain the original parameter set θ from the mapping Φ.

It is worth noting that there is not a unique way to select the pseudo-outputs because it is an election done by the user, based on *a priori* knowledge of the specific case. Further details are provided in Appendix C.

3.1.2. Rotational discrimination (RD) method

This method uses the spectral decomposition of the search space to deal with the near singularity of the Hessian matrix. It projects the least-squares direction onto a reduced space where the objective function decreases the most.

Given the optimization problem of the parameter estimation as:

$$\begin{aligned} &\min_{\theta} f(\theta) = \sum_{j=1}^{m} r_j(\theta)\ v_j^{-1} r_j(\theta) \\ &s.t.: \quad l \le \theta \le u \end{aligned} \tag{3.1}$$

where $\theta \in \mathbb{R}^n$ is the vector of parameters, $r(\theta) = [r_1(\theta), r_2(\theta), ..., r_m(\theta)]^T$ is the residual vector. In this specific case, it is the difference between the model prediction and the measured value, $r_j(\theta) = (\hat{y}_j(\theta) - y_j)_{j=1,2,...,m}$. v_j is the diagonal matrix of measurement variance, l and u are the parameter lower and upper bounds, respectively.

The derivatives of $f(\theta)$, $\nabla f(\theta)$ and $\nabla^2 f(\theta)$, can be written as function sensitivities of r, $S(\theta) = \left[\frac{\partial r_j}{\partial \theta_i}\right]_{\substack{j=1,2,...,m \\ i=1,2,...,n}}$, as stated by eq.(3.2) and (3.3).

$$\nabla f(\theta) = g(\theta) = 2\sum_{j=1}^{m} r_j(\theta)\ v_j^{-1} \nabla r_j(\theta) = 2S(\theta)^T (V^{-1}) r(\theta) \ \in \mathbb{R}^n \tag{3.2}$$

$$\begin{aligned} \nabla^2 f(\theta) = H(\theta) &= 2\sum_{j=1}^{m} \nabla r_j(\theta)\ v_j^{-1}\ \nabla r_j(\theta)^T + 2\sum_{j=1}^{m} r_j(\theta)\ v_j^{-1}\ \nabla^2 r_j(\theta) \\ &= 2S(\theta)^T V^{-1} S(\theta) \quad + 2\sum_{j=1}^{m} r_j(\theta)\ v_j^{-1}\ \nabla^2 r_j(\theta) \end{aligned} \quad \in \mathbb{R}^{n\,X\,n} \tag{3.3}$$

Since the first term of the last equation is often dominant, the second may be neglected, either because of near-linearity of the model close to the solution or because of the residuals are small (NOCEDAL; WRIGHT, 1999). As a result, the second derivative of $f(\theta)$ is simply given by:

$$\nabla^2 f(\theta) = H(\theta) = 2\ S(\theta)^T V^{-1} S(\theta) \quad \in \mathbb{R}^{n\,X\,n} \tag{3.4}$$

Several authors (BARD; LAPIDUS, 1970; BARD, 1970, 1974; MARQUARDT, 1963) suggested a Hessian matrix reconditioning, H^{rec}, to avoid numerical errors in the matrix decomposition and inversion steps,

$$H^{rec} = P^{-1} H P^{-1} \tag{3.5}$$

where P is a diagonal matrix with elements defined by:

$$p_{ii} \begin{cases} \sqrt{h_{ii}} & \text{if} \quad h_{ii} \geq \varepsilon_{rec} \\ \sqrt{\varepsilon_{rec}} & \text{otherwise} \end{cases} \qquad \varepsilon_{rec} = 1e-3 \tag{3.6}$$

In the next stage, the reconditioned Hessian matrix is decomposed in eigenvalues and eigenvectors to perform a principal component analysis, which excludes eigenvalues smaller than a defined tolerance ε_{cp} (VAJDA et al., 1989), obtaining the reduced eigenvalues matrix, Λ_{red}, and their associated eigenvectors R_{red}.

$$R \Lambda R^T = H^{rec} \tag{3.7}$$

$$\lambda_{red_{ii}} \begin{cases} \lambda_{ii} & if \quad \lambda_{ii} \geq \varepsilon_{cp} \\ 0 & otherwise \end{cases} \qquad \varepsilon_{cp} = \max[1e-6,\ 1000^{-0.5} \max_i(\lambda_{ii})] \tag{3.8}$$

where λ_{ii} are the eigenvalues of Λ and $\lambda_{red_{ii}}$ the eigenvalues of the reduced eigenvalues matrix, Λ_{red}. Then, the inverse matrix of the reduced Hessian is given by:

$$H_{red}^{-1} = P^{-1} R_{red} \Lambda_{red}{}^{-1} R_{red}{}^{T} P^{-1} \quad (3.9)$$

With this information, the search direction for minimization of the objective function can be found by the Gauss-Newton method (NOCEDAL; WRIGHT, 1999):

$$s_k = -P^{-1} R_{red} \Lambda_{red}^{-1} R_{red}^{T} P^{-1} . g(\theta) \quad (3.10)$$

Then, this direction is used to obtain a new parameter set, θ^{k+1},

$$\theta^{k+1} = \theta + k_{opt} . s_k \quad (3.11)$$

where k_{opt}, the optimum step length, is determined by line search procedure using two different criteria. The first one takes into account the parameters bounds through Cauchy point computation at the variables limits, clipping the maximum step size ($k_{\max}$) or reducing the parameter space, in case of active set. The second one caries out a quadratic interpolation algorithm, respecting $k_{\max}$, until the strong Wolfe conditions are satisfied (NOCEDAL; WRIGHT, 1999).

A block diagram describing the main procedures of the rotational discrimination method is shown in Figure 3.2.

Figure 3.2 - Rotational discrimination algorithm.

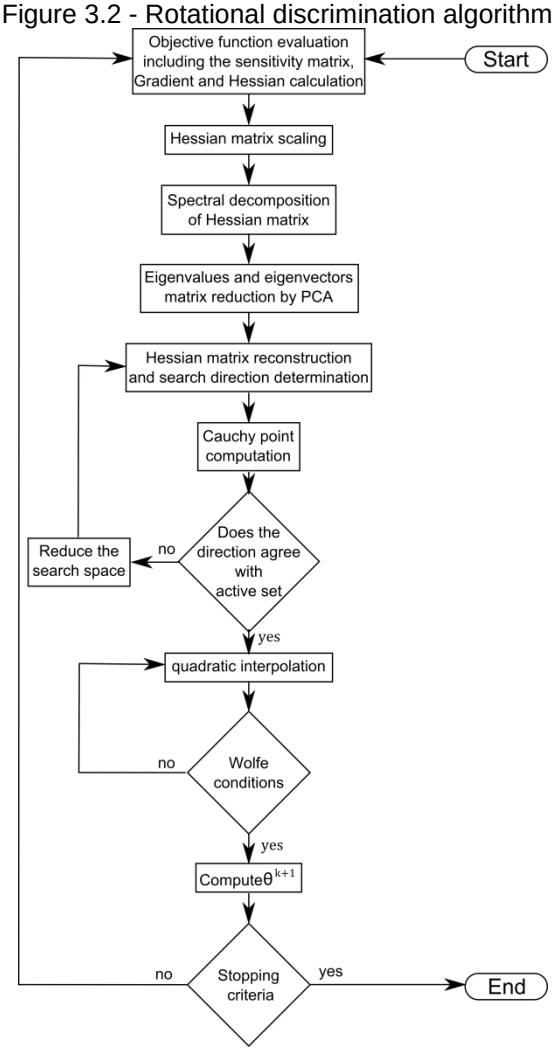

3.1.3. Automatic selection and parameter estimation (APS)

The main objective of the APS method is to chose a subset of parameters to fit the process model (SECCHI et al., 2006), reducing the probability of model overfit. First of all, the method starts by computing the approximate Fischer Information Matrix (FIM) from the sensitivity and normalized variance of outputs measurement.

$$FIM = \frac{\partial r}{\partial \theta}^{T} (V_y)^{-1} \frac{\partial r}{\partial \theta} \quad \in \mathbb{R}^{n\,X\,n} \tag{3.12}$$

where V_y is the diagonal of the matrix of measurement variances, obtained from repetitions of physical experiments or, in the case of computer experiments, is known

a priori. The overall parameter effect index, *E*, is calculated from the spectral decomposition of the FIM (LI; HENSON; KURTZ, 2004):

$$E = \frac{|V_k D_k|}{trace(D_k)} \tag{3.13}$$

where V_k and D_k denote the eigenvector and eigenvalue matrices of the k largest eigenvalues of FIM (where, $k = \min\{n, m\}$ minimum value between the number of parameters , n , or the number of measurements, m).

The highest ranked parameter, given by E , is selected to make part of the estimated parameters set, Ω_q , which is used to compute the reduced Fisher information matrix, F_q , and then, the correlation coefficients, $\overline{\rho}_y$ and $\overline{\rho}_\theta$, from the covariance matrices of the predicted outputs and parameters, V_y and V_θ , and finally, the condition number κ .

$$F_q = \frac{\partial r}{\partial \theta_{\Omega q}}^T (V)^{-1} \frac{\partial r}{\partial \theta_{\Omega q}} \quad \in \mathbb{R}^{q X q} \tag{3.14}$$

$$V_\theta = F_q^{-1} \quad \text{and} \quad V_{\hat{y}} = \frac{\partial r}{\partial \theta_{\Omega q}}^T V_\theta \frac{\partial r}{\partial \theta_{\Omega q}} \tag{3.15}$$

$$\rho_\theta = V_\theta \otimes^{-1} \sqrt{V_\theta V_\theta^T} \quad , \quad \overline{\rho}_\theta = \left\| \rho_\theta - I_n \right\|_\infty \tag{3.16}$$

$$\rho_y = V_{\hat{y}} \otimes^{-1} \sqrt{V_{\hat{y}} V_{\hat{y}}^T} \quad , \quad \overline{\rho}_{\hat{y}} = \left\| \rho_{\hat{y}} - I_m \right\|_\infty \tag{3.17}$$

$$\kappa = \left\| F_q \right\| . \left\| V_\theta \right\| \tag{3.18}$$

where $\otimes^{-1}$ denotes element-by-element division and $\| . \|_\infty$ is the largest element in a matrix. Then, the model is adjusted using Ω_q and keeping the other parameters at

their nominal values; after that, the predictability degradation index, τ_q , and parameter correlation degradation index, η_q , are calculated to be used as stopping criteria.

$$\xi = \left[\hat{y}(\theta_{\Omega q}) - y_m \right] \otimes^{-1} y_m \tag{3.19}$$

$$\tau_q = \overline{\rho}_y + \left\| \xi \right\|_\infty \tag{3.20}$$

$$\eta_q = \overline{\rho}_\theta + \delta_{1,q} \tag{3.21}$$

where y_m corresponds to the measured outputs and $\delta_{1,q}$ is the Kronecker delta (necessary to avoid premature termination in the first iteration).

The next step is evaluating the stopping criteria. A useful criterion, suggested by Secchi and coworkers (2006), is to end the parameter estimation routine if:

- $\{ [\tau_{q-1} < \tau_q]$ **and** $[(\tau_{q-1} < 1)$ **or** $(\eta_{q-1} < \rho_{\max}$ **and** $\eta_q > \rho_{\max})] \}$, **or**
- The inverse of the condition number is smaller than ε ($\kappa^{-1} < \varepsilon$).

where $\rho_{\max}$ denotes the maximum allowed parameter correlation (e.g., 0.95) and ε the minimal condition number of FIM (e.g., 10^{-16}).

If the stop criterion is not satisfied, the correlation index between the selected and not selected parameters is evaluated, and the not selected parameter with lowest correlation is added to the estimable parameters set Ω_q, closing the algorithm loop. A block diagram describing the algorithm APS is shown in Figure 3.3.

Figure 3.3 - APS algorithm.

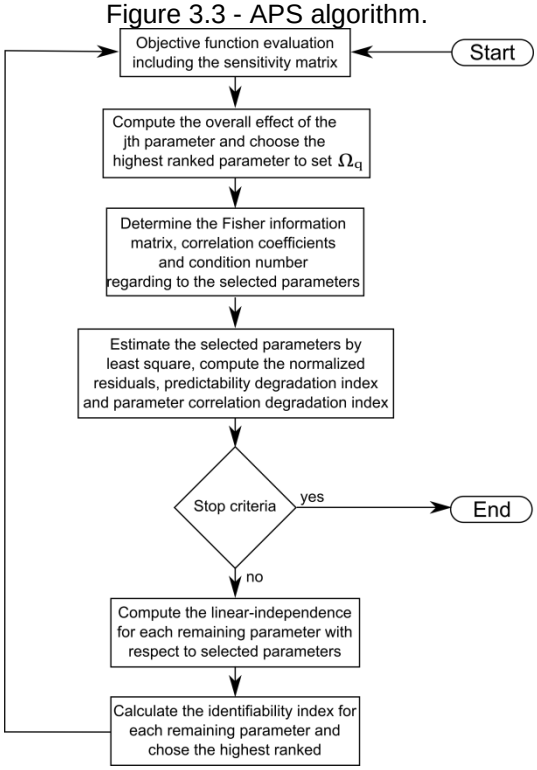

3.1.4. Least squares (LSq) method

A simple (unweighted) nonlinear least-squares function, using trust-region-reflective algorithm as minimization method (Matlab, R2009a), is used to estimate all parameters involved in the model. This estimation method is implemented in Matlab in the function *lsqnonlin.* This method does not take into account the identifiability issue at all, and serves to contrast the solutions obtained by the other methods.

3.2. Local Parametric sensitivity

RD and APS methods use local parametric sensitivity to analyze the parameter influence on the output variables, to estimate the gradient of the objective function and to approximate the hessian matrix (e.g., using Gauss-Newton approach). There are three major numerical methods for calculating local sensitivities (SALTELLI; CHAN; SCOTT, 2000): finite-difference approximation, direct method and Green's function method. The second method is used in this work to calculate the local

parametric sensitivities of the system because it tends to be more accurate than finite difference approximation and it is simpler than the Green's function method, without compromising accuracy and speed.

The direct method computes the sensitivity matrix evaluating the ODE or DAE sensitivity problem created by the analytical differentiation of the model with respect to its parameters,

$$M\frac{d}{dt}\left(\frac{\partial y}{\partial \theta}\right)=\frac{\partial F}{\partial \theta}+\frac{\partial F}{\partial y}\frac{\partial y}{\partial \theta} \tag{3.22}$$

where F denotes the right side of the system equation and *M* is a diagonal matrix partitioned as $[I/O]^T$ (I for the differential equations and O for the algebraic equations).

3.3. Case Study: Three-phase batch reactor

The parameter estimation approaches presented previously are compared using the case study proposed by Ben-zvi (2008), where it is applied the RDG method to estimate the parameters of a three-phase industrial batch reactor. The chemical transformations within the system follow the scheme:

$$\begin{aligned} A_s &\rightarrow A_l \quad (R_{MT}) \\ A_l + B &\rightarrow C + D \quad (r_1) \\ B + C &\rightarrow E + D \quad (r_2) \\ B + E &\rightarrow F + D \quad (r_3) \\ B + F &\rightarrow P + D \quad (r_4) \end{aligned} \tag{3.23}$$

The first expression in this scheme corresponds to the dissolution of the solid *A*, the other ones are reaction steps involved in the production of the product of interest *P*. The reactions, carried out under laboratory conditions, allow fast removal of component *D*, therefore the reverse reactions involving *D* can be neglected.

The dynamics of the isothermal reactor, neglecting reverse reactions, is given by the material (component) balances:

$$\begin{aligned}
\frac{dn_{A_s}}{dt} &= -R_{MT} \\
\frac{dn_{A_l}}{dt} &= R_{MT} - r_1 V \\
\frac{dn_B}{dt} &= (-r_1 - r_2 - r_3 - r_4)V \\
\frac{dn_C}{dt} &= (r_1 - r_2)V \\
\frac{dn_E}{dt} &= (r_2 - r_3)V \\
\frac{dn_F}{dt} &= (r_3 - r_4)V \\
\frac{dn_P}{dt} &= r_4 V
\end{aligned} \tag{3.24}$$

The mass transfer, R_{MT}, and reaction rates, r_i's, follow the expressions:

$$\begin{aligned}
R_{MT} &= 3(n_{A_s}^0 MW_A)^{1/3}(n_{A_s} MW_A)^{2/3}\frac{k_{MT}}{\rho_A R_{Po} V}(n_{A_l}^{eq} - n_{A_l}) \\
r_1 &= k_1 \frac{n_B n_{A_l}}{V^2} \\
r_2 &= k_2 \frac{n_B n_C}{V^2} \\
r_3 &= k_3 \frac{n_B n_E}{V^2} \\
r_4 &= k_4 \frac{n_B n_F}{V^2}
\end{aligned} \tag{3.25}$$

where n_{A_s}, n_{A_l}, n_B, n_C, n_E, n_F and n_P are the mole numbers of the components in the reactor, $n_{A_s}^0$ is the initial mole number of the solid A. Parameters MW_A, ρ_A, R_{Po}, $n_{A_l}^{eq}$ and V are assumed to be known, while k_1, k_2, k_3, k_4, k_{MT} are unknown and shall be estimated. A description of these parameters is given in Table 3.1.

Table 3.1 – Values of the parameters for the three-phase reactor model

Parameter	Description	Value	Unit
MW_A	Molecular weight of *A*	1.0	kg/mol
ρ_A	Density of A_s	500	kg/m^3
R_{Po}	Initial A_s radius	0.001	m
$n_{A_l}^{eq}$	Equilibrium solubility of A	0.1	mol
V	Reactor volume	1.0	m^3
k_{MT}	Solid-liquid mass transfer coefficient	0.10	m/s
k_1	Rate constant	1.0	m^3/mol s
k_2	Rate constant	1.5	m^3/mol s
k_3	Rate constant	0.50	m^3/mol s
k_4	Rate constant	1.2	m^3/mol s

The comparative experiment is designed as Monte Carlo samples. First, the model previously described is simulated using the original value of the parameters in the calibration initial conditions (see Table 3.2). Discrete samples of two state variables, the concentration of species *B* and *P* (measured variables), are taken in triplicate, between 0 and 25 seconds (one sample each five seconds), constituting a three-output data set used to fit the reactor model.

Table 3.2 – Initial conditions for the computational experiments

State variables	Calibration	Validation
n_{A_S}	0.50	0.20
n_{Al}	0	0
n_B	1	1
n_C	0	0
n_E	0	0
n_F	0	0
n_P	0	0

3.3.1. Case study – Experimental Design

A Monte Carlo methodology is employed to generate the statistical information required to assess the quality of each approach. In this analysis, each parameter estimation method is run several times employing random initial values (guesses) for the optimization step and randomly drawn measurement noise for the experimental

data. This analysis presents advantages over the common practice in which parameter estimation methods are evaluated using few data sets (BIEGLER et al., 1986; SECCHI et al., 2006; SURISETTY et al., 2010) since it is possible to investigate the behavior of the estimation methods under a wide range of conditions, which sheds light on their overall performances (BARD, 1974).

The algorithm loop starts adding a zero mean noise with normal distribution and standard deviation of 0.05 and 0.0167 for *B* and *P* concentrations, respectively (BEN-ZVI, 2008). A random initial guess for the parameters is provided for all the identification methods, following a uniform distribution between their lower and upper bounds (Table 3.3). The idea is to represent the arbitrary choice by a random variable with a uniform distribution, since there is no *a priori* information about these values. At each iteration, the noise added to the output sets and the parameter guesses are chosen randomly. This procedure is repeated 1000 times.

The computer simulation comprises two stages. In the first (model calibration) the model parameters are estimated by each method, using the unweigthed least squares objective function that combines the data set corresponding to the calibration conditions shown in Table 3.2. In the second stage (model validation) the parameters obtained in the calibration step are used to predict the reactor behavior under new conditions (Validation, Table 3.2).

Table 3.3 – Upper and lower bounds of the guess of model parameters.

Parameters	Original. value	Guess	
		Lower bound	Upper bound
k_1	1.00	0.5	1.5
k_2	1.50	0.75	2
k_3	0.50	0.25	1
k_4	1.20	0.6	1.8
k_{MT}	0.10	0.06	0.15

Table 3.4 - Upper and lower bounds of the guess of the nominal values for the RDG method.

Nominal State variables	Lower bound	Upper bound
V	0.5	5.0
n_{Al}	0.1	1.0
n_B	0.1	1.0
n_C	0.1	1.0
n_E	0.1	1.0
n_F	0.1	1.0

3.4. Case study 2: The Dow chemical identification problem

The parameter estimation problem formulated by the Dow Chemical Co. is an industrial problem presented to 165 research groups after the FOCAPO (Foundations of Computer-Aided Process Design) congress in 1980. Eleven of those groups accepted the proposed challenge, but only five of them submitted acceptable solutions. The problem consists of an isothermal batch reactor, which produces the desired product AB, from the reactants HA and BM. The mechanism shown in Equations (3.26) and (3.27) represents the chemical process, which is catalyzed by QM, completely dissociated at the initial condition.

Slow reactions:

$$\begin{aligned} M^- + BM &\Leftarrow k_{-1}\ k_1 \Rightarrow MBM^- \\ A^- + BM &\qquad k_2 \Rightarrow ABM^- \\ M^- + AB &\Leftarrow k_{-3}\ k_3 \Rightarrow ABM^- \end{aligned} \tag{3.26}$$

Fast reactions:

$$\begin{aligned} MBMH &\Leftarrow K1 \Rightarrow MBM^- + H^+ \\ HA &\Leftarrow K2 \Rightarrow A^- + H^+ \\ HABM &\Leftarrow K3 \Rightarrow ABM^- + H^+ \end{aligned} \tag{3.27}$$

This process is modeled as a system of six differential and four algebraic equations (BIEGLER; DAMIANO; BLAU, 1986). $K1$, $K2$ and $K3$ are ionic equilibrium constants; and $k_1, k_{-1}, k_2, k_3, k_{-3}$ are temperature-dependent rate constants, modeled as reparametrized Arrhenius equation (PRITCHARD; BACON, 1978), see Appendix

D. In the original problem, a simplification is proposed to reduce the number of parameters from 13 to 9, this assumption can be represented in our parameter space as:

$$\begin{aligned} \varphi_3 &= \varphi_1 \\ \varphi_{-3} &= \varphi_{-1} - \ln(2) \\ \psi_3 &= \psi_1 \\ \psi_{-3} &= \psi_{-1} \end{aligned} \tag{3.28}$$

where φ and ψ are parameters of the reparametrized Arrhenius equation (see Appendix D). Table 3.5 shows the original parameter values used to provide the experimental data for the Monte Carlo analysis.

Table 3.5. Nominal reference parameter values for Dow Chemical parameter estimation problem.

φ_1	ψ_1	φ_{-1}	ψ_{-1}	φ_2	ψ_2	$K1$	$K2$	$K3$
0.7735	9.1375	8.2288	9.4809	1.2312	9.1694	-35.8955	-30.6519	-36.2600

To apply the parameter estimation techniques discussed in this work, the sensitivities of the outputs variables with respect to parameters are calculated by the direct method eq.(3.22). The whole equation system of this problem, including mass balance and sensitivity analysis, is a stiff DAE system with 60 differential and 40 algebraic equations, solved using NDF (Numerical Differentiation Formulas) implemented in the Matlab® solver ode15s.

3.4.1. Case study 2 - Experimental design

The same Monte Carlo methodology proposed for the first case study is applied to evaluate the performance of three parameter estimation methodologies, viz. LSq, RD and APS. The RDG method is not evaluated in this case study due to the difficulty in generating an analytic nonlinear transformation to obtain the pseudo-outputs. This drawback has been recognized by Ben-zvi, (2008) as a current limitation for the application of his method.

Experiments are generated using the nominal parameter values in Table 3.5 for three different initial conditions and temperatures, indicated in Table 3.6. A normal distribution error with zero mean and standard deviation, equal to the maximum between 1% of the measured value or 0.0167, is added to the measured state variables (HA, BM, $HABM$ and AB), at instants corresponding to the time vector presented in Appendix D. The initial parameter guesses are randomly drawn between the lower and upper bounds, listed in Table 3.7 following a uniform distribution. This procedure is repeated 900 times.

Table 3.6 - Initial conditions for the computational experiments for case study 2.

	Calibration set			Validation set
Concentration*	40°C	67°C	100°C	120°C
$[HA]$ (gmol/kg)	1.7066	1.6497	1.5608	1.5608
$[BM]$ (gmol/kg)	8.3200	8.2262	8.3546	8.3546
$[HABM]$ (gmol/kg)	0.0000	0.0104	0.0082	0.0082
$[AB]$ (gmol/kg)	0.0000	0.0017	0.0086	0.0086

*The initial condition for the other variables are given in the Appendix B

Table 3.7 - Upper and Lower bounds for the parameters initial guess and optimization step for case study 2

	φ_1	ψ_1	φ_{-1}	ψ_{-1}	φ_2	ψ_2	$K1$	$K2$	$K3$
Upper*	1.3337	10.1383	7.2412	10.1383	1.3336	10.1381	-39.1439	-25.3284	-39.1439
Lower*	1.2125	9.2168	6.5831	9.2168	1.2125	9.2168	-43.0467	-27.8599	-43.0529
Upper**	1.5470	18.2750	16.4577	18.9618	2.4624	18.3388	-17.9478	-15.3259	-18.1300
Lower**	0.3867	4.5687	4.1144	4.7404	0.6156	4.5847	-71.7910	-61.3037	-72.5201

* For the initial guess
** In the estimation

3.5. Results

3.5.1. Case study 1

The stopping criteria for the algorithms presented are that the relative change of the objective function between iterations k and $k+1$ is less or equal to a predetermined tolerance of 10^{-8} or that the number of iterations exceeds the maximum allowed number (1500). The tolerance used in the Hessian reconditioning step of the RD method is set to $\varepsilon_{cp} = 3.162 \times 10^{-2}$, while the maximum allowed parameter correlation for the APS method is set at $\rho_{\max} = 0.99$.

3.5.1.1. Calibration set

The objective function frequency distribution achieved by each method is presented in Figure 3.4. It can be appreciated that LSq, RD and APS reach similar final model fits, however, there is a significant difference among the variance of RD method in comparison to that of the other two ones. The RDG method shows the poorest results both in the mode and variance of the objective function distribution.

Figure 3.4 – Objective function values obtained for the calibration set

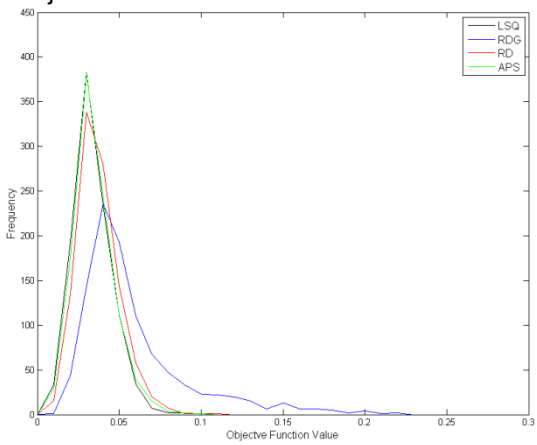

The frequency distributions of the estimated parameters by APS and LSq methods (Figure 3.5) are similar. The most interesting feature is that both exhibit a bimodal behavior for parameters k_1, k_2, k_3 and k_4 (possibly related to parameter inflation), with the modes located near their upper and lower bounds. On the other hand, the parameter distributions obtained by the RD and RDG methods are unimodal, with modes close to the true parameters.

Figure 3.5 – Frequency distribution of the estimated parameters by each method and true parameter values (vertical line). Figure A, B, C, D and E represents the parameters k1, k2, k3, k4 and kMT, respectively.

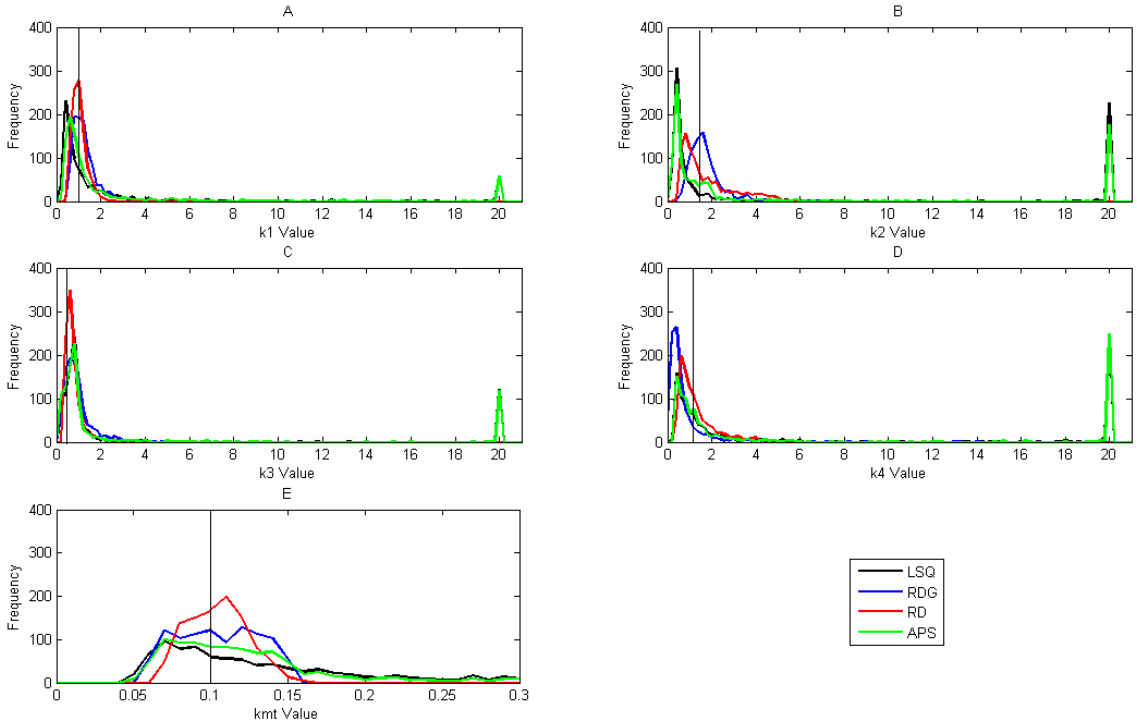

A comparison of the mean values of the estimated parameters (Table 3.8) shows that the RD method presents four out of five parameters (k_1, k_3, k_4, k_{MT}) close to the nominal values while the RDG just one, k_2, but with a small difference from the mean presented by the RD method.

Table 3.8 – Mean values of the parameters obtained in the MC analysis.

Method	Parameters' mean								
	k_1		k_2		k_3		k_4		k_{MT}
	*Peak 1**	*Peak 2**	*Peak 1*	*Peak 2*	*Peak 1*	*Peak 2*	*Peak 1*	*Peak 2*	*Peak 1*
nominal	1.0000		1.5000		0.5000		1.2000		0.1000
LSQ	1.3335	18.8162	1.0309	19.5102	0.8557	19.6007	1.3895	19.5276	0.2009
RDG	1.3031	--------	1.7128	--------	0.9936	--------	0.7047	--------	0.1044
RD	1.0396	--------	1.7551	--------	0.7406	--------	1.3496	--------	0.1041
APS	1.3313	19.0540	1.1137	19.5905	0.9464	19.8286	1.3579	19.6623	0.1521

***Peak 1**- values between 0 and 10; **Peak 2** - values between 10 and 20

The variance of the estimated parameters (Table 3.9) shows that RDG and RD methods present the smallest variances for the 5 parameters compared to the other two methods.

Table 3.9 – Variance of the parameters obtained in the MC analysis

Method	Parameters' variance								
	k_1		k_2		k_3		k_4		k_{MT}
	*Peak 1**	*Peak2**	*Peak 1*	*Peak 2*	*Peak 1*	*Peak 2*	*Peak 1*	*Peak 2*	*Peak 1*
LSQ	2.2392	7.3902	2.0638	3.5477	0.6437	2.7442	2.0141	2.7826	0.1686
RDG	0.3673	--------	0.7191	--------	0.5660	--------	0.8168	--------	0.0007
RD	0.1103	--------	1.3893	--------	0.1617	--------	0.8183	--------	0.0004
APS	1.9971	6.4786	1.9391	3.0219	1.1909	1.0909	1.9280	2.2659	0.0470

*__Peak 1__- values between 0 and 10; __Peak 2__ - values between 10 and 20

The fitted parameters in the APS method varies between 2 and 5 (two parameters are adjusted in 2.10% of the runs, three in 21.20%, four in 14.00% and five in 62.70%). The ranking criterion used by the APS method shows the following order (from most to least important): k_3, k_4, k_1, k_2 and k_{MT}. This classification is obtained from the number of times that a parameter occupies a position within the ranking presented in Table 3.10. It is worth noting that the parameter ranking obtained by the APS method shows, in most cases, that k_{MT} is the last parameter to be adjusted. This result agrees with the reparametrization performed by the RDG method, where k_{MT} belongs to the inestimable set, see (GRACIANO; MENDOZA; LE ROUX, 2014). At the same time, it can be noticed the APS method does not lead to the same parameter choice, since this election depends on the initial guess and data noise.

Table 3.10 – Parameter ranking (as percentage) according to the criteria used in the APS method.

Parameter	Ranking				
	1	2	3	4	5
k_1	01.70	37.20	53.52	01.17	05.90
k_2	00.10	01.60	23.39	71.06	09.57
k_3	50.80	27.10	03.37	14.34	00.32
k_4	42.20	33.80	18.28	05.08	00.00
k_{MT}	05.20	00.30	01.43	08.34	84.21

The four estimation methods are shown to be robust, for this specific case, since they converged for all 1000 random initial values. The average execution time of each method (run in a personal computer Intel® core™ i5-2400 CPU at 3.10 GHz, measured by the Matlab® function "tic", "toc") reveals that the RD method is the fastest (6.698 s), followed by LSq (22.374 s), RDG (31.186 s) and APS (43.143 s).

3.5.1.2. Validation set

The quality of each method is evaluated using the frequency distribution of the objective function in the validation set (Figure 3.6). This function measures the difference between the concentration profiles estimated by the validation set and the concentration profiles calculated by the true parameters (experimental data). The frequency distribution of the objective function presents a better prediction when it uses the parameter sets estimated from methods devised to address the identifiability problem (RDG, RD and APS) than from the method that adjusts all model parameters (LSq). The results obtained in the validation set present an opposite behavior compared to that obtained in the calibration set, where the LSq method achieves the lowest value (Table 3.11), illustrating the effect of overfitting in predictions.

Table 3.11 – Objective function statistics in calibration and validation sets

	Objective Function			
	Calibration		Validation	
Method	Mean	Variance	Mean	Variance
LSq	0.0333	0.0001	0.1101	0.0093
RDG	0.0588	0.0011	0.0508	0.0005
RD	0.0372	0.0002	0.0493	0.0003
APS	0.0344	0.0002	0.0825	0.0044

Figure 3.6 – Objective function values obtained for the validation set

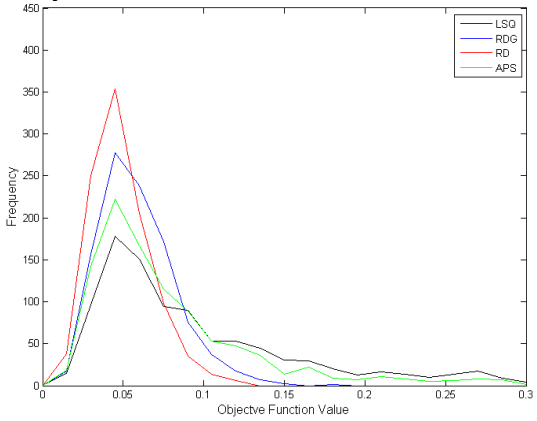

The 1000 concentration profiles of *B* and *P*, predicted by the model, using the parameter sets estimated by the different methods and the true concentration profiles are shown in Figure 3.7. The parameters estimated by the LSq method generate a model with the greatest discrepancy with respect to the real profiles. In contrast,

almost any parameter set provided by the RD algorithm can be used to adequately predict the system behavior.

The APS and RDG methods present good results for *P* and *B* profiles. Nevertheless, the predicted concentration profiles are more dispersed than those obtained by the RD method.

Figure 3.7 – Concentration profiles of B and P predicted by LSq (A), RD (B), RDG (C) and APS (D) methods. (--) True concentration profile

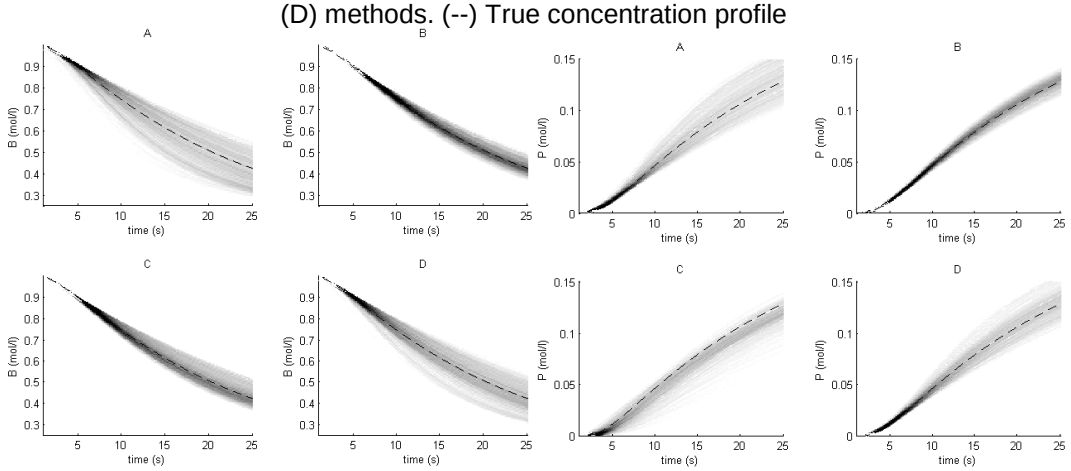

3.5.2. Case study 2

For these experiments, the relative tolerances of the optimization algorithms are again set at 10^{-8} and the maximum number of iterations at 1500. The tolerance for the RD method and the maximum allowed parameter correlation for the APS method are set at $\varepsilon_{cp} = 3.162 \times 10^{-5}$ and $\rho_{\max} = 0.98$.

3.5.2.1. Calibration set

The objective function distribution (Figure 3.8) presents three well-defined regions for the final value of the objective function: from 0 to 1.5, from 1.5 to 3 and from 58 to 63. The RD method has the best fit, reaching mostly the first region (from 0 to approximately 1.5), however, it is the method with the highest number of results in the third region (between 58 and 63). The LSq method mainly converges to the

second region (1.5 to 3), while the results obtained by the APS method are concentrated in the first and second regions, but more scattered than the two other methods.

From these numerical outcomes, it can be concluded that the LSq was unable to converge to the minimal solution. The points towards which it converges correspond to Objective Function values larger than those obtained by the RD. The fact that LSq does not present overfit is due to inherent numerical difficulties. In fact, instead of overfitting, LSq underfits the problem, as the Objective Function values are typically larger than those obtained by the RD method. The RD method is known as a biased estimator because it does not converge to the minimum. In this case the LSq performance is poor because it does not even converge to solutions as precise as those proposed by the RD.

Figure 3.8 – Objective function values obtained in second case study on calibration set, from 0 to 5 (A) and from 58 to 63 (B).

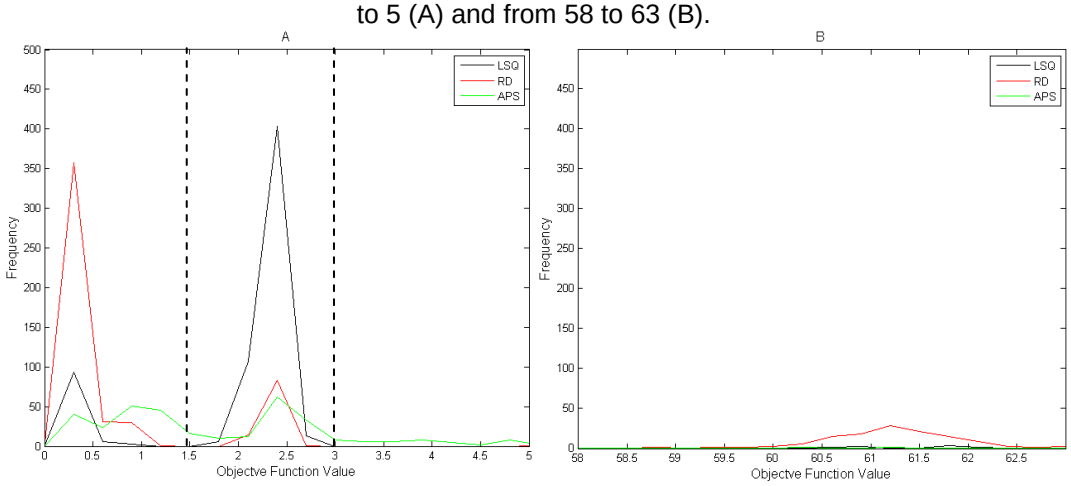

The parameter frequency distributions obtained by the estimation methods (Figure 3.9) show that parameters $K1$ and $K3$ have similar profiles for the three studied methods, which may indicate a similar influence over the output and a dependence between them, as observed by Biegler et al. (1986). Furthermore, $K1$, $K2$, $K3$ and ϕ_{-1} parameter profiles are far from the nominal values. This is particularly prominent for the last one, which shows the largest dispersion band with peaks close to the upper bound.

Figure 3.9 - Frequency distribution of the estimated parameters by each method and true parameter values (vertical line) – Case study 2.

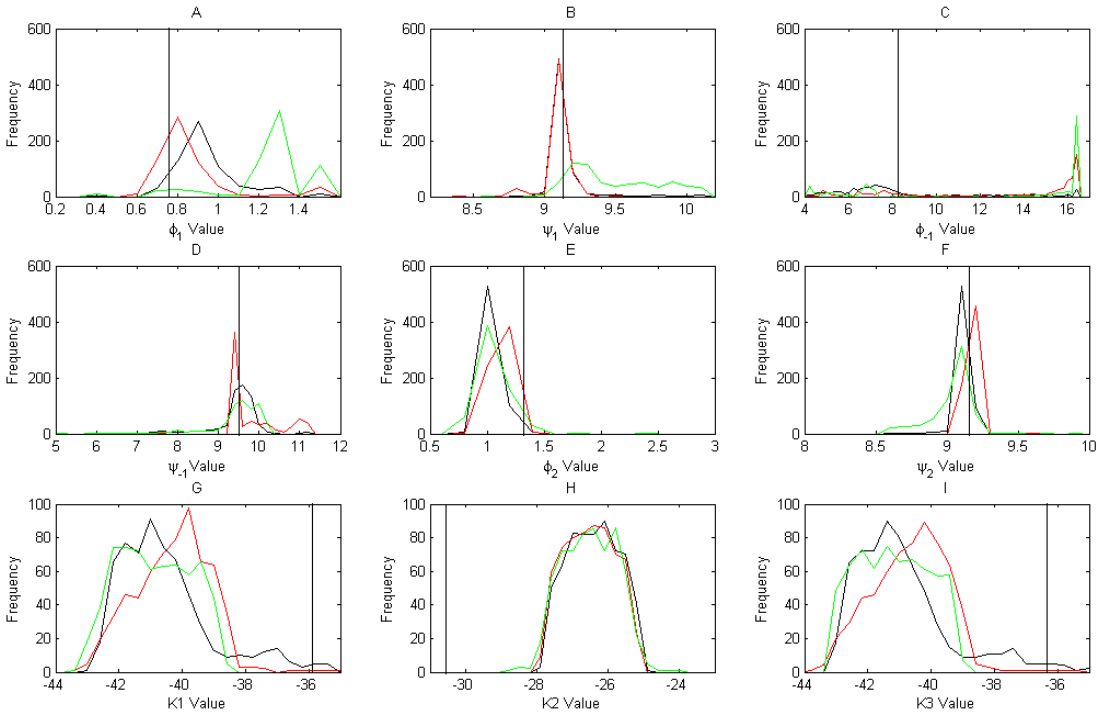

In this case study, the number of parameters adjusted by the APS methods is between 2 and 8 (2.51%, 33.91%, 2.20%, 5.97%, 1.57%, 48.04% and 5.81%, respectively). Moreover, it can be noticed from Table 3.12 that ψ_2 is the most influential parameter and $K3$ the least one. It is worth noting, as done in case study 1, that the parameter ranking in the APS method depends on the nominal values (initial guess) used for the parameters.

Table 3.12 - Parameter ranking (as percentage) according to the criteria used in the APS method – study case 2.

Ranking	φ_1	ψ_1	φ_{-1}	ψ_{-1}	φ_2	ψ_2	$K1$	$K2$	$K3$
1	0,00%	0,00%	0,31%	0,31%	5,34%	88,23%	5,81%	0,00%	0,00%
2	0,00%	1,10%	42,23%	5,18%	38,15%	7,54%	5,81%	0,00%	0,00%
3	1,61%	4,83%	28,34%	13,85%	13,69%	0,64%	12,40%	24,64%	0,00%
4	5,43%	7,65%	7,41%	12,84%	15,56%	1,73%	12,10%	37,28%	0,00%
5	4,60%	4,35%	4,35%	17,39%	13,55%	1,02%	22,51%	32,23%	0,00%
6	14,73%	8,22%	5,67%	26,91%	11,90%	1,13%	25,21%	6,23%	0,00%
7	29,15%	30,03%	4,08%	16,62%	5,25%	0,00%	13,12%	0,29%	1,46%
8	27,03%	56,76%	0,00%	2,70%	0,00%	0,00%	10,81%	0,00%	2,70%

The average execution time shows that the LSq method is the fastest (133.9 s, because it is not able to proceed further, since the increment in theta is lower than the tolerance), followed by RD (289.9 s) and APS (473.3 s). Regarding robustness, the RD algorithm shows the best characteristics converging in 95% of the cases followed by LSq (86%) and APS (75%) methods.

3.5.2.2. Validation set

The values of the objective function in the validation set are depicted in Figure 3.10. In this case, there are two well-defined solution regions, instead of the three present in the calibration set. The distributions in the first and second regions are similar to that obtained in the same regions for the calibration set. The RD method mostly lies in the first region, while the LSq converges mainly to the second. The APS presents the biggest dispersion with three small peaks, one in the first and other two in the second region. In other words, the algorithm with the best result for the calibration set (RD) also presents the best prediction, which differs from the results obtained in the first case study, where RD presented the best prediction but not the best calibration.

Figure 3.10 – Objective function values obtained in second case study on validation set.

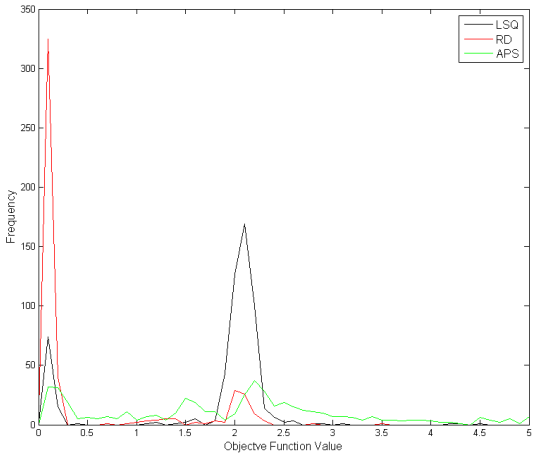

The distribution of concentration profiles obtained in the validation set (Figure 3.11) shows that the parameters estimated by the RD allows the most accurate prediction of the system behavior. The predictions by the LSq method are imprecise, since it frequently estimates faster reaction rates than the real process. The profiles predicted by the APS method present the largest dispersion, as for the calibration.

Figure 3.11 - Concentration profiles of measured components predicted by LSq (A), RD (B), and APS (C) methods – Case study 2.

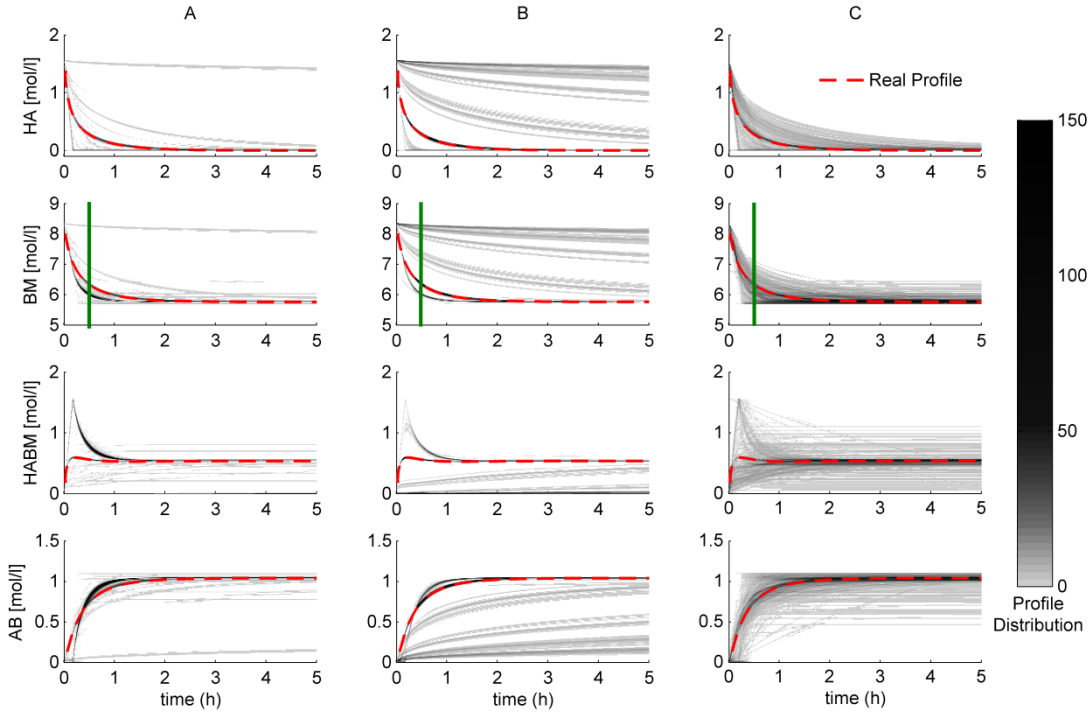

Figure 3.12 - Cross section histogram of BM's concentration profile at time 0.5 hours

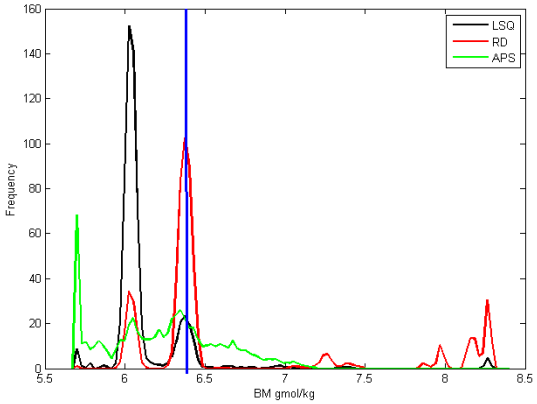

To make the information about the predicted concentration profiles on the validation set clearer, an histogram of BM's profiles of Figure 3.12 at time 0.5 hours (this point is indicated in Figure 3.11 using green lines) is plotted in Figure 3.12. It can be noticed that there are three well-defined regions regarding the RD method, which correspond to the three regions found in the objective function values analysis in the calibration set. The vertical blue line represents the nominal concentration value of BM at 0.5 hours; the region around this line correspond to the prediction from the

region of Figure 3.8 (the smallest values of objective function), where the RD method has the highest frequency of convergence. The peaks on the left side correspond to the prediction from the second region of Figure 3.8, where the LSq has the highest rate of convergence. The RD peaks on the right side are related to the third region in Figure 3.8.

3.6. Discussion

Under the experimental conditions chosen for this study case, the first case study is unidentifiable in practice since the available information makes the problem ill-conditioned and makes it difficult to obtain unique parameter estimates (BEN-ZVI, 2008). The same behavior can be observed in the second case study, since parameters $K1/K3$ produce linearly dependent sensitivities, as observed by Biegler et al. (1986) and confirmed by the frequency distributions for these parameters (Figure 3.9 G and I). This characteristic is the main reason to use methods that tackle the identifiability problem.

3.6.1. Case study 1

A comparison between Figures 3.1 and 3.3 shows the degradation of the objective function value in the LSq method. This degradation comes from the fact that this method overfits the model in the calibration set. This overfitting generates the degradation of least-squares estimator as a consequence of its incapacity to discriminate the random and deterministic parts of the data sets. As the flexibility of a model increases, this ineffectiveness gets worst because the LSq method is unbiased (EFRON, 1975), generating unreliable parameter estimates. Thus, the small values of the objective function obtained by the LSq method are misleading, since they come from fitting noise components which decreases the prediction capacity of the model in the validation set.

Model overfitting can be corroborated by evaluating the noise influence on the model prediction; for this purpose two MC simulations are performed (1000 estimations

each): one noise-free and the other normal distribution with standard deviation twice larger than that of the base case. The results (Figures 3.13 and 3.14) show that the LSq method has the best predictive capacity adjusting noise-free measurements, while the presence of noise considerably lessens its prediction capability. It is worth noting that the quality of the parameters obtained using the RD does not change as much as for the other biased estimation methods.

Figure 3.13 – Concentration profiles of B and P predicted by LSq (A), RD (B), RDG (C) and APS (D) methods. (--) Nominal concentration profile. Noise-free Case 1

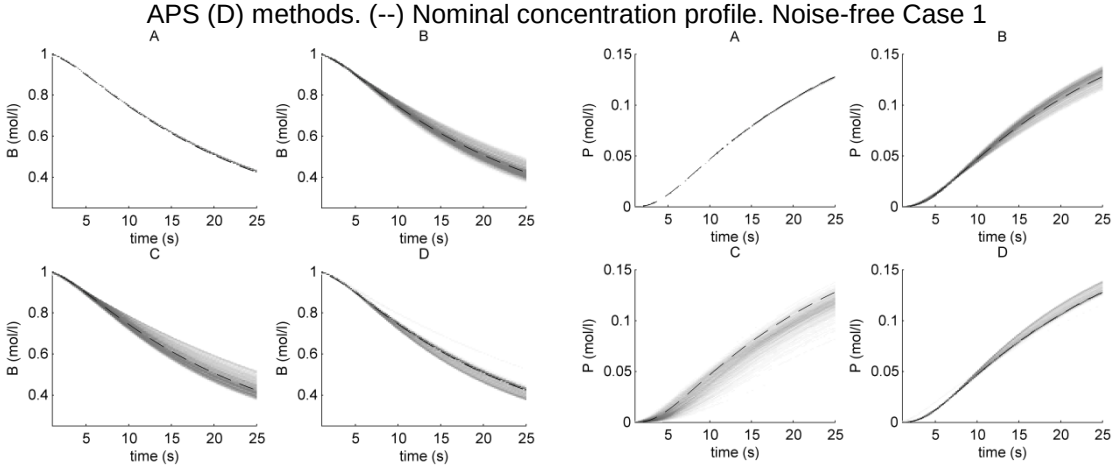

Figure 3.14 – Concentration profiles of B and P predicted by LSq (A), RD (B), RDG (C) and APS (D) methods. (--) Nominal concentration profile. Noise with standard deviation twice larger than the one used in base Case 1

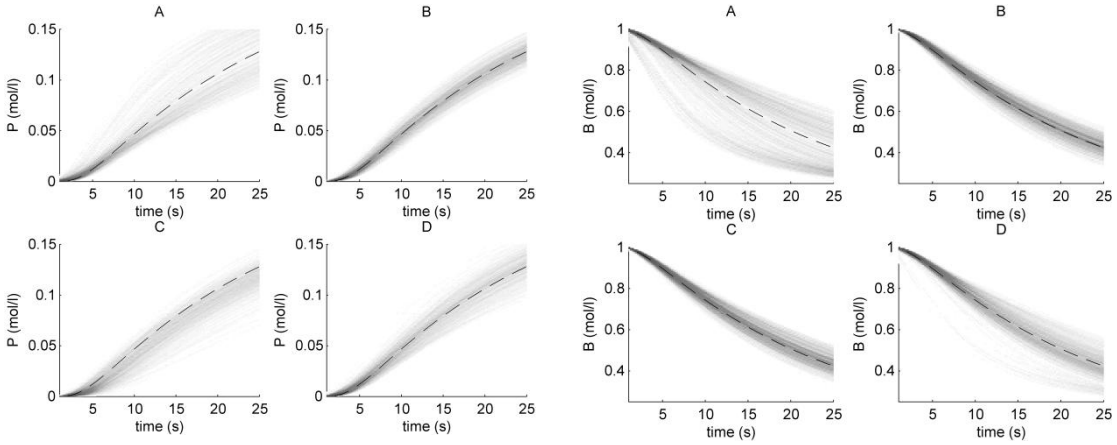

A very important result is that the values of parameters k_1, k_2, k_3 and k_4 obtained by the APS and the LSq methods are close to the upper and lower bounds allowed for the parameters in the minimization step. This behavior reinforces the previous analysis, showing that there is a region where the objective function is not sensitive to variations in the parameters, what makes the optimization method to keep varying the parameter values, trying to improve the cost function value without success, and

eventually obtaining parameter values close to their lower or upper bounds, in order to use a constraint for limiting the practical rank-deficient problem (parameter inflation phenomenon). Additionally, in the case of the APS method, the nominal values of the unadjusted parameters might influence the values of the adjusted ones.

3.6.2. Case study 2

It can be noticed from Figure 3.8 that the LSq method cannot converge to the optimal solution, avoiding the model overfit caused by it. This fact is related to the ill-conditioning of the Hessian Matrix of this case study, which also prevents the solutions of the proposed algorithms to reach the first region more frequently. The RD method, on the other hand, obtained the best results because it is able to handle the ill-conditioning problem, although, the RD algorithm fails to converge when poor initial guesses are used. This feature is responsible for the fact that it converges to solutions in the third region in Figure 3.8, whilst the others do not. In practice, a hybrid algorithm could be devised, in which LSq is applied when RD fails to converge, and then switched to RD as far as the LSq is unable to evolve. For recurrent problems like those found in RTO, typical objective function values are known *a priori*, and the conception of such an algorithm is absolutely natural.

The three different convergence regions (Figure 3.8) are a consequence of the different concentration profiles solution (Figure 3.12). The solutions obtained for the smallest values of the objective function (Figure 3.8) fit better the original concentration profiles. It is worth noting that the frequency distribution of the APS method, in the interval from 0 to 0.15, is smaller than the one of the LSq method (Figure 3.10), however, the frequencies of these methods in the concentration profile, when compared to the nominal values, are similar (Figure 3.12). In other words, despite APS having an objective function distribution with larger values in the validation set, its predictions are as good as the ones presented by the LSq method.

It can be observed in Figure 3.9 C, G, H and I that the parameter distribution profiles are displaced from the nominal parameter values, but this fact does not jeopardize the achievement of a good parameter fit able to predict the system behavior in the

validation set (Figure 3.10). This behavior, typical of quantitatively unidentifiable systems, suggests that the suitability of a parameter estimation method for inestimable models cannot be judged on the ability of proposing a "true" parameter set. A more sensible criterion is that the estimated parameters enable the model to predict accurately in the intervals of interest. Thus, it is always desirable to reserve a data subset to analyze the prediction accuracy of a model.

The utility of a mathematical model is that it represents a real process in a given range of process conditions. The way a model is used determines some characteristics of the parameter estimation algorithm, such as robustness, speed and accuracy of prediction. The first two requirements, though desirable, are not mandatory in off-line applications (e.g. process design) since the time slot is not as stringent as in on-line applications, that require fast and robust parameter computation to implement a new operating point for the real plant (e.g., real time optimization). Nonetheless, the prediction capacity is a common requirement for both, on-line and off-line applications, since only accurate predictions may guarantee suitable choices. The results presented in this Chapter show that the RD method is able to handle model quantitative identifiability problems, with the best prediction capacity, compared to the other methods. Regarding the speed, RD method is the fastest. Moreover, the RD method proposes more effective changes in parameters values, resulting in well-posed differential equations and better predictions. The analysis of the parameters confidence region could be implemented in these case studies to confirm theirs outcomes, and for this reason, it should be considered in future works.

3.7. Partial Conclusions

The performance of four parameter estimation approaches was evaluated using two case studies. These methods were assessed according to their robustness, computational speed and prediction capacity. The LSq method does not take into account the practical unidentifiability of the model. In this method all the parameters are adjusted, leading to model overfit (case study 1) or underfit (case study 2). The former is characterized by poor discrimination between noise and deterministic

features, whereas the latter happens when the ill-conditioning is too pronounced and LSq is unable to converge to reasonable solutions. In the first case study, the LSq and APS methods presented the lowest values of the objective function in the calibration set, however, the LSq prediction is the worst among the evaluated methods. This points out that the best fit in the calibration set is not an adequate criterion to define how good the estimated parameters are. A more sensible way to assess the goodness of the estimation is by using the information provided by a validation set. The RDG method handles the identifiability problem using *a priori* information to reparameterize the model, demanding knowledge about model structure, process behavior and differential geometry expertise to find the diffeomorphic transformation. These requirements, together with the lower performance compared to RD method, limits the application of RDG at its actual state, and for these reasons, it is not applied in the second case study. The APS method presents better results than the LSq, nonetheless it is the slowest method. The results obtained in this work show that RD method is the most suitable among the evaluated methods, because it presents the best prediction capacity and robustness, with reasonable computational time. These outcomes suggest a possible successful application of the RD method in a RTO system, which is accomplished in Chapter 5 of the present thesis.

Most of the material presented in Chapter 3 corresponds to the paper "Performance Comparison of Parameter Estimation Techniques for Unidentifiable Models", published in the journal Computers & Chemical Engineering, volume 64, pages 24-40, 2014.

4. LOW SET POINT UPDATE FREQUENCY

The Real-Time Optimization method claims to be an online method, but it can be performed only when steady state information of the system is available. Therefore, after an incoming disturbance it is necessary to wait until the system settles down to obtain new steady state information, and then update the economic set point (ENGELL, 2007). The plant operates at suboptimum conditions over the transient period, which should not be a problem when the process settling period is short, but it is a concerning issue when the process takes some hours to settle down after an inlet disturbance. Such is our main case study, the vapor recompressed distillation (VRD) system for propylene production (see Chapter 5).

An alternative to overcome this problem is to build a control layer that is robust to the main disturbances affecting the economic performance. It can be done by choosing controlled variables (CVs) with set points insensitive to these disturbances, which is the main idea of Self Optimizing Control (SOC) approach. Skogestad (2000) presented a procedure to find a set of self-optimizing controlled variables using information provided by a steady state model. This technique was successfully applied to large-scale chemical processes as described by de Araújo; Govatsmark and Skogestad (2007); Larsson et al. (2001).

Another alternative to implement SOC is to create artificial CVs (c), economically insensitive to the disturbances, using linear combinations of measured variables (y), $c = Hy$. Several studies have been conducted in this area, using steady state process models. Examples include the Exact Local method developed by Halvorsen and coworkers (2003), which considers a second order approximation around the optimal point to obtain measured combinations that are less affected by disturbances and implementation error. In addition, the Null Space method, by Alstad and Skogestad (2007), uses the optimum output sensitivity to disturbances to find a matrix of measurement combinations (H). In this case, the artificial controlled variables present zero loss with respect to the analyzed disturbances. Alstad and coworkers (2009) extended the Null Space method, using extra measurements to reduce the loss assigned to measurement noise by minimizing the worst-case loss. Kariwala and

coworkers (2008) developed a method using the average loss criterion, which presented superoptimal solutions with respect to the worst-case scenario. In other words, the solution of the average loss criterion also minimizes the worst-case condition.

Jäschke and Skogestad (2013) developed a method to identify combinations of measured variables using only process data. In this method, several plant experiments are performed to compute the measured gain matrix, while the reduced Hessian matrix is computed from a second order black box model adjusted to the process data. Despite the fact that it does not require a process model, this method demands large amounts of process data, which is difficult to accomplish in practice.

Ye et al. (2013) incorporated concepts of necessary conditions of optimality (NOC) in SOC to determine controlled variables that approximate the economic objective function gradient with respect to the manipulated variables. These controlled variables are represented by parametric models that are identified with measurements from the entire operating space, reducing the profit loss for a larger disturbance region, when compared to local methods.

The concepts developed in SOC theory explore the disturbance region around the optimum point. However, when the disturbances become more significant, this method presents poor results and it needs to be updated for another region. Following this idea, Ye et al. (2014) extended their previous work combining NOC and SOC by implementing a statistical criterion to decide when the controlled variables should be updated for another region, using SOC in an RTO-like framework.

In this setting, the SOC methodology is complementary to the RTO method, and it can be an alternative to address low frequency set point updates in RTO (JÄSCHKE; SKOGESTAD, 2011; MANUM; SKOGESTAD, 2012). However, the practical implementation of SOC in the control layer still has some challenges to be addressed, such as the active set changes due to an incoming disturbance.
Conceptually, the SOC implementation strategy primarily implies the control of active constrains, and then, the control of a sufficient number of SOC variables to deplete

the number of degrees of freedom of the control problem (SKOGESTAD, 2000). When a disturbance changes the number of active constraints, it is necessary to modify the control structure by adding or reducing SOC variables, and for this reason, the control layer needs to be flexible to meet this requirement.

Some methods have already been proposed in the literature to handle this problem, for instance, Cao (2005) proposed a cascade control approach in which the inner control loop is responsible for constraint control, while the outer loop provides set points for the inner loop by maintaining the self-optimizing control variables constant, using a saturation block to handle the constraints satisfactorily.

Another alternative to handle the active set change problem is through a split range control. Lersbamrungsuk et al. (2008) applied this method to a heat exchange network, by performing an offline optimization to determine all possible active constraints regions, and then used a simple integer linear program to identify where the process is placed and which constraints should be controlled.

Hu and coauthors (2012) extended the exact local method (ALSTAD; SKOGESTAD; HORI, 2009) to account for process constraints. This proposed method presents a simpler control structure than the cascade or the split rage control, consequently, it yields worse economic result than the previous approaches, indicating conservativeness.

The previously mentioned approaches are based on PID (proportional-integral-derivative) controllers, which have clear disadvantages compared to MPC, i.e. the difficulties in handling multiple input and multiple output problems. Seeing that, Manum and Skogestad (2012) proposed an alternative by exploiting the link between SOC and a linear quadratic MPC. In their work, different active set regions were identified by a parametric program. Then, the self-optimizing control variable values were used to select the region where the process currently lies, as well as the best choice of controlled variables for that specific region. The challenge faced by this method is the need to identify all the different active set regions and their corresponding set of self-optimizing control variables (in the whole operational map). This makes their strategy more complex compared to the method developed in the

present work., which only requires the local active-set and self-optimizing variables information.

Our results are based on the control of self-optimizing control variables, as well as enforcing the feasibility of the constrained states through a zone control approach, which is similar to the method based on PID control previously discussed in (CAO, 2005). In other words, the RTO layer provides the ideal controlled variables values to the MPC, which drives them to their set points. In the presence of active constraints, the zone control approach will enforce the constraint satisfaction while the MPC targets will steer the self-optimizing control variables as close to their set points as possible.

The active set change problem can be summarized in two possible cases, as follows. After an incoming disturbance:

Case 1: one or more inactive constraints become active. In this case, there is a reduction in the number of degrees of freedom. Therefore, one self-optimizing control variable must be replaced by satisfying the new active constraint.

Case 2: one or more active constraints become inactive. In this case, the number of degrees of freedom increases, and then a previously controlled active constraint must be replaced by a self-optimizing control variable.

The MPC developed in the present work aims to tackle the first case, which is the most important with regard to economical loss, once it presents proportional loss with respect to the error (BERTSEKAS; NEDIÂC; OZDAGLAR, 2003). The second case, which presented only a minor effect on the economic loss, is managed by the RTO layer that is able to identify a constraint becoming inactive, and then to update this information in the MPC layer.

In summary, the method developed in the present work is inspired from the implementation discussed by Manum and Skogestad (2012) and aims to handle larger disturbances by the integration of SOC and RTO. However, it is simpler, because it does not require: (i) the offline computation of constraints map, (ii) logical

assessment to detect in which constrained region the process is placed, (iii) extra measurements due to change in the control structure.

This Chapter is organized as follows: Section 4.1 describes the proposed RTO and MPC framework. Section 4.2 develops an MPC with self-optimizing control variables used as targets and a zone control approach to assure the constraints satisfaction. Then, two case studies are presented in Sections 4.3 and 4.4. Finally, partial conclusions are given in Section 4.5.

4.1. RTO framework implementation with SOC

The MPA (model parameter adaptation) structure is used to develop the new framework with SOC. First of all, the optimization problem given by the MPA in Chapter 2 is complemented with the vector of analyzed disturbances ($d \in \mathbb{R}^{n_d}$).

$$\begin{aligned} u^* = \arg\min_{u} \quad & \varphi(u, \hat{y}, d) \\ \text{s.t.} \quad & \hat{y} = F(u, \theta, d) \\ & g(u, \hat{y}, d) \leq 0 \end{aligned} \tag{4.1}$$

The optimum result obtained from eq.(4.1) is implemented in the process by the hierarchical structure depicted in Figure 4.1. The algorithm starts with the detection of the steady state condition of the plant. Then the process measurements (y) are screened, regarding their consistency and presence of gross errors in the reconciliation module. After that, filtered data are used to update the process model in the parameter estimation module. The next stage comprises the optimization of an economic objective function subject to the updated model (eq.4.1), but differently from the classic MPA method, this new framework provides more information to the MPC layer, namely: the set of self-optimizing controlled variables ($c \in \mathbb{R}^{n_c}$), their set points ($c^* \in \mathbb{R}^{n_c}$) and the constrained variables ($r \in \mathbb{R}^{n_r}$). Lastly, the MPC layer is responsible to drive the self-optimizing control variables to their set points and to satisfy the process constraints.

Figure 4.1 - Proposed framework for the implementation of SOC in the RTO

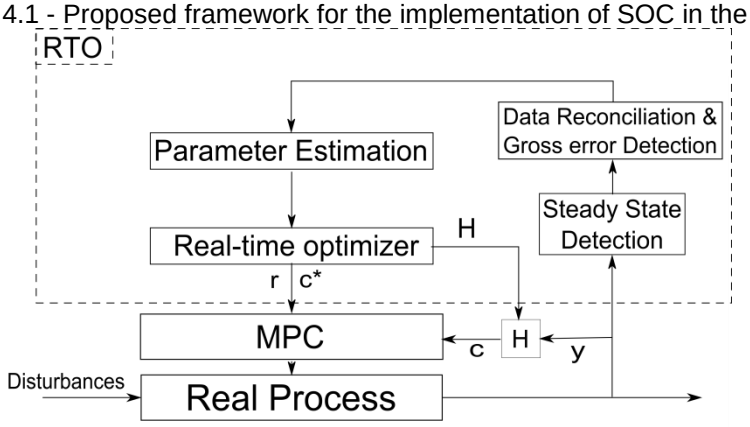

The artificial self-optimizing control variables (c) are calculated as linear combinations of measured variables by the Null Space method (ALSTAD and SKOGESTAD, 2007). In this method, the vector of artificial variables is given by $c = Hy$, where H is a selected matrix in the left null space of F:

$$F = \frac{\partial y^{opt}}{\partial d} = \begin{bmatrix} \frac{\partial y_1^{opt}}{\partial d_1} & \cdots & \frac{\partial y_1^{opt}}{\partial d_{nd}} \\ \vdots & \ddots & \vdots \\ \frac{\partial y_{ny}^{opt}}{\partial d_1} & \cdots & \frac{\partial y_{ny}^{opt}}{\partial d_{nd}} \end{bmatrix}; \quad HF = 0 \qquad (4.2)$$

where F is the optimum NLP sensitivity matrix of outputs with respect to the vector of analyzed disturbances (d), which is obtained by considering the economic objective function. Here, the NLP sensitivity matrix is computed by solving the Optimization (eq.4.1) for each finite difference perturbation of the disturbances space. Based on eq.(4.2), the number of artificial self-optimizing variables is equal to $n_c = n_y - n_d$, implying that the number of measurements should be greater than the analyzed disturbances, which is enough to meet the necessary number of degrees of freedom.

The presented framework aims to increase the overall system robustness by updating the artificial self-optimizing control variables, their set points and the current constrained variables, at each RTO sampling period. Consequently, the control layer is able to guarantee the variables bounds and will lead to near-optimum adjustments

of the inputs in between the RTO runs, for the Case 1 described in the previous Section, without needing to wait for the next RTO update.

4.2. Development of an MPC with zone control and artificial SOC variables targets for RTO implementation

Controlling artificial SOC variables may lead to violation of uncontrolled process constraints after an active set change. The basic idea behind this new method is to enable the MPC to guarantee the feasibility of constrained inputs and outputs variables, while it controls the set of self-optimizing control variables.

Figure 4.2 summarizes the suggested control idea to handle the Case 1 (discussed in the previous sections). Here, the outputs variables are divided in two classes: constrained variables (e.g. product properties specification or safe operation temperatures) and controlled variables (artificial self-optimizing control variables).

Figure 4.2 – MPC with zone control and SOC

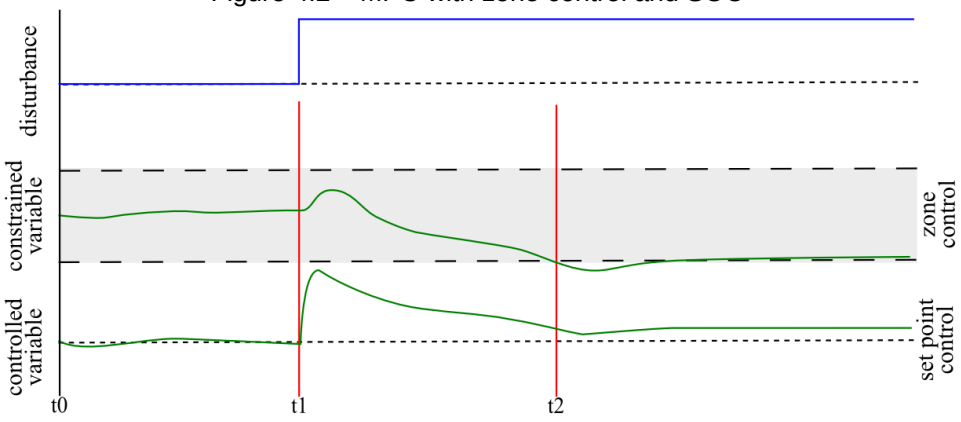

At *t*0, the controller keeps the controlled variable at its set point and the constrained variable does not have any influence on the objective function (since it is within its zone). When a disturbance affects the system at *t*1, the controller tries to drive the controlled variable to its set point, but at the expense of moving the constrained variable toward one of its bounds. At *t*2, the constrained variable reaches its lower bound, then, the controller is forced to keep the constrained variable inside its zone, leading to an offset in the controlled variable.

This strategy allows for the imposition of the constraint satisfaction within an RTO cycle, while keeping the controlled variables as close to their set points as possible (Case 1), until a new RTO cycle updates the controlled variables set points to values compatible with the actual set of disturbances (Case 2).

While the classic MPC with zone control uses the input (manipulated variables) targets as controlled variables (GONZÁLEZ; ODLOAK, 2009), the present work uses a set of SOC variables and active constraints as controlled variables in order to assure acceptable profit loss in case of known disturbances.

Modified dynamic model

The formulation of the MPC with zone control and SOC targets considers a linear dynamic model with nu inputs and ny outputs (eq.4.3). This model is rearranged in an incremental form (eq.4.4 and 4.5), in order to eliminate output offset (MAEDER; BORRELLI; MORARI, 2009).

$$\begin{aligned} x(k+1) &= A\,x(k) + B\,u(k) \\ y(k) &= C\,x(k) \end{aligned} \tag{4.3}$$

$$\begin{aligned} \begin{bmatrix} x(k+1) \\ u(k) \end{bmatrix} &= \begin{bmatrix} A & B \\ 0 & I_{nu} \end{bmatrix} \begin{bmatrix} x(k) \\ u(k-1) \end{bmatrix} + \begin{bmatrix} B \\ I_{nu} \end{bmatrix} \Delta u(k) \\ y(k) &= \begin{bmatrix} C & 0 \end{bmatrix} \begin{bmatrix} x(k) \\ u(k-1) \end{bmatrix} \end{aligned} \tag{4.4}$$

$$\begin{aligned} \bar{x}(k+1) &= D\,\bar{x}(k) + E\,\Delta u(k) \\ y(k) &= M\,\bar{x}(k) \end{aligned} \tag{4.5}$$

Here, $y(k)$ is the vector of measured output variables (including the constrained and unconstrained measured variables), $\Delta u(k)$ is the difference between $u(k)$ and $u(k-1)$ and I_{nu} is an identity matrix with dimension nu (number of inputs). The dynamic model eq.(4.5) is the basis of a new dynamic model with two output vectors (see eq.4.6), namely: a vector of controlled variables $c(k)$ in which the number of variables is equal to number of degrees of freedom, and a vector of constrained variables $r(k)$.

$$\begin{aligned} \bar{x}(k+1) &= D\,\bar{x}(k) + E\,\Delta u(k) \\ c(k) &= H\,M\,\bar{x}(k) \\ r(k) &= W\,M\,\bar{x}(k) \end{aligned} \tag{4.6}$$

The vector of controlled variables $c(k) \in \mathbb{R}^{ndf}$ is selected from $y(k)$ using the map H (matrix of measurements combination obtained from the Null Space method). Basically, the number of rows of matrix H is equal to number of degrees of freedom, in which each row represents a combination of measurements (SOC variable given by eq.4.2). The vector $r(k) \in \mathbb{R}^{n_r}$ is the vector of constrained variables (e.g. product composition) selected by a diagonal matrix W of zeros and ones. Then, the dynamic model used in here is simplified to eq.(4.7).

$$\begin{aligned} \bar{x}(k+1) &= D\,\bar{x}(k) + E\,\Delta u(k) \\ \bar{c}(k) &= U\,\bar{x}(k) \\ \bar{r}(k) &= V\,\bar{x}(k) \end{aligned} \tag{4.7}$$

Both vectors of predicted outputs – $\bar{c}(k) \in \mathbb{R}^{(nc.p)}$ and $\bar{r}(k) \in \mathbb{R}^{(nr.p)}$, controlled and constrained variables respectively – are extended over p intervals, and the input movements are extended over m intervals, i.e., $\Delta U_k = \left[\Delta u_k, \Delta u_{k+1} \ldots\right]^T \in \mathbb{R}^{(m.nu)}$, according to eq.(4.8) and (4.9); Ψ, Θ, Ω and T are defined by eq.(E1) and (E2) of Appendix E. We admit that the input values are constant after m, i.e. $u(k+m) = u(k+m+1) = \ldots = u(k+m+p) \therefore \Delta u(k+m+i) = 0, \quad i = 0, \ldots, p-m$.

$$\bar{c}(k) = \Psi \bar{x}(k) + \Theta \Delta U_k \tag{4.8}$$

$$\bar{r}(k) = \Omega \bar{x}(k) + \mathrm{T}\,\Delta U_k \tag{4.9}$$

Zone constraints

Using the vector of constrained predicted variables $\bar{r}(k)$, it is possible to determine a set of inequality constraints that implement the zone control strategy shown in figure 4.2. The eq.(4.10) describes this set of inequality constraints.

$$\Omega\,\bar{x}(k)+\mathrm{T}\,\Delta U_k \geq b_{\min} \quad ; \quad \Omega\,\bar{x}(k)+\mathrm{T}\,\Delta U_k \leq b_{\max}$$
$$-\mathrm{T}\,\Delta U_k \leq \Omega\,\bar{x}(k)-b_{\min} \quad ; \quad \mathrm{T}\,\Delta U_k \leq b_{\max}-\Omega\,\bar{x}(k) \tag{4.10}$$

Furthermore, the input (manipulated) variables should also be constrained due to physical limits imposed by the plant equipment, for instance, maximum or minimum flow rate for a particular stream. The nominal values of the input variables with respect to the inputs increments are given by eq.(4.11) and the set of their inequality constraints is given by eq.(4.12).

$$U_k = \tilde{M}\Delta U_k + \tilde{I}u(k-1); \quad \tilde{M} = \begin{bmatrix} I_{nu} & 0 & \cdots & 0 \\ I_{nu} & I_{nu} & \cdots & 0 \\ \vdots & \vdots & \ddots & \vdots \\ I_{nu} & I_{nu} & \cdots & I_{nu} \end{bmatrix}; \quad \tilde{I} = \begin{bmatrix} I_{nu} \\ I_{nu} \\ \vdots \\ I_{nu} \end{bmatrix} \tag{4.11}$$

$$\tilde{M}\Delta U_k \leq U_{\max} - \tilde{I}u(k-1) \quad ; \quad -\tilde{M}\Delta U_k \leq \tilde{I}U(k-1) - u_{\min} \tag{4.12}$$

By grouping all the inequality constraints (eq.(4.10) and (4.12)) and including L_1 penalty functions to transform hard constraints into soft constraints (to avoid infeasibilities in the optimization step of the control problem), the set of inequality constraints in eq.(4.13) and (4.14) is obtained, which implements the zone control policy (see figure 4.2).

$$\begin{bmatrix} T & -I & 0 & 0 & 0 \\ -T & 0 & -I & 0 & 0 \\ \tilde{M} & 0 & 0 & -I & 0 \\ -M & 0 & 0 & 0 & -I \end{bmatrix} \begin{bmatrix} \Delta U_k \\ s_U^O \\ s_L^O \\ s_U^I \\ s_U^I \end{bmatrix} \leq \begin{bmatrix} b_{\max} - \Omega\,\bar{x}(k) \\ \Omega\,\bar{x}(k) - b_{\min} \\ U_{\max} - \tilde{I}u(k-1) \\ \tilde{I}u(k-1) - U_{\min} \end{bmatrix} \tag{4.13}$$

$$\tilde{A} \begin{bmatrix} \Delta U_k \\ s_U^O \\ s_L^O \\ s_U^I \\ s_L^I \end{bmatrix} \leq \tilde{b} \tag{4.14}$$

Here, s are the slack variables, the superscripts O and I indicate constrained outputs and input variables respectively, and the subscripts U and L indicate upper and lower bounds.

Target control

The MPC set point control (see figure 4.2) is implemented using a classic quadratic control objective function in which the outputs are predicted within a finite prediction horizon of p intervals, and the input moves are considered over m time intervals, and using the vector of predicted artificial SOC variables $\bar{c}(k)$:

$$J_k = (\bar{c}(k) - \bar{c}^{sp})^T \bar{Q}(\bar{c}(k) - \bar{c}^{sp}) + \Delta u_k{}^T \bar{R} \Delta u_k \qquad (4.15)$$

where $\bar{c}^{sp} = \left[\underbrace{c^{sp^T} \ldots \ c^{sp^T}}_{p} \right]^T$ is the Self Optimizing Control variables set point vector, $\bar{Q} = diag\left[\underbrace{Q \ \ldots \ Q}_{p} \right]$ is a diagonal weighting matrix on the differences between the controlled variables and their set points and $\bar{R} = diag\left[\underbrace{R \ \ldots \ R}_{m} \right]$ is a diagonal weighting matrix on the input movements.

Substituting eq.(4.8) into (4.15) leads to the control objective function in terms of Δu_k eq.(4.16) and its quadratic form, shown in eq.(4.17).

$$J_k = (\Psi \bar{x}(k) + \Theta \Delta U_k - \bar{c}^{sp})^T \bar{Q}(\Psi \bar{x}(k) + \Theta \Delta U_k - \bar{c}^{sp}) + \Delta U_k{}^T \bar{R} \Delta U_k \qquad (4.16)$$

$$J_k = \Delta U_k{}^T \Gamma \Delta U_k + 2\bar{a}_f{}^T \Delta U_k + \bar{a} \qquad (4.17)$$

where:

$$\Gamma = \Theta^T \bar{Q} \Theta + \bar{R}$$
$$\bar{a}_f{}^T = (\Psi x(k) - \bar{c}^{sp})^T \bar{Q} \Theta$$
$$\bar{a} = (\Psi x(k) - \bar{c}^{sp})^T \bar{Q} \ (\Psi x(k) - \bar{c}^{sp})$$

MPC with zone control and artificial SOC variables targets

Now, it is necessary to combine the target and zone control approaches into the same objective function. For this reason, the set of slack variables is included into the objective function eq.(4.17) as a L_1 penalty function, leading to eq.(4.18).

$$\begin{aligned} J_k &= \Delta u_k{}^T Y \Delta u_k \;\; + 2\bar{a}_f{}^T \Delta u_k + [s_U^{OT} \;\; s_L^{OT} \; s_U^{IT} \;\; s_L^{IT}]\, M\, e \\ e &= [1,1,1,\ldots]^T \end{aligned} \tag{4.18}$$

where M is a sufficiently large diagonal weighting matrix to make sure that the input movements will maintain the feasibility of the constrained variables.

Finally, the control problem is defined by eq.(4.19):

$$\begin{aligned} &\min_{\Delta u_k, s} J_k \\ &\text{subject to:} \\ &\Delta u_{\min} \le \Delta u \le \Delta u_{\max} \\ &s_U^O \ge 0,\;\; s_L^O \ge 0,\; s_U^I \ge 0,\;\; s_L^I \ge 0 \\ &\tilde{A} \begin{bmatrix} \Delta u_k \\ s_U^O \\ s_L^O \\ s_U^I \\ s_L^I \end{bmatrix} \le \tilde{b} \end{aligned} \tag{4.19}$$

4.3. Case Study 1: Ammonia production

The MPC with zone control and SOC targets developed in the previous section is implemented in a case study of ammonia production, defined in Manum and Skogestad (2012), and presented in Figure 4.3. In this process, the feed stream (composed of hydrogen H_2 and nitrogen N_2) is compressed and mixed with the recycle stream to generate stream S2. Then, this mixture reacts at pressure P_{reac} to produce ammonia, which is cooled to temperature T_{flash} and then separated from the light components (H_2 and N_2). The recycle stream (S5) is split, generating stream S7

that is purged and stream S6 that is compressed and mixed with the feed stream (S1).

Figure 4.3 - Schematic representation of ammonia production process

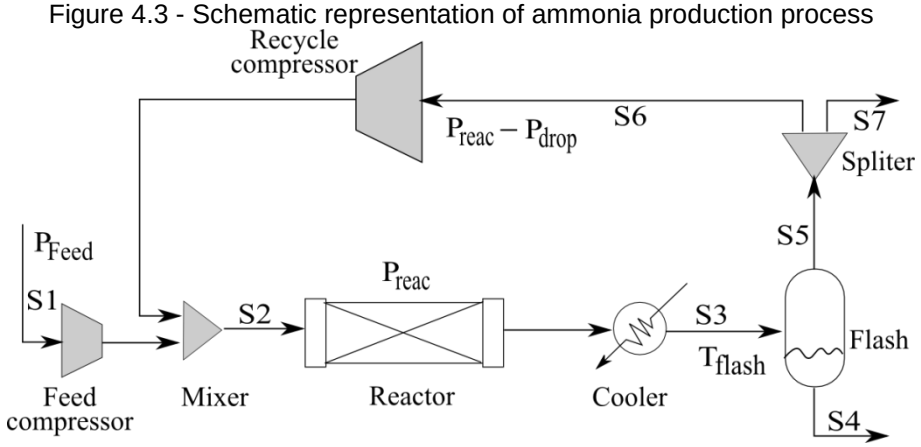

The ammonia production process is modeled at steady state by a set of mass and energy balances and equilibrium equations, simulated in the software AMPL® (the complete model is given in Appendix F). Equation (4.20) describes the optimization problem with the economic objective function composed by the production costs (compressors and cooling work) and profit (ammonia stream, S4).

$$\begin{aligned} \min_{u} \quad & Cost^{opt} = P_{feed}W_{feed} + P_{recy}W_{recy} + P_{cool}W_{cool} - P_{NH3}S4_{NH3} \\ \text{subject to: Steady State Model} & \\ & 266 \le T_{flash} \le 288 \qquad [\text{K}] \\ & 0 \quad \le S6 \quad \le 3.5 \qquad [\text{mol/time}] \end{aligned} \tag{4.20}$$

where u=[P_{reac}, T_{flash}, sf] is the vector of decision variables (reactor pressure, flash temperature and split fraction of stream S5); W_{feed}, W_{recy} and W_{cool} are respectively the work performed by the feed compressor, recycle compressor and cooler; $S4_{NH3}$ is the molar flow rate of ammonia in the product stream; P are the prices given in Table F2 (see Appendix F). The operating regions of this process are defined by a set of inequality constraints on the flash temperature (T_{flash}) and the recycle molar flow rate (S6).

Two disturbances are considered, *d1* in the feed flow rate and *d2* in the feed composition. These disturbances can be mathematically represented by eq.(4.21).

Figure 4.4 depicts the process profit function with respect to the disturbances and Figure.4.5 shows the active set map for the operating space, including the minimum cooler temperature (T_{flash}) and the maximum flow rate S6 and split fraction (sf).

$$S1 = 5.1 + d1 \quad \text{[mol/time]}$$
$$x^{S1} = \begin{bmatrix} 0.8 + d2 \\ (1 - 0.8) - d2 \\ 0 \end{bmatrix} \begin{matrix} \rightarrow H_2 \\ \rightarrow N_2 \\ \rightarrow NH_3 \end{matrix} \tag{4.21}$$

Figure 4.4 - Profit of ammonia plant with respect to disturbances (This surface would be the cost if there were no active set changes)

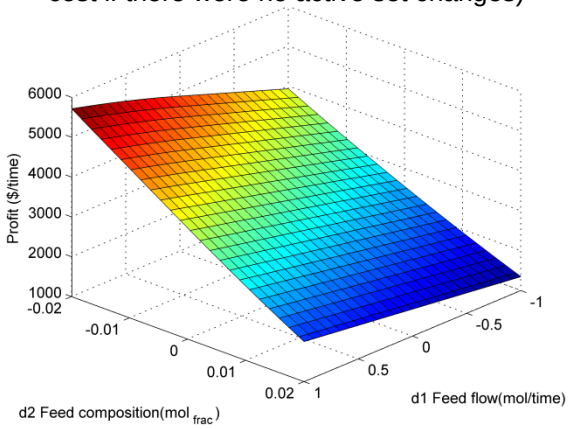

Figure 4.5 - Active set map for the disturbance region, ammonia production case study. (Each color denotes a region where the active set does not change. The variable names within the regions denote the constraints that are active)

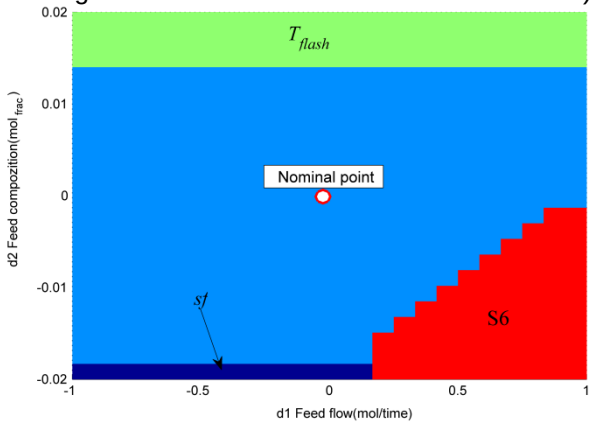

4.3.1. Steady state analysis

Three steady state cases are carried out to compare the economic performance of different MPC approaches under presence of disturbances. Case A simulates the "classical" control approach (controlling only given set points), where three process variables, flash temperature (T_{fash}), reactor pressure (P_{reac}), and recycle flow rate (S6),

are the controlled variables. Case B applies the control of three SOC variables computed as the linear combination of 6 measurements $y=[S2_{H2}, S2_{N2}, S6, P_{reac}, T_{flash}, sf]^T$. In this case, the zone control of the constrained variables (molar flow rate, S6) is not considered. Case C simulates our new MPC with zone control and SOC targets; in this case, the same artificial SOC variables are controlled as in Case B. However, the zone constraints are enforced to respect the upper bounds on S6 stream.

These cases are conducted by the solution of the optimization problem in eq.(4.22) (which corresponds to the steady state solution for a nonlinear model predictive controller), for a given disturbance value, among $-1.00 \le d1 \le 1.00$ $-0.02 \le d2 \le 0.02$ regions:

$$\begin{aligned} \min_{u} \quad & Obj = \left(c1 - c1^{sp}\right)^2 + \left(c2 - c2^{sp}\right)^2 + \left(c3 - c3^{sp}\right)^2 \\ \text{subject to:} \quad & \text{Nonlinear Steady State Model} \\ & Cost^{\exp} = P_{feed}W_{feed} + P_{recy}W_{recy} + P_{cool}W_{cool} + P_{NH3}S4_{NH3} \\ & 266 \le T_{flash} \le 288 \qquad [K] \\ & 0.4 \le sf \le 0.8 \end{aligned} \tag{4.22}$$

where c are the controlled variables defined in Table 1.1 and c^{sp} are their set point values computed at the nominal point ($d1=0$ and $d2=0$). The sensitivity information required for the null space matrix, F, is also computed at this point, by solving problem eq.(4.20), nested within finite difference perturbations. Additionally, Case C, considers the constraint in eq.(4.23):

$$S6 \le 3.5 \qquad [\text{mol/time}] \tag{4.23}$$

The performance of the three Cases is compared through the loss function, computed by the difference between the cost (negative of profit) achieved by the solution of the optimization problem in eq.(4.22) ($Cost^{\exp}$) and the optimum cost ($Cost^{opt}$, solution of eq.(4.20)). The results can be observed in figure 4.6, which shows the loss profile with respect to the disturbances for each Case.

Table 4.1. - Set of controlled variables for each Case
(AV: artificial variable)

Case	c1	c2	c3
A	P_{reac}	T_{flash}	S6
B	AV	AV	AV
C	AV	AV	AV

Figure 4.6 - Steady state analysis results: (A) “classic” MPC, (B) MPC with artificial SOC variables and (C) MPC with zone control and SOC targets

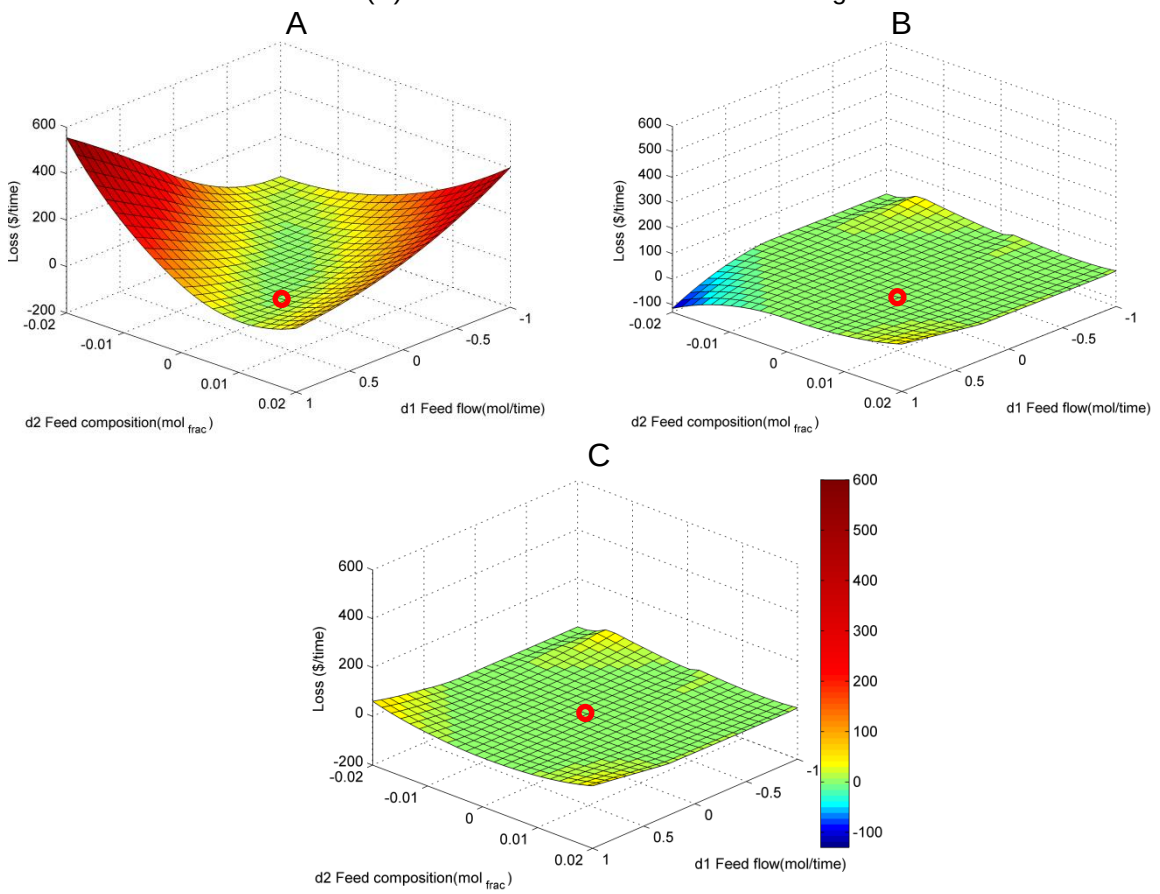

The results observed in Figure 4.6 show that the classical MPC approach (Case A) obtained the worst steady state performance with maximum profit loss value of approximately 10 percent. In comparison, the control of SOC variables (Cases B and C) presented only 1 percent of loss in the worst case. It is important to notice the difference between the performances of Cases B and C. As long as Case B does not consider the constraint satisfaction of all process variables, this case obtained a negative loss region where constraint eq.(4.23) is violated (it represents a better economic performance, but for an infeasible operating point). On the other hand, Case C enforces constraint eq.(4.23), since the controlled variable S6 is handled in the zone control approach. For this reason, Case C does not present the same behavior (negative loss region) observed in Case B.

4.4. Case Study 2: BTX separation process

In this Section, the novel MPC with zone control and SOC targets is implemented in a second case study, a BTX (Benzene, Toluene and p-Xylene) separation by a multi-column distillation process, described by Leer (2012) and depicted in figure 4.7. In this process, a BTX mixture feeds the first column, where benzene is removed in the top flow rate. The bottom product, rich in Toluene and p-Xylene, feeds the second column where Toluene is removed in the top flow rate and Xylene from the bottom.

Figure 4.7 – BTX process schematic representation

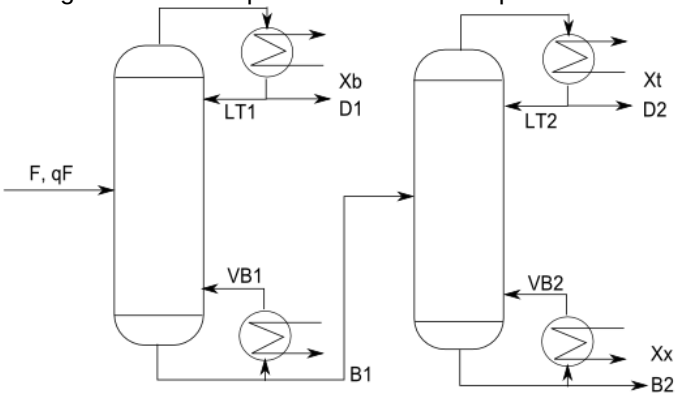

The columns are modeled as a sequence of ideal equilibrium stages, with constant relative volatility and vapor flow rate through all the stages. The liquid flow rate is given by the Francis weir formula. Both columns have 41 theoretical equilibrium stages, including the total condenser and the partial reboiler, and the feed tray corresponds to stage 21, counting from the bottom to the top. More details about this model as well as the model built in AMPL® can be found in Leer (2012).

In the first column, seven states are considered as measured variables, including the distillate Benzene composition Xb, 3 stage temperatures at the rectification section and 3 at the stripping section. The second column has eight measured variables, including the Toluene and p-Xylene molar compositions (Xt and Xx), and equivalent stage temperatures of first column. All of these states comprise the vector of measured variables, $y(k)$ in eq.(4.5).

It is assumed that the molar holdups in the condenser drums and reboilers are controlled by the distillate and bottom flow rates, respectively. Thus, the problem has four steady state degrees of freedom, which are chosen as $u = \left[LT1, VB1, LT2, VB2 \right]$ in the economic optimization problem given by eq.(4.24).

$$\begin{aligned} \min_{u} \quad & Cost^{opt} = p_F F + p_V (VB1 + VB2) - p_B D1 - p_T D2 - p_X B2 \\ & Xb \geq 0.95 \\ & Xt \geq 0.95 \\ & Xx \geq 0.95 \\ & VB1 \leq 4.080 \quad [\text{mol/min}] \\ & VB2 \leq 2.405 \quad [\text{mol/min}] \end{aligned} \tag{4.24}$$

where D and B are the distillate and bottom flow rates, F is the feed flow rate, and p_F, p_V, p_B, p_T and p_X are respectively the prices of feed, vapor, benzene, toluene and xylene streams. Relevant model parameters are given in table 4.2.

Table 4.2 – Parameters values

Feed F [kmol/min]	Liquid fraction qF	Vapor price p_V [$/kmol]	Feed price p_F [$/kmol]	Benzene price p_B [$/kmol]	Toluene price p_T [$/kmol]	p-Xylene price p_X [$/kmol]
1.41	1.00	0.035	1.00	1.00	3.00	2.00

The two disturbances acting on the system are the molar fraction of benzene and toluene in the feed stream, described by eq.(4.25).

$$\begin{aligned} z_{ben}^{F} &= 0.40 + d1 \\ z_{tol}^{F} &= 0.20 + d2 \\ z_{xyl}^{F} &= 1 - z_{ben}^{F} - z_{tol}^{F} \end{aligned} \tag{4.25}$$

Figure 4.8 depicts the cost profile with respect to the disturbances ($d1$ and $d2$), within a range of 5% mole fraction. The active set map for this region is shown in Figure 4.9, which presents four different active sets, including the minimum toluene product concentration Xt, and the maximum boil up rates for the reboilers $VB1$ and $VB2$.

Figure 4.8 – Cost profile with respect to disturbances

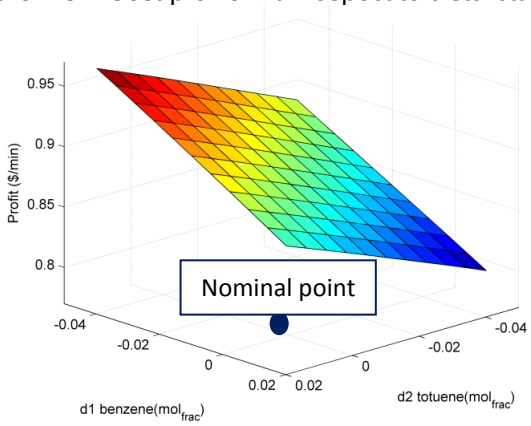

Figure 4.9 – Active set map

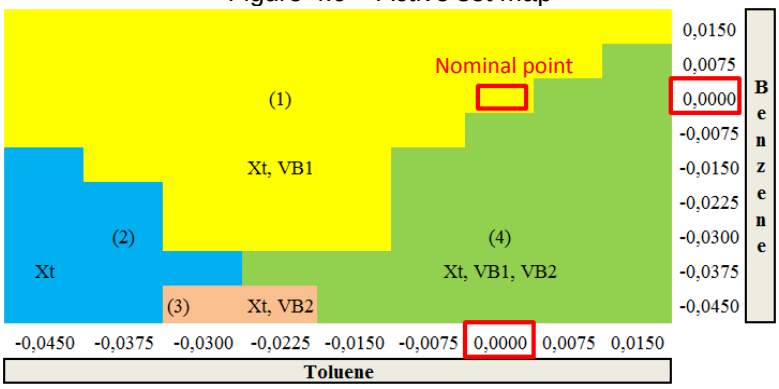

4.4.1. Steady state analysis

Three steady state experiments are carried out to compare the economic performance of different MPC approaches under presence of disturbances. Once more, Case A simulates the classical MPC control approach, where the three product concentrations and one tray temperature in the first column ($TC1_{10}$) are controlled variables. Case B applies the control of four artificial SOC variables computed by the linear combination of 12 measured tray temperatures defined in Section 4.4. In this case, zone control of the constrained variables (product concentrations) is not considered. Experiment C illustrates the new MPC with zone control and SOC targets developed in the present work; in this case, the same artificial SOC variables are controlled as in Case B. However, the zone constraints are enforced to respect the lower bounds on product concentrations.

Mathematically, the experiments are conducted by the solution of the optimization problem in eq.(4.26), for a given disturbance value ($d1$ and $d2$).

$$
\begin{aligned}
\min_{u} \quad & Obj = \left(c1 - c1^{sp}\right)^2 + \left(c2 - c2^{sp}\right)^2 + \left(c3 - c3^{sp}\right)^2 + \left(c4 - c4^{sp}\right)^2 \\
\text{subject to:} \quad & \text{Steady State Model} \\
& \text{Cost}^{\exp} = p_F F + p_V (VB1 + VB2) - p_B D1 - p_T D2 - p_X B2 \\
& VB1 \le 4.080 \qquad [\text{kmol/min}] \\
& VB2 \le 2.405 \qquad [\text{kmol/min}] \\
& -0.015 \le d1 \le 0.045 \quad [\text{mol frac}] \\
& -0.015 \le d2 \le 0.045 \quad [\text{mol frac}]
\end{aligned}
\tag{4.26}
$$

where c are the controlled variables summarized in Table 4.3 and c^{sp} are their set point values computed at the nominal point ($d1 = 0$ and $d2 = 0$). The sensitivity information required for the null space matrix, F, is also computed at this point, by solving problem (4.26), nested within finite difference perturbations. Additionally, Case C, considers the constraints in eq.(4.27).

Table 4.3 – Set of controlled variables for each experiment

Experiment	c1	c2	c3	c4
A	Xb	TC1_10	Xt	Xx
B	AV*	AV	AV	AV
C	AV	AV	AV	AV

*AV – Artificial variable computed by the null space method;

$$
\begin{aligned}
& Xb \ge 0.95 \\
& Xt \ge 0.95 \\
& Xx \ge 0.95
\end{aligned}
\tag{4.27}
$$

Performance of the three experiments is compared regarding the Profit Loss function, computed by the difference between the cost achieved by the solution of the optimization problem in eq.(4.26) ($Cost^{\exp}$) and the optimum cost ($Cost^{opt}$, solution of eq.(4.24)). The results can be observed in figure 4.10, which shows the Loss profile with respect to the disturbances for each experiment.

Figure 4.10 – Steady state analysis results: (A) “classic” MPC, (B) MPC with artificial SOC variables and (C) MPC with zone control and SOC targets

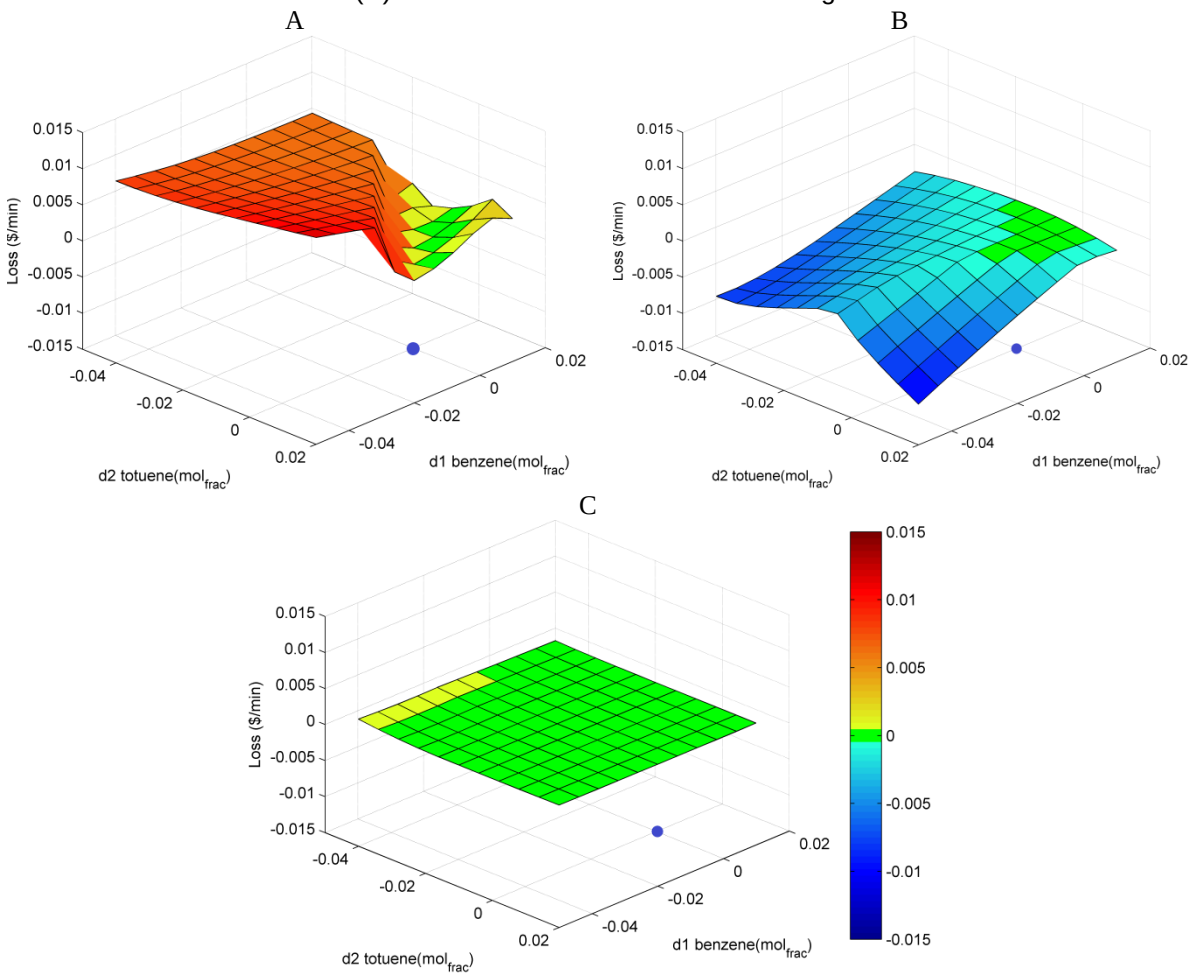

The results show that the Loss function is largely influenced by the choice of the control structure (see figure 4.10). Note that Case A, the “classical” control approach, has once again the worst performance regarding this set of disturbances, yielding lower values of profit loss close to the nominal point, while the largest part of its area presents losses greater than 0.005 $/min with a maximum of 0.01173 $/min. In this case, it was expected that the “classical” MPC approach would lead to suboptimal operation after a given disturbance, at least until the RTO module updates the set point values.

On the other hand, Case B simulates the control of the artificial SOC variables without enforcing the product constraints. This case shows a profit loss close to zero around the nominal point and negative profit Loss in the remaining area. This behavior is explained by the violation of the product concentration constraints. In other words, in presence of the analyzed disturbances, control of these set points

without a policy of constraint satisfaction (zone control) leads to an increased profit because the product stream does not satisfy specifications. (Here the toluene concentration is less than 95% at top of the second column).

In conclusion, Case C shows the best performance among the analyzed approaches, with a flat Loss profile surface close to zero, and maximum profit Loss value of 0.00076 $/min. In this case, the constraints in eq.(4.27) enforce the minimum product concentration values, at the expense of yielding offsets in the controlled variables, as expected by the prerogatives of this new method.

4.4.2. Dynamic analysis

The BTX process described in section 4.4 is now modeled dynamically in Matlab® and simulated as a system of 246 non-linear ordinary differential equations, to represent the process. The linear dynamic models used in the MPC formulations are identified by transfer functions in step response experiments at the nominal point, and then, converted to a state-space model (eq.(4.5)). The "classical" MPC is implemented in the case study through the MATLAB® MPC Toolbox 4.1.2, using the controlled variables defined in Case A of table 4.3. On the other hand, the MPC with zone control and SOC target (Case C) is applied by solving the optimization problem defined in eq.(4.19) using the interior-point algorithm implemented in the MATLAB® function "*quadprog*". Case B was not considered because product specifications were already violated at steady state.

The dynamic experiment comprises the simulation of both MPC approaches starting from the optimum economic point. At time zero, the RTO layer computes the optimum economic set points and the sensitivity analysis (matrix F of eq.(4.2)). Then, a disturbance is introduced ($d1 = -0.04$) and the controllers drive the process towards a new operational steady state point. Finally, the RTO layer updates the set point values to the actual economical optimum. Figure 4.11 depicts the profit obtained by approaches A and C in these settings.

Figure 4.11 – Comparison of the profit obtained by each MPC approach

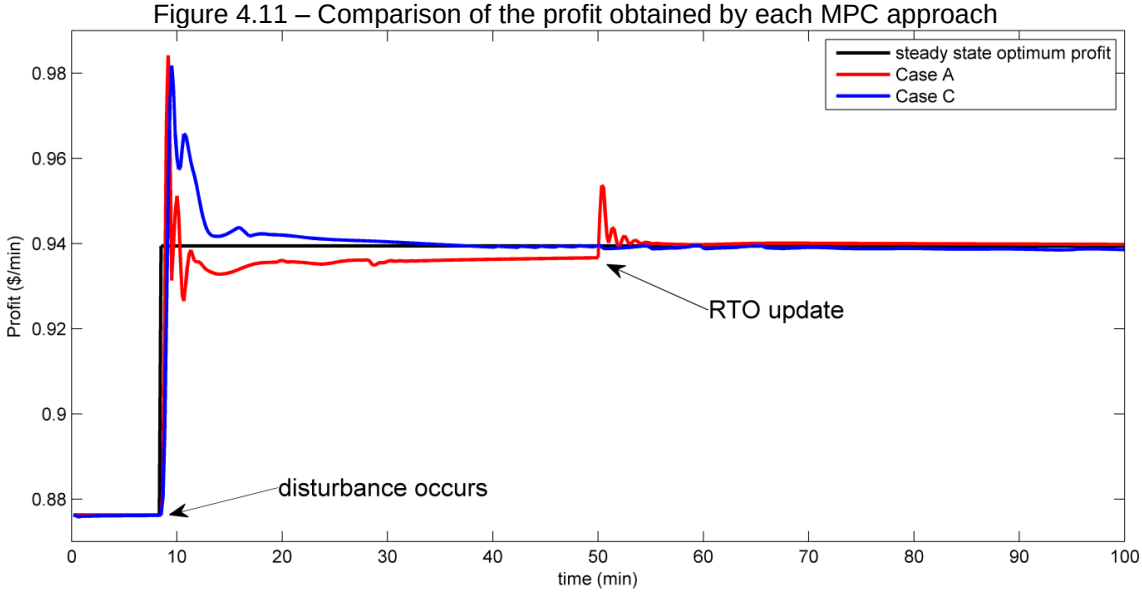

Note that in figure 4.11 the MPC with zone control and SOC targets (Case C) yields higher profit than the conventional MPC (Case A) during the transient period between the RTO runs (from 9 to 50 minutes). After introducing the disturbance at t = 8 min, the new MPC approach settles to the economic optimum, whereas the classical approach maintains the process at a suboptimum operating point. At 50 minutes, when a new RTO cycle is performed, the system is subject to a new upset in the classical approach implementation, in order to drive the process to the new optimum economic set point. This is not observed in the implementation of zone control MPC.

Figure 4.12 – Constrained variables profile

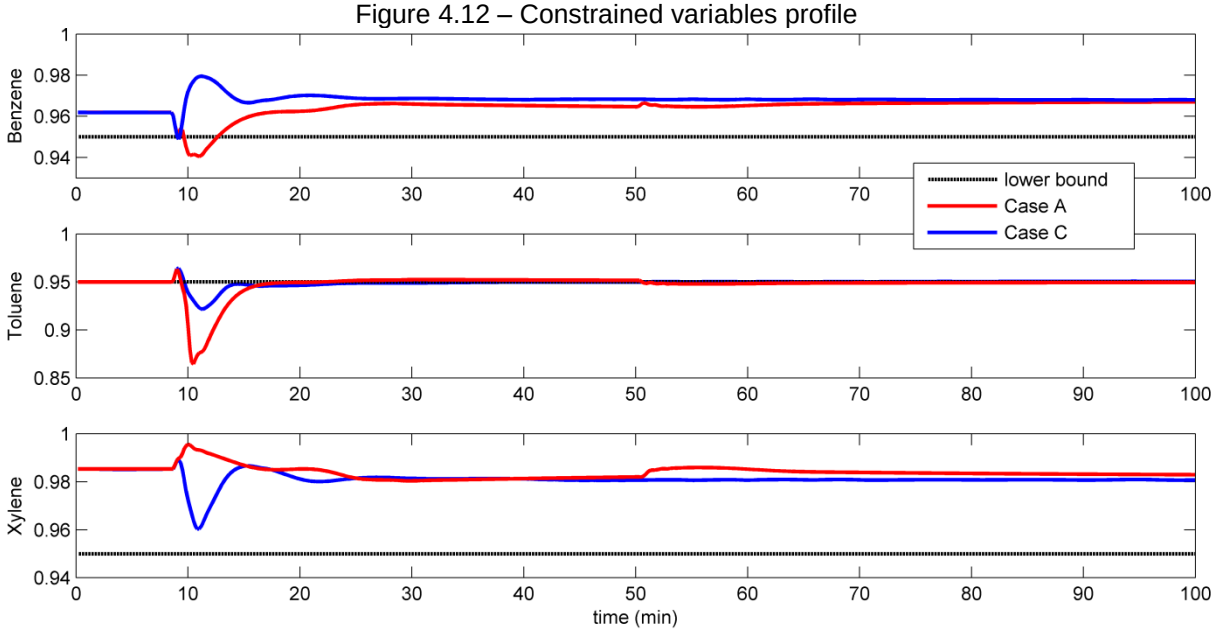

Figure 4.12 shows the concentration profile of each product stream. It can be observed that, after the disturbance, the Benzene concentration starts to decrease in both cases; however, only Case A violates the specification stream constraint. Observing the concentration profile of the Toluene stream, we observe better performance of the zone control policy, which yields out of specification product over a shorter period. In particular, the product stream has a minimum toluene purity of 92.2%, compared to 86.6% yielded by the classical approach. Moreover, it can be noticed that Case C does not present any constraint violation for the inactive constraints (Benzene and Xylene).

Figure 4.13 – Manipulated variables

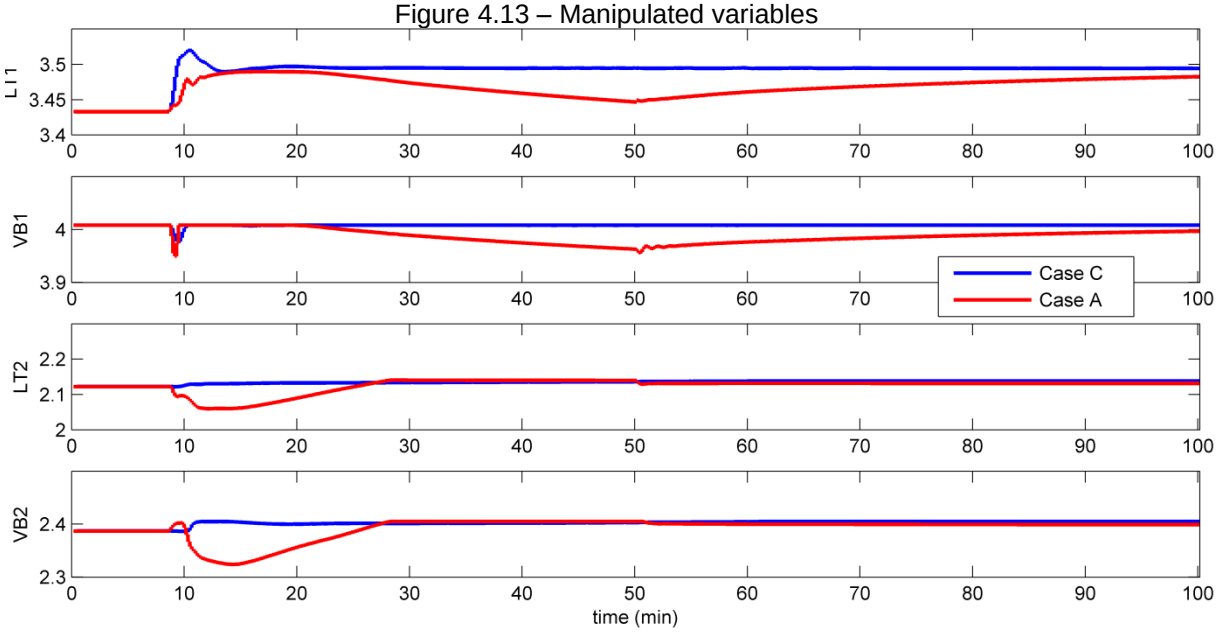

Lastly, manipulated variable profiles are depicted in Figure 4.13. It is important to notice that the MPC with zone control and SOC targets yields smaller control actions than the classical approach. This is mainly observed in the manipulated variable behavior of the first Column, which does not change in comparison to Case A. Another important consideration is the ability of the new approach to stabilize the system after the disturbance, which is not observed in the classical approach before the RTO updates the set point values, at 50 minutes.

4.5. Partial conclusions

This study presents a RTO framework with a new MPC algorithm based on zone control and SOC variable targets. The new approach is demonstrated on two case studies: an ammonia production plant and a multi-column distillation process. The results at steady state and dynamic operation show better economic performance of the new approach in comparison with classical RTO/MPC, requiring less effort from the manipulated variables to keep the process under control. This characteristic improves the process stability, since it requires less process changes when the RTO is evaluated. Moreover, the zone constraint policy outperforms the classical target approach regarding the constraints satisfaction, showing faster responses to drive the concentration profile back to their zones or targets. These facts indicate that the integration between RTO and SOC can be a good alternative to alleviate the drawback of low frequency updates in RTO. Furthermore, the zone control policy is a reliable option to handle the problem of active set changes observed in the SOC methodology.

The concepts of SOC methodology are used in the next Chapter to evaluate different structures of the VRD process, and then, to estimate possible improvements of integrating RTO with SOC in this kind of process.

The main findings presented in Chapter 4 corresponds to the paper "Integrating self-optimizing control and real-time optimization using zone control MPC", published in the Journal of Process Control, volume 34, pages 35-48, 2015.

5. Practical implementation of an RTO approach

The objective of this Chapter is to discuss the practices of the RTO implementation in a Vapor Recompression Distillation (VRD) process. This is carried out by performing a complete RTO cycle (in open loop), using information provided by the real plant.

As a typical rule of thumb the RTO benefits may range from 0 to 50%, which is justified by day-to-night variations and changing market conditions. For this reason, the RTO approach has been largely used in chemical and petrochemical industry. Some estimates point out around 250 to 300 RTO implementations using commercial software, not including in-house applications (DARBY et al., 2011b).

Several practical RTO implementations are reported in literature for a number of different petrochemical processes. For instance, Sildir *et al*. (2013) applied the RTO methodology to a hydrocracking process including fractionation columns. The results showed that the control framework is able to drive the process to the optimum condition determined by the economic optimization. Shokri *et al.* (2009) discussed the applicability of the RTO methodology in refineries, showing several successful implementations around the world and their economical benefits. Ramdial *et al.* (2009) applied an RTO like framework to a petroleum field, which was able to meet the gas market demands with increase of 7% in the condensate production. Bader and Guesneux (2007) implemented the RTO methodology in a hydrodesulphurization (HDS) unit with capacity to process about 870,000 ton per year, reducing in about 20% the H_2 makeup and the reactor octane loss. Rotava and Zanin (2005) compared the potential of implementing multivariate control (MVC) and RTO. The analysis of two industrial cases studies showed that RTO is preferable, since it considered the trade-off between energy consumption and production with a rigorous nonlinear model. Basak et al. (2002) developed an in-house RTO solution for an industrial crude distillation unit, increasing the profit around 8.5 million dollars per year. Geourgiou et al. (1998) discussed the application of RTO in an ethylene production unit, pointing out improvements in plant operations and maintenance.

All the papers above describe the implementation and the benefits of RTO approaches. This is conducted in this Chapter for the VRD case study. Firstly, Section 5.1 describes the phenomenological steady-state model used in our RTO cycle. Then, Section 5.2 comments about the steady-state identification procedure used to obtain the plant information. Further, the description of the parameter estimation is performed in Section 5.3, where the plant/model adequacy is evaluated. Section 5.4 discusses the economical improvements reached by the RTO approach. The comparison between the implementation of RTO or MPC alone is carried out in Section 5.5. Finally, the partial conclusions are drawn in Section 5.6.

5.1. Process description

The present section describes a mathematical model suitable for RTO implementation on an industrial-scale depropanizer column (in Paulínea refinery owned by Petrobras S.A.). VRD is a well-known highly integrated energy process, widely used in the chemical industry to split close-boiling mixture, such as propylene and propane (ANNAKOU; MIZSEY, 1995). The main characteristic of VRD process is that additional mechanical energy is added to the overhead vapor stream by a compressor; then this stream is used to boil up the mixture in the reboiler, reducing the total amount of demanded energy compared to a traditional distillation scheme.

The highly interlinked structure involved in the VRD process, coupled to the nonlinearities and the large number of equations (around 8000 in this specific case) make the simulation particularly difficult to converge in sequential modular simulators (AYDIN; BENALI, 2009; HEYEN; LEDENT; KALITVENTZEFF, 1994), requiring an equation oriented approach to handle the convergence obstacles generated by this recycle system (MEIXELL; GOCHENOUR; CHEN, 2010). In the present work the VRD process is modeled in the software EMSO (Environment for Modeling, Simulation and Optimization), which is an equation oriented simulator conceived and developed in a joint effort of Brazilian universities, Petrobras and Braskem, to be a tool for educational and industrial purposes (RODRIGUES; SOARES; SECCHI, 2010). Some features that make EMSO adequate to RTO implementation are the

calculation of first order derivatives via automatic differentiation, robust nonlinear algebraic solver and modules for parameter estimation and optimization.

The schematic structure of VRD process is depicted in Figure 5.1. First, a low molecular weight hydrocarbon mixture (mainly propylene and propane) enters the distillation column, where high-purity propylene (99.95%) is obtained as overhead product stream D, and propane (95%) is obtained as the main product at the bottom stream B. The overhead stream is mixed with vapor stream from the distillate drum, and then, it is compressed to increase its condensing temperature. After that, the largest part of the compressor outlet stream feeds the reboiler (F_{boil}), while the rest (about 10%) is condensed with cooling water (F_{cool}) to control the column pressure. Subsequently, the propylene streams (hot stream) from reboiler and condenser expand through throttle valves, returning to the distillate drum, where a portion of the liquid is sent to the column as reflux stream (R), and the other part is stored as high purity propylene (D).

Figure 5.1 - Schematic representation of the VRD process

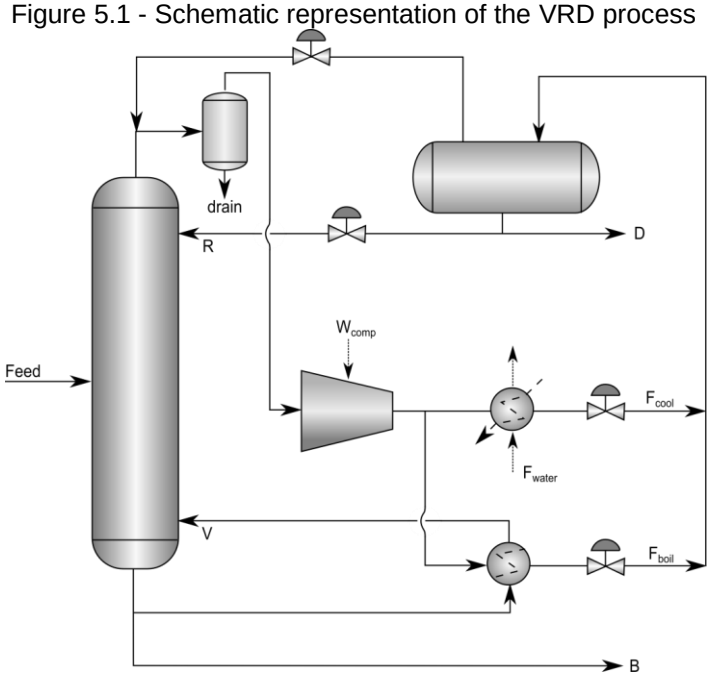

The equipment in this process are modeled considering thermodynamic aspects only, using thermodynamic properties calculated with Peng and Robinson (PR) equation of state and predictive-SRK mixing rule (HOLDERBAUM; GMEHLING,

1991), which is provided by the IISE (Industrial Integrated Simulation Environment) thermodynamic package of VRtech® company.

The main characteristics of each equipment are given below and the summary of equipment equations is shown in Appendix G.

Distillation Tower

This equipment is modeled as a collection of individual trays (numbered from top to bottom), which are described by rigorous mass, equilibrium, summation and heat (MESH) equations. The column has 197 theoretical plates with feed stream at 157th tray. The pressure profile is given by a linear approximation where the top and the bottom pressures are set at constant values. Mass transfer aspects are included in the model via vapor Murphree efficiencies (adjustable parameter), two for the rectification and one for the stripping section.

Compressor

The rotary compressor is modeled using isentropic efficiency, η_{CP} , and specified discharge pressure. The problem with this formulation is that, in the real process, the isentropic efficiency is not a constant value, changing from different operating points. For this reason, it is proposed to replace the constant value of η_{CP} by a function of the product of delta pressure (ΔP_{CP}) times mass flow rate (Q_{CP}). Figure 5.2 shows the measurements of three years of process operation where it is possible to observe a linear correlation between these variables.

Figure 5.2 - Measured efficiency against the product $\Delta P_{CP}.Q_{CP}$

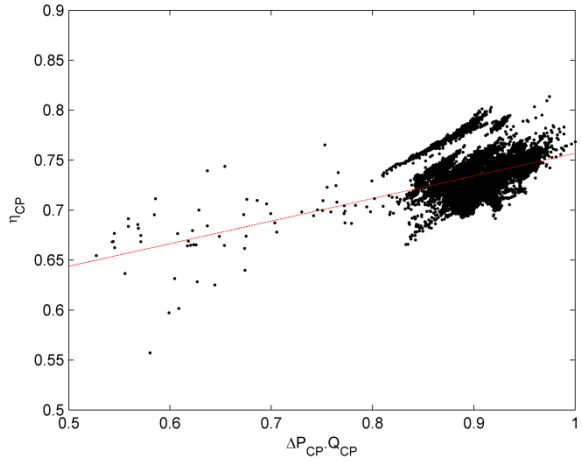

Equation 5.1 describe the linear correlation obtained from this data and Figure 5.3 shows the comparison of the predicted and measured compressor power using the correlation in eq.(5.1). It is worth to notice that the model is able to predict the power consumption with small deviations.

$$\eta_{CP} = 0.5307 + 3.4619e^{-4}\left(Q_{CP}.\Delta P_{CP}\right) \qquad 5.1$$

Figure 5.3 - Comparison of predicted and measured power

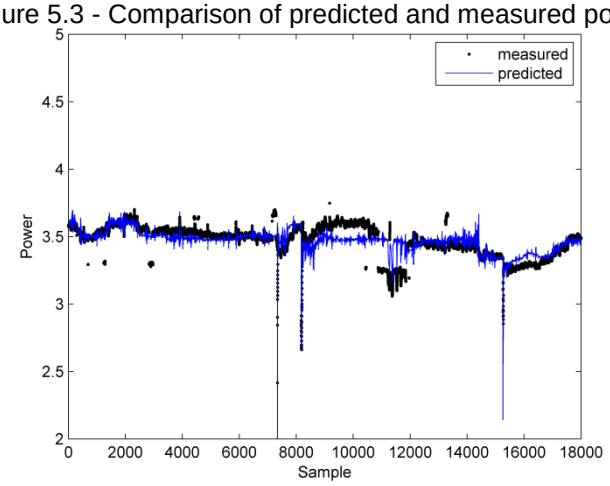

Reboiler

The reboiler is modeled as an adiabatic countercurrent heat exchanger, in which the temperature of the inlet streams is given by the solution of column and compressor models. The vapor fraction of the cold outlet stream (propane to column) is set by an adjustable parameter and the temperature of the propylene outlet stream is

empirically determined using plant historical data. The histogram, given in Figure 5.4 B, demonstrates that the difference of temperatures between the propylene outlet stream and propane inlet stream is approximately constant, about 0.547°C. For this reason, the propylene outlet temperature is set to 0.547°C higher than the propane inlet stream.

Figure 5.4 - Historic data of the reboiler temperature profile

A

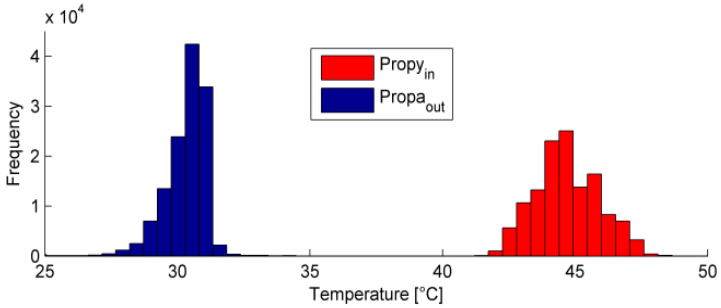

B

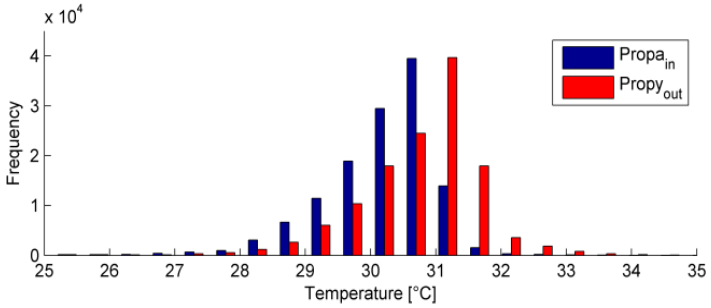

Cooler

The model of this equipment is similar to the reboiler, but in this case the cooling water flow rate is estimated by a function of propylene flow rate, overall heat transfer coefficient (adjustable parameter) and the logarithmic mean temperature difference. This formulation requires the specification of the temperature in the outlet hot stream, which is given by analysis of the historical data. Figure 5.5 depicts the histogram of measured temperatures in the cooler. One can see that the difference between hot outlet stream and cooling water inlet stream temperature is almost constant at 0.05 °C. justifying the temperature of the hot outlet stream to be set 0.05 °C higher than the measured temperature of cooling water.

Figure 5.5 - Historic data of the cooler temperature profile

A

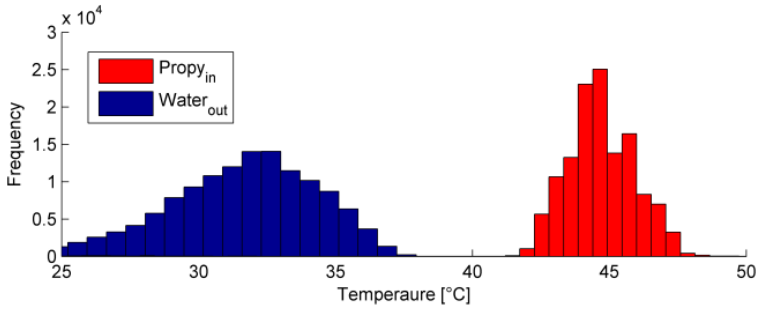

B

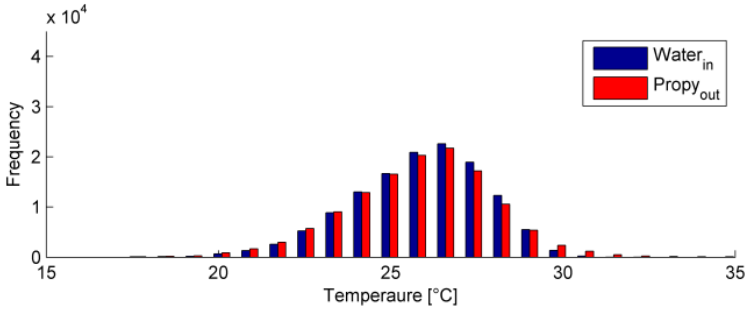

Throttle valves

The expansion valves are modeled as an adiabatic and isenthalpic process, in which the outlet stream is in liquid-vapor equilibrium. The outlet stream pressure is set as the measured pressure in the distillate drum.

Feedstock characteristics

Figure 5.6 shows the distribution profile of the feed stream flow rate (A) and components concentration (B and C), in a period of three operating years. It is important to notice that the process operates in a large range of feed conditions, but in about 72% of times the flow rate is between 7.5 and 12 mass/time units, while the concentration profiles distribution is similar to an uniform distribution, varying from 60 to 80% for propylene and 20 to 40% for propane.

Figure 5.6 - Feed stream characteristics

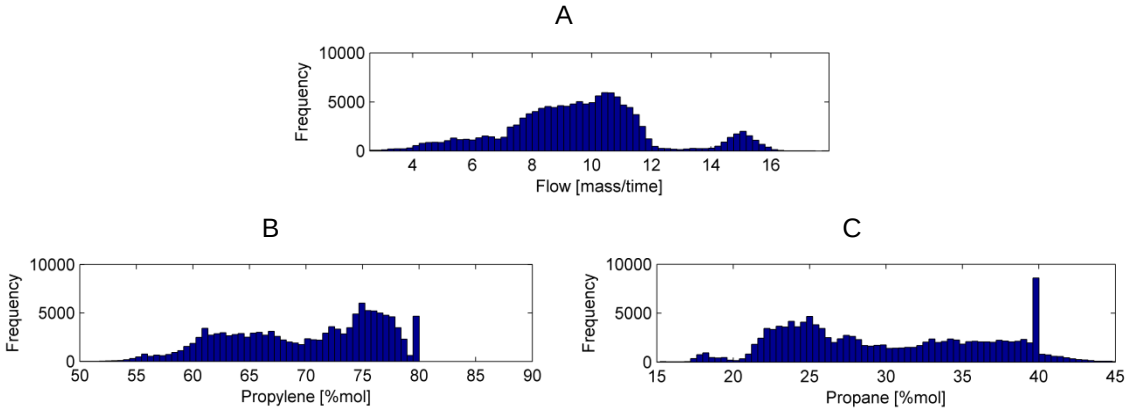

Product stream characteristics

Figure 5.7 displays the distribution profile of the mass flow rate and contaminant concentration in the overhead and bottom product streams. It may be appreciated that the process is able to handle the disturbances in the feedstock, keeping the contaminant concentration in the overhead stream less than its upper bound (5000 ppm), at least for 97.11% of sample times. In contrast, the contaminant concentration in the bottom stream is greater than its upper limit (5%) in 47.50% of time, resulting in economic loss due to large amount of propylene sent to the bottom stream.

Figure 5.7 - Products characteristics

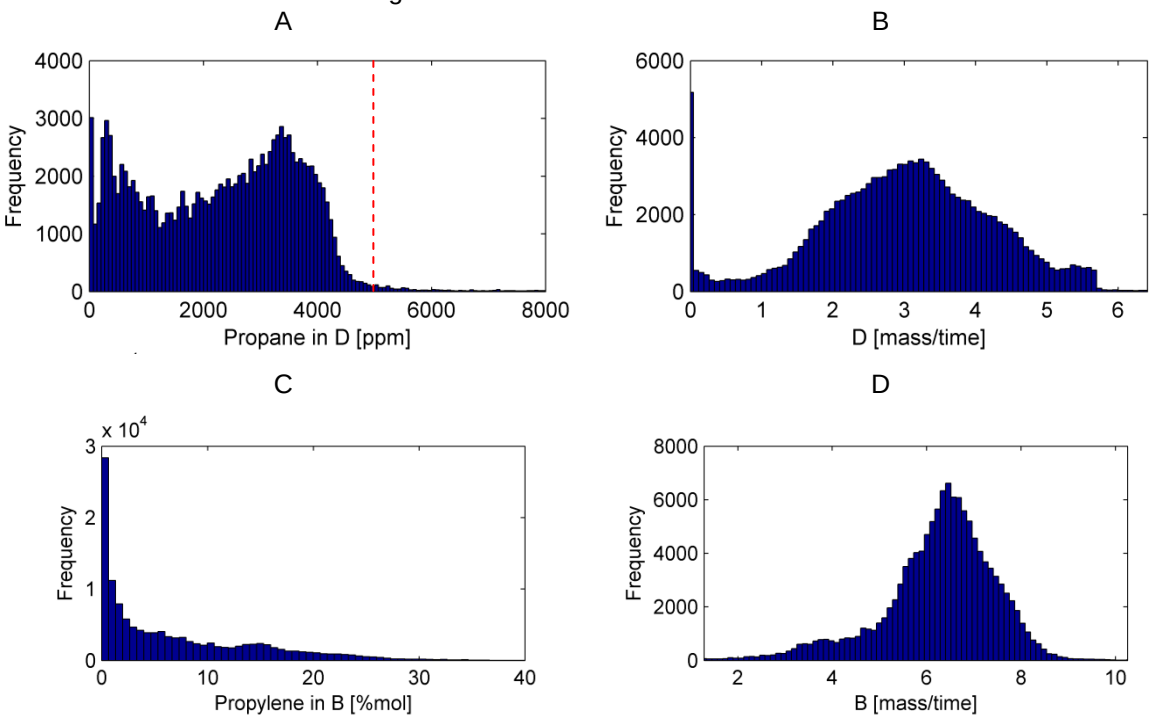

5.2. Steady state identification

As discussed in previous Chapters, the RTO methodology is based on steady-state phenomenological models, requiring stationary information to update the key parameters at each iteration. In this subsection, the steady-state identification (SSI) method used in this work is presented.

Several different approaches of SSI have been developed in the literature, for instance, methods based on F-like test (CAO; RHINEHART, 1995a), wavelet theory (JIANG et al., 2003), polynomial equations (LE ROUX et al., 2008) and ARX (Auto-Regressive with eXogenous inputs) models (RINCON; LIMA; LE ROUX, 2015). Basically, each of these methods compute quantities from the measured states that are compared to critical values; if this comparison satisfies a determined condition the process is considered to be in steady-state. The problem associated with all these approaches is the need for adequate tuning, which relies on specific measurements characteristics such as noise and frequency. Rincon and coworkers (2015) compared different approaches and found that, after proper tuning, the F-like test presents similar levels of performance than more complex methods, which motivated its application in our case study.

The Cao and Rhinehart (1995) SSI method is an F-like test, which basically compares two variance estimates computed in different ways. First of all, the measured state (X_i) is filtered by an exponential filter, using λ_1 as smoothing factor (eq.(5.2)). Then the filtered value ($X_{f,i}$) is used to compute the first variance estimate ($\upsilon_{f,i}^2$) in eq.(5.3), while the second variance estimate ($\delta_{f,i}^2$) is calculated only based on the measured states (X_i and X_{i-1}), eq.(5.4). After that, the ratio between these two variance estimates is used in the SSI index R_i (see, eq.(5.5)), which is finally compared to a critical value R_{cr}. If R_i is less than R_{cr} the process is considered at steady-state. Otherwise, the process is assumed in transient regime.

$$X_{f,i} = \lambda_1 X_i + (1-\lambda_1) X_{f,i-1} \tag{5.2}$$

$$\upsilon_{f,i}^2 = \lambda_2 \left(X_i - X_{f,i-1} \right)^2 + \left(1 - \lambda_2 \right) \upsilon_{f,i-1}^2 \tag{5.3}$$

$$\delta_{f,i}^2 = \lambda_3 \left(X_i - X_{i-1} \right)^2 + \left(1 - \lambda_3 \right) \delta_{f,i-1}^2 \tag{5.4}$$

$$R_i = \frac{\left(2 - \lambda_1 \right) \upsilon_{f,i}^2}{\delta_{f,i}^2} \tag{5.5}$$

Seven measured variables are chosen to detect the process steady-state: three stream flow rates (feed, overhead and bottom product) and four concentration measurements (propylene composition of feed and bottom product and propane composition in feed and overhead streams). The smoothing factors λ_1, λ_2 and λ_3 are determined by visual inspection, resulting in 0.7, 0.05 and 0.006 respectively, while the R_{cr} value is set equal to 2. Representative steady-states are selected as information for the parameter estimation performed in the following subsection.

5.3. Parameter estimation

In this section the Rotational Discrimination (RD) methodology is applied to the VRD case study, using real information from the propylene production unit of REPLAN refinery of Petrobras. The tests are conducted in the software EMSO by using a RD routine written in C++ language (see the algorithm depicted in Figure 3.2).

Firstly, the RD routine is tested in a small case study to evaluate the correctness of its implementation, where these outcomes are compared with a classical weighted least squares (LSq) approach already available in the EMSO software package. The case study chosen in this test is the Williams Otto chemical reactor, previously described in Section 2.3 of this thesis. Basically, this process is composed of a CSTR reactor, which is fed with components *A* and *B* to produce the products *P* and *E*, and a waste byproduct *G*.

Five different operating points are simulated with the original parameters values (Region 1 of Table 2.1). Then, the obtained values of *P* and *E* concentrations are used as measured variables for the parameter estimation problem, which is solved with RD and LSq routines. Both methods are set with the same termination criteria tolerance (1e-9).

Table 5.1 summarizes the results obtained by both approaches, where the values of the objective function and parameters are compared. It is worth to observe that RD approach presents smaller values of the objective function, but with a larger number of objective function evaluations than the LSq method. The difference in the number of objective functions evaluations does not necessarily represent a significant discrepancy in computational time, which is 0.108 and 0.056 seconds for RD and LSq respectively, at least for this small case study.

Another important remark about the RD results is related to the parameters values. One may notice that RD approach presents smaller parameter deviations from the initial values in comparison to LSq. This fact indicates that the algorithm is able to perform what it is aimed to do, which is to minimize the objective function without increasing the parameter inflation resulting from identifiability issues.

Table 5.1 - Summary of the parameter estimation results for the WO case study

	Parameter values			**Parameter deviation from the initial value**	
	Initial value	**LSq**	**RD**	**LSq**	**RD**
*ObF value	-----	2.85831e-04	2.80622e-04	-----	-----
*ObF evaluations	0	22	69	-----	-----
$\eta p1$	1.6e06	5.2544e06	1.4081e06	228.40%	-11.99%
$\eta p2$	7.2e08	2.2928e09	7.8325e08	218.45%	8.78%
$\eta p3$	2.6e12	1.9400e13	2.2481e12	646.14%	-13.53%
$Ea1$	6600	7154	6646	8.39%	0.70%
$Ea2$	8300	8109	8271	-2.30%	-0.35%
$Ea3$	11000	11275	11051	2.50%	0.47%

*ObF: objective function

The results of the first case study show that the RD algorithm written in C++ is well implemented. The next step is to conduct the parameter estimation in the VRD case study using the representative steady-state found by the procedure described in Section 5.2.

In this parameter estimation problem, 6 model parameters are used to fit the process data and other 5 measured states are set as "parameters" in order to be reconciliated; the detailed list of parameters can be appreciated in Table 5.2. In addition, 9 states are set at their measured values and 23 measured states are used in the objective function (see Table 5.3). The standard deviations used in the objective function are also computed from the historical data and displayed in Table 5.3.

Table 5.2 - Parameters used in the VRD estimation

Parameter type	Description	Unit	Lower bound	Upper bound
Model parameter	Column - Murphree efficiency section 1	------	0.5	1.2
	Column - Murphree efficiency section 2	------	0.5	1.2
	Column - Murphree efficiency section 3	------	0.5	1.0
	Column - heat exchanged with the environment	W	0	5000
	Cooler - overall heat transfer coefficient	W/m^2K	200	1000
	Reboiler - vapor fraction of the outlet propane stream	------	0.25	1.0
Reconciliated data	Propylene composition in feed stream	%-mol	20	90
	Feed stream flow rate	mass/time	6.4e3	1.5e4
	Reflux flow rate	mass/time	6.4e4	1.1e5
	Bottom product flow rate	mass/time	2.6e2	5.1e3
	Column top pressure	kgf/cm^2	8	12

The parameter estimation algorithm is executed and converges in about 17 minutes, which is a small period when compared to the process settling time of 10-12 hours. Figure 5.8 shows the temperature profile of the column after the parameter estimation. It can be seen that the prediction has a good agreement with the measured values.

Figure 5.8 - Temperature profile of VRD column after parameter estimation

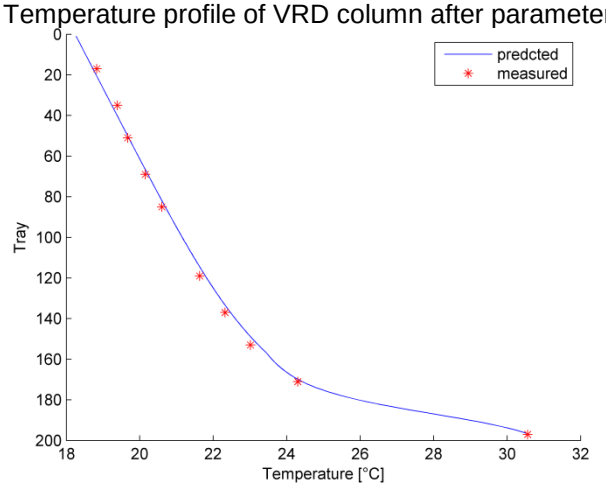

Table 5.3 displays the values of the measured and predicted states, organized by equipment. One can observe that the deviation between the process and the model is not greater than 5% for most of the measured states. The highest deviation is obtained in the propane concentration at the overhead stream, which is not an issue since the observed deviation is still smaller than measurement variance ($559ppm^2$ against $900\ ppm^2$).

Four out of six parameters used in the parameter estimation reach their limits. The three Murphree efficiencies are adjusted to their upper bounds, probably to compensate possible inaccuracies of the thermodynamic model. Moreover, the vapor fraction at the reboiler outlet stream (vapor to the column) reaches its lowest value.

In general, the results demonstrate that the model is able to reproduce the process behavior and can be applied to the RTO algorithm. The next section presents the economic optimization of this updated model, in order to evaluate the economical benefits related to the RTO implementation.

Table 5.3 - Summary of the parameter estimation results for the VRD process case study

	Process variable	Unit	Measured value	Std	Predicted value	Deviation %
Feed stream	Temperature*	°C	24.96	0.03	24.96	------
	Pressure*	kgf/cm²	11.49	0.01	11.49	------
	Flow rate**	mass/time	7.32	0.26	7.19	-1.72
	Propylene concentration**	%-mol	78.03	0.15	77.26	-0.98
	Propane concentration**	%-mol	22.00	0.14	22.73	3.32
	Ethane concentration*	ppm	0.13	0.14	15.84	------
Compressor	Suction temperature	°C	19.20	0.03	18.27	-4.85
	Discharge temperature	°C	44.88	0.06	46.77	4.22
	Suction Pressure	kgf/cm²	10.14	0.00	9.92	-2.16
	Discharge Pressure*	kgf/cm²	16.17	0.02	16.17	------
	Power	MW	3.51	0.01	3.36	-4.12

continue...

...

	Process variable	Unit	Measured value	std	Predicted value	Deviation %
Tower	Top pressure**	kgf/cm²	10.04	0.01	9.92	-1.19
	Tray 17th**	°C	18.83	0.02	18.73	-0.54
	Tray 35th**	°C	19.39	0.02	19.24	-0.77
	Tray 51st**	°C	19.67	0.02	19.70	0.13
	Tray 69th**	°C	20.15	0.02	20.22	0.34
	Tray 85th**	°C	20.60	0.02	20.69	0.46
	Tray 119th**	°C	21.63	0.02	21.78	0.73
	Tray 137th**	°C	22.32	0.02	22.47	0.66
	Tray 153rd**	°C	23.01	0.02	23.23	0.94
	Tray 171st**	°C	24.30	0.07	24.42	0.50
	V stream temperature	°C	30.56	0.06	30.73	0.57
	Bottom pressure**	kgf/cm²	11.37	0.01	11.36	-0.04
Reboiler	Propylene inlet temperature	°C	44.88	0.00	46.77	4.22
	Propane outlet temperature**	°C	30.56	0.06	30.73	0.57
	Propylene outlet temperature	°C	30.94	0.05	31.15	0.71
	Propylene flow rate**	mass/time	88.49	0.37	88.73	0.27
Cooler	Propylene inlet temperature	°C	44.88	0.00	46.77	4.22
	Cooling water inlet temperature*	°C	25.90	0.48	25.90	------
	Cooling water outlet temperature**	°C	30.55	0.59	30.54	-0.06
	flooding level*	%	50.20	1.29	50.20	------
	Cooling water flow rate	mass/time	------	-------	195.32	------
	Propylene outlet temperature*	°C	25.84	0.49	26.05	0.82
	Propylene flow rate**	mass/time	10.85	0.52	10.28	-5.22
Bottom product	Flow rate**	mass/time	1.73	0.40	1.77	2.45
	Temperature	°C	30.88	0.12	30.70	-0.59
	Propylene concentration**	%-mol	4.42	0.43	4.64	4.89
Overhead product	Temperature	°C	30.40	0.04	30.35	-0.16
	Propane concentration**	ppm	312.32	30.28	871	178.85
	Flow rate**	mass/time	5.66	0.31	5.43	-4.11
Reflux stream	Pressure*	kgf/cm²	15.89	0.01	15.90	------
	Flow rate**	mass/time	92.59	0.75	93.43	0.91
Reflux drum	Pressure*	kgf/cm²	13.45	0.01	13.45	------
	Outlet stream temperature	°C	30.29	0.03	30.35	0.20

** measured states used in the estimation objective function

* measured states set in the model

5.4. Optimization

With the updated model at hand, it is possible to optimize the model according to the economic objective function. Essentially, the main objective of this plant is to produce high purity propylene at overhead stream, which is sold to a polymer industry at a higher price compared to the bottom stream (propane incorporated in LPG). Therefore, the economic objective function is composed of the operating cost given by the sum of profits (overhead and bottom products) minus the sum of utilities (compressor energy and cooling water) and feedstock cost.

The problem of the above objective function formulation is that the feedstock stream is an intermediate stream, which does not have an assigned market price, and cannot be compared to the cost of other streams. An alternative to circumvent this is to employ a wide-plant approach and to optimize several units at the same time, in which all inlet and outlet streams have assigned market prices. However, this approach is not efficient because it is almost impossible that all units achieve steady-states at the same time in order to be optimized (RINALDO; UNGAR, 2000).

Another possibility is to optimize the process using decomposition techniques, to obtain fictitious prices (shadow prices) for the intermediate streams, which are then used to optimize each unit at a time (CONEJO et al., 2006; GUIGNARD, 2003). The implementation of decompositions techniques in the propylene production unit was previously studied in our research group, resulting in the shadow price used in this thesis; the complete study can be found in (ACEVEDO et al., 2015). The list of prices used in the VRD case is displayed in Table 5.4.

Table 5.4 - Price list

Cost component	Unit	Value
Feed stream	currency/mass	397.25
Overhead stream	currency/mass	893.86
Bottom stream	currency/mass	229.08
Compressor energy	currency/MWh	19.92
Cooling water	currency/mass	0.013

Due to current problems found in the solver implementation of the EMSO environment, it is impossible to solve large scale problems by an equation oriented optimization approach. Therefore, the economic optimization problem is conducted

using a derivative-free approach (Nelder-Mead method) in the reduced space of this problem.

Originally, the VRD process has two degrees of freedom to be optimized that are chosen to be one internal flow rate (reflux stream) and the bottom stream flow rate. The constraints for the products concentration are handled as ℓ_1 penalty functions added to the objective function and the solver is tuned with relative and absolute accuracy set at 10^{-8}. With this tuning, the problem converges after 101 iterations with 191 objective function evaluations, in approximately 5 min.

Table 5.5 summarizes the economical gains obtained by the optimization, where it is displayed the costs computed at the current operating point and the optimal solution. It is important to notice that the utility cost is not significant with respect to the total profit (approximately 0.8%); which is different from traditional distillation columns schemes without energy integration. Furthermore, the optimization outcomes show that it is possible to reduce the utility cost and also to increase the production of the most valuable product (propylene), improving the total profit in 2.98% that represents saves of around 2 million dollars per year.

Table 5.5 - Summary of the economic optimization result (cost components)

	Unit	Current	Optimal solution	Deviation %
Total profit	currency/ time	9073.87	9352.51	2.98%
Feed cost		2856.23	2856.23	0.00%
Overhead profit		4847.84	4934.12	1.75%
Bottom product profit		404.66	382.57	-5.78%
Compressor cost		67.04	60.76	-9.37%
Cooling water cost		2.59	1.62	-37.57%

The values of the most relevant process variables, before and after optimization, are listed in Table 5.6. It can be seen that the internal flow rates (reflux, reboiler and compressor) are significantly reduced to decrease the utility costs. However, as the utility costs are rather negligible in comparison to the total profit, the optimization tends to increase the amount of overhead product until the product concentrations achieve their upper and lower bound in the overhead and bottom streams.

Table 5.6 - Summary of the economic optimization result (process variables)

Variable	Unit	Current	Optimal solution	Deviation %
Distillate Flow	mass/time	5.43	5.52	1,66%
Distillate concentration	ppm	870.92	5000.00	474,10%
Bottom Flow	mass/time	1.77	1.67	-5,65%
Bottom concentration	%-mol	4.64	0.30	-93,53%
Reflux Flow	mass/time	93.43	80.42	-13,92%
Reboiler Flow	mass/time	88.73	77.03	-13,19%
Compressor Flow	mass/time	99.01	86.48	-12,66%

Actually, the optimization raises the column temperature (about 0.60ºC per tray) in order to propel more propylene to the column top, as may be observed in Figure 5.9. This behavior also sends more propane to the overhead stream, achieving its upper bound of 5000ppm.

Figure 5.9 - Optimized temperature profile

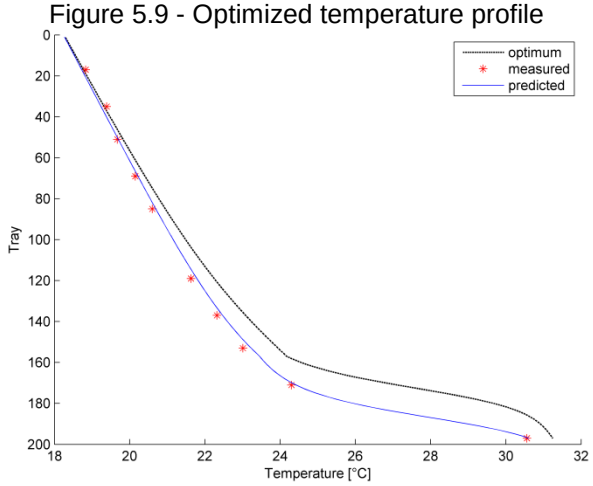

5.5. Control structure

Darby et al. (2011) pointed out the importance to compare the benefits of RTO to those than can be obtained from MPC or PID alone. This evaluation is carried out in the present section.

In the previous section, the economical benefits of RTO are demonstrated, and it can be seen that due to heat integration provided by the VRD process, the utilities costs are almost irrelevant with respect to the total profit. As a consequence, the process optimization tends to increase the overhead flow rate until the propane concentration

reaches its upper bound (5000ppm), while the propylene concentration reaches its lowest value in the bottom stream (0.3%mol).

That characteristic motivates the control of both concentrations (at their bounds) to obtaining the maximum profit at any operating point, without need of an RTO. However, the “dual” control (control of two products composition) is known to be difficult to be implemented due to the strong interactions (JOGWAR; DAOUTIDIS, 2009; MUHRER; COLLURA; LUYBEN, 1990; SKOGESTAD; MORARI, 1987; SKOGESTAD, 2000), so the implementation of an MPC with a fixed set point using both concentrations as controlled variables may be impractical.

A possible alternative could be to control the propane concentration in the overhead stream together with another measured state, which preferentially does not change its value for different disturbances. Table 5.7 shows the optimal values of several measured variables, considering disturbances in flow rate and composition of feed stream. It can be seen that all variables change their values in comparison to the nominal state, with exception of the products concentrations.

Table 5.7 - Optimal values for different disturbances

Variable		Unit	Nominal value	Dist1	Dist2	Dist3	Dist3**
Feed flow rate		mass/time	7.19	7.55	7.91	7.19	7.19
Feed composition	propylene	%-mol	77.26	77.26	77.26	73.40	69.54
R		mass/time	80.42	84.39	88.35	77.07	73.69
F_{boil}		mass/time	77.03	81.03	85.04	73.61	70.17
D		mass/time	5.52	5.80	6.07	5.23	4.95
B		mass/time	1.67	1.76	1.84	1.96	2.24
Overhead composition	propylene	%-mol	5000	5000	5000	5000	5000
Bottom composition	propylene	%-mol	0.30	0.30	0.30	0.30	0.30
R/Feed		------	11.18	11.17	11.17	10.71	10.24
F_{boil}/Feed		------	10.71	10.73	10.75	10.23	9.76
R/D		------	14.56	14.55	14.55	14.72	14.89
D/Feed		------	0.77	0.77	0.77	0.73	0.69
B/Feed		------	0.23	0.23	0.23	0.27	0.31

** Disturbance

The integration between RTO and SOC is discussed in Chapter 4. That study inspires the proposition of a pair of controlled variables for the VRD process, one

would be the propane concentration at overhead stream and the other an artificial self-optimizing control variable made-up of a linear combination of the overhead (D) and bottom (B) streams flow rates and of the ratio $\frac{F_{boil}}{Feed}$. The SOC variable is calculated in accordance to the Null Space method (ALSTAD; SKOGESTAD, 2007), with optimal sensitivities computed by finite differences at the nominal point. Equation 5.6 presents the new pair of controlled variables.

$$\begin{aligned} c1 &= x_{D,propy} \\ c2 &= -0.10701D + 0.2962B + 0.9491\frac{F_{boil}}{Feed} \end{aligned} \tag{5.6}$$

To evaluate the performance of the proposed alternative, an experiment is conducted with disturbances of 10% in the feed composition and feed flow rate, employing $c1$ and $c2$ as controlled variables. The results show that the profit loss that can be attributed to the control of both variables is small, about 0.09% of the optimal profit. This outcome is an important indication that the optimum control of the VRD process using an RTO with SOC approach may yield excellent results, since the SOC is able to handle small disturbances and the RTO can manage larger ones.

For sure, the previous analysis is not conclusive and dynamic experiments need to be conducted to draw a general conclusion about the ideal VRD control structure. However, these experiments are not in the scope of the present thesis and are to be considered for future works.

5.6. Partial Conclusions

In this Chapter the practical aspects of RTO implementation in a VRD unit are discussed. First of all, the phenomenological model is presented using process data to determine some relevant fixed parameters. After that, the steady-state identification method is presented, and then, the model parameters are estimated by the Rotational Discrimination method. The parameter estimation outcomes show that the model is flexible enough to represent the process data with small deviations and

can be successfully used in the RTO cycle. The economical optimization is conducted by using the operational cost as objective function, resulting in a profit improvement of 2.98%, equivalent to 2 million dollars per year. Finally, the improvements obtained by the RTO approach are compared to the ones obtained by the MPC alone. Although the dual control of both products composition is enough to keep the process at the economical optimum, this control strategy may have poor results, due to strong interaction between the controlled variables (SKOGESTAD; MORARI, 1987). This fact motivates the proposition of a new control structure using SOC variables. Preliminary results show that the proposed control approach (RTO plus SOC) could lead to small profit losses and would be a good alternative to the VRD control. However, more experiments need to be conducted to guarantee the superiority of RTO plus SOC in comparison to MPC alone. Moreover, other methods to calculate SOC variables should also be considered that include implementation errors, for instance.

6. General Conclusions and Future Works

In the thesis the Real Time Optimization methodology applied to chemical processes has been studied. This is an attractive alternative to control many process systems, because it has a high acceptance among process operators. Although the large number of RTO implementations in industry, its benefits are not always self-evident because this method has some drawbacks that need to be reduced for proper operation, namely: plant/model mismatch, non-identifiability problems and low frequency of set points updates. Each of these problems was separately analyzed and alternatives were proposed to mitigate their influence on the RTO cycle, resulting in an improved RTO framework. Then, the proposed approaches were successfully applied to an industrial case of study.

The main conclusions of this thesis may be summed up as following:

a) The comparison between RTO strategies shows that the classical RTO method (Model Parameter Adaptation) may be reliable, provided that a flexible model to represent process topology, a parameter estimation method suitable to handle process noise characteristics, lack of model identifiability and a method to improve the quality of measurements (Dual methodology) are used in combination.

b) The evaluation of the parameter estimation methodologies demonstrates that the Rotational Discrimination (RD) method is likely the most appropriate among the evaluated methods to be used in a RTO-like framework, because it presents the best prediction capacity and robustness, with reasonable computational time, in the examples that studied in this thesis.

c) The results obtained in the development of the MPC integrating Self-Optimizing Control (SOC) and RTO point out that the combination of these methodologies may be a good alternative to alleviate the inconvenience of low frequency set point updates in RTO. Moreover, the zone control policy is a consistent option to handle the problem of active set point changes observed in the SOC methodology.

d) The RTO implementation in an industrial case study shows that it is possible to increase the VRD process profit in 2.98%, which is equivalent to saves around 2 million dollars per year. Moreover, the comparison between the control structures shows that the integrated approach between RTO and SOC may be an interesting alternative for this process.

e) One of the main drawbacks in the RTO methodology is that it is necessary that the process be at steady-state. This limits the frequency of application of the estimation, re-optimization cycle, and it depends solely on the control performance, the characteristics of perturbations of the system and on the dynamics of the process.

Some of the drawbacks in RTO were studied in detail in this thesis, but some are inherent to the methodology. In this sense, it would be interesting to provide some suggestions for future works:

a) The Rotational Discrimination method may be extended using redescending estimators to integrate parameter estimation and reconciliation modules. This approach would be able to handle simultaneously, and in a robust way, gross errors and identifiability problems.

b) It is necessary to analyze other methods to compute SOC variables including measurement errors, and then integrate these methods to the MPC developed in the present work.

c) It would be interesting to develop a general alternative to handle both problems related with changes in the active set (see Chapter 4). One possibility is to employ only unconstrained variables as controlled variables and calculate the optimum sensitivity matrix via surface response methods, similar to the work of Ye *et al.* (2013).

d) Development of an MPC integrating RTO and SOC with for example using infinity horizon to guarantee Lyapunov stability.

f) The dynamic comparison among different control structures for the VRD case study including possible SOC variables is necessary to evaluate economic and stability benefits of RTO methodology in this process.

g) The identification of continuous processes by steady-state models is a difficult task, mainly because the information used in the parameter estimation is punctual and the time is crucial. An alternative to handle this problem is to use a dynamic model to take advantage of measurements in the transient period, improving the parameter estimation. This approach would be similar to the Dynamic Real Time Optimization (DRTO) with the difference that the economic optimization could be performed by the steady-state model, such as done in the classic RTO, which would reduce at least one dynamic optimization problem.

REFERENCES

ACEVEDO, A. M.; GRACIANO, J.E.A.; LIPORACE, F.; LE ROUX, G.A.C. **Decomposition Techniques for the Real-time Optimization of a Propylene Production Unit**25th European Symposium on Computer Aided Process Engineering. Copenhagen: Elsevier, 2015

ALSTAD, V.; SKOGESTAD, S. Null Space Method for Selecting Optimal Measurement Combinations as Controlled Variables. **Industrial & Engineering Chemistry Research**, v. 46, n. 3, p. 846–853, jan. 2007.

ALSTAD, V.; SKOGESTAD, S.; HORI, E. S. Optimal measurement combinations as controlled variables. **Journal of Process Control**, v. 19, n. 1, p. 138–148, jan. 2009.

ANNAKOU, O.; MIZSEY, P. Rigorous investigation of heat pump assisted distillation. **Heat Recov. Syst. CHP**, v. 15, n. 3, p. 241, abr. 1995.

ARORA, N.; BIEGLER, L. T. Redescending estimators for data reconciliation and parameter estimation. **Comput. Chem. Eng.**, v. 25, n. 11-12, p. 1585, nov. 2001.

AYDIN, B.; BENALI, M. **Simulation and optimization of depropanizer, C3-splitter and debutanizer**Spring Meeting & 5th Global Congress on Process Safety. Tampa: 2009

BADER, J.-M.; GUESNEUX, S. Use real-time optimization for low-sulfur gasoline production. **Hydrocarbon processing**, v. 86, n. 2, 2007.

BAMBERGER, W.; ISERMANN, R. Adaptive on-line steady-state optimization of slow dynamic processes. **Automatica**, v. 14, n. 3, p. 223–230, may 1978.

BARD, Y. Comparison of Gradient Methods for the Solution of Nonlinear Parameter Estimation Problems. **SIAM Journal on Numerical Analysis**, v. 7, n. 1, p. 157–186, mar. 1970.

BARD, Y. **Nonlinear parameter estimation**. New York: Academic Press, 1974.

BARD, Y.; LAPIDUS, L. Nonlinear System Identification. **Industrial & Engineering Chemistry Fundamentals**, v. 9, n. 4, p. 628–633, nov. 1970.

BASAK, K.; ABHILASH, K.B.; GANGULY, S.; SARAF, D.N. On-Line Optimization of a Crude Distillation Unit with Constraints on Product Properties. **Ind. Eng. Chem. Res.**, v. 41, n. 6, p. 1557, mar. 2002.

BELLMAN, R.; ÅSTRÖM, K. J. On structural identifiability. **Mathematical Biosciences**, v. 7, n. 3-4, p. 329–339, abr. 1970.

BEN-ZVI, A. Reparameterization of inestimable systems with applications to chemical and biochemical reactor systems. **AIChE Journal**, v. 54, n. 5, p. 1270–1281, maio

2008.

BERTSEKAS, D. P.; NEDIÂC, A.; OZDAGLAR, A. E. **Convex analysis and optimization**. e.1. ed. Belmont: Athena Scientific, 2003.

BIEGLER, L. T.; DAMIANO, J. J.; BLAU, G. E. Nonlinear parameter estimation: A case study comparison. **AIChE Journal**, v. 32, n. 1, p. 29–45, jan. 1986.

BIEGLER, L. T.; GROSSMANN, I. E.; WESTERBERG, A. W. A note on approximation techniques used for process optimization. **Computers & Chemical Engineering**, v. 9, n. 2, p. 201–206, 1985.

BRDYS, M. A.; TATJEWSKI, P. **Iterative Algorithms for Multilayer Optimization Control**. London: Imperial College Press, 2005.

BUNIN, G. A.; FRANÇOIS, G.; BONVIN, D. Performance of Real-Time Optimization Schemes – I. Sufficient Conditions for Feasibility and Optimality. **Computer and Chemical Engineering (subimitted)**, v. submitted, 2013a.

BUNIN, G. A.; FRANÇOIS, G.; BONVIN, D. Performance of Real-Time Optimization Schemes – II. Implementation Issues. **Computer and Chemical Engineering (subimitted)**, v. submitted, 2013b.

BUNIN, G. A.; FRANÇOIS, G.; BONVIN, D. Sufficient Conditions for Feasibility and Optimality of Real-Time Optimization Schemes - I. Theoretical Foundations. 12 ago. 2013c.

BUNIN, G. A.; FRANÇOIS, G.; BONVIN, D. Sufficient Conditions for Feasibility and Optimality of Real-Time Optimization Schemes - II. Implementation Issues. p. 56, 12 ago. 2013d.

BUNIN, G. A.; FRANÇOIS, G.; BONVIN, D. From Discrete Measurements to Bounded Gradient Estimates: A Look at Some Regularizing Structures. **Industrial & Engineering Chemistry Research**, v. 52, n. 35, p. 12500–12513, 4 set. 2013e.

CAO, S.; RHINEHART, R. R. An efficient method for on-line identification of steady state. **Journal of Process Control**, v. 5, n. 6, p. 363–374, 1995a.

CAO, S.; RHINEHART, R. R. An efficient method for on-line identification of steady state. **Journal of Process Control**, v. 5, n. 6, p. 363–374, dez. 1995b.

CAO, Y. Direct and indirect gradient control for static optimisation. **International Journal of Automation and Computing**, v. 2, n. 1, p. 60–66, jul. 2005.

CHU, Y.; HUANG, Z.; HAHN, J. Global Sensitivity Analysis Procedure Accounting for Effect of Available Experimental Data. **Industrial & Engineering Chemistry Research**, v. 50, n. 3, p. 1294–1304, 2 fev. 2011.

CONEJO, A. J. et al. **Decomposition techniques in mathematical programming: engineering and science applications**. [s.l.] Springer Science & Business Media,

2006.

DARBY, M. L.; NIKOLAOU, M.; JONES, J.; NICHOLSON, D. RTO: An overview and assessment of current practice. **J. Process Contr.**, v. 21, n. 6, p. 874, jul. 2011a.

DARBY, M. L. et al. RTO: An overview and assessment of current practice. **Journal of Process Control**, v. 21, n. 6, p. 874–884, jul. 2011b.

DE ARAÚJO, A. C. B.; GOVATSMARK, M.; SKOGESTAD, S. Application of plantwide control to the HDA process. I—steady-state optimization and self-optimizing control. **Control Engineering Practice**, v. 15, n. 10, p. 1222–1237, out. 2007.

EFRON, B. Biased versus unbiased estimation. **Advances in Mathematics**, v. 16, n. 3, p. 259–277, jun. 1975.

ENGELL, S. Feedback control for optimal process operation. **Journal of Process Control**, v. 17, n. 3, p. 203–219, mar. 2007.

FARISS, R. H.; LAW, V. H. An efficient computational technique for generalized application of maximum likelihood to improve correlation of experimental data. **Computers & Chemical Engineering**, v. 3, n. 1-4, p. 95–104, jan. 1979.

FORBES, J. F.; MARLIN, T. E. Model Accuracy for Economic Optimizing Controllers: The Bias Update Case. **Industrial & Engineering Chemistry Research**, v. 33, n. 8, p. 1919–1929, ago. 1994.

FORBES, J. F.; MARLIN, T. E.; MACGREGOR, J. F. Model adequacy requirements for optimizing plant operations. **Comput. Chem. Eng.**, v. 18, n. 6, p. 497, jun. 1994.

GEORGIOU, A.; SAPRE, A.V.; TAYLOR, P.; GALLOWAY, R.E; CASEY, L.K. Ethylene optimization system reaps operations and maintenance benefits. **Oil and Gas Journal**, v. 96, n. 10, 1998.

GONZÁLEZ, A. H.; ODLOAK, D. A stable MPC with zone control. **Journal of Process Control**, v. 19, n. 1, p. 110–122, jan. 2009.

GRACIANO, J. E.; MENDOZA, D. F.; LE ROUX, G. A. C. Performance comparison of parameter estimation techniques for unidentifiable models. **Computers & Chemical Engineering**, v. 64, p. 24–40, may 2014.

GUIGNARD, M. Lagrangean relaxation. **Top**, v. 11, n. 2, p. 151–200, 2003.

HAAKER, M. P. R.; VERHEIJEN, P. J. T. Local and Global Sensitivity Analysis for a Reactor Design with Parameter Uncertainty. **Chemical Engineering Research and Design**, v. 82, n. 5, p. 591–598, may 2004.

HALVORSEN, I. J. et al. Optimal Selection of Controlled Variables †. **Industrial & Engineering Chemistry Research**, v. 42, n. 14, p. 3273–3284, jul. 2003.

HANGOS, K.; CAMERON, I. **Process system engineering : process modeling**

and modeling analysis. London: Academic Press, 2001.

HEYEN, G.; LEDENT, T.; KALITVENTZEFF, B. A modular package for simultaneous calculation of complex interlinked separation processes. **Comput. Chem. Eng.**, v. 18, p. S69, jan. 1994.

HOLDERBAUM, T.; GMEHLING, J. PSRK: A Group Contribution Equation of State Based on UNIFAC. **Fluid Phase Equilibria**, v. 70, n. 2-3, p. 251–265, dez. 1991.

HU, W. et al. Local self-optimizing control of constrained processes. **Journal of Process Control**, v. 22, n. 2, p. 488–493, fev. 2012.

JASCHKE, J.; SKOGESTAD, S. **Using Process Data for Finding Self-optimizing Controlled Variables**International Symposium on Dynamics and Control of Process Systems. **Anais**...Mumbai: 2013

JÄSCHKE, J.; SKOGESTAD, S. NCO tracking and self-optimizing control in the context of real-time optimization. **Journal of Process Control**, v. 21, n. 10, p. 1407–1416, dez. 2011.

JIANG, T. et al. Application of steady-state detection method based on wavelet transform. **Computers & Chemical Engineering**, v. 27, n. 4, p. 569–578, abr. 2003.

JOGWAR, S. S.; DAOUTIDIS, P. Dynamics and control of vapor recompression distillation. **Journal of Process Control**, v. 19, n. 10, p. 1737–1750, dez. 2009.

JOSE, R. A.; UNGAR, L. H. Pricing interprocess streams using slack auctions. **AIChE Journal**, v. 46, n. 3, p. 575–587, mar. 2000.

KARIWALA, V.; CAO, Y.; JANARDHANAN, S. Local Self-Optimizing Control with Average Loss Minimization. **Industrial & Engineering Chemistry Research**, v. 47, n. 4, p. 1150–1158, fev. 2008.

KEESMAN, K. J.; SPANJERS, H.; STRATEN, G. VAN. Analysis of endogenous process behavior in activated sludge. **Biotechnology and Bioengineering**, v. 57, n. 2, p. 155–163, 1998.

LARSSON, T. et al. Self-Optimizing Control of a Large-Scale Plant: The Tennessee Eastman Process. **Industrial & Engineering Chemistry Research**, v. 40, n. 22, p. 4889–4901, out. 2001.

LE ROUX, G. A. C. **Strategie d'identification de modeles algebro-diferentiels. Application aux systemes reactionnels complexes**. [s.l.] Institut national polytechnique de tolouse, 1995.

LE ROUX, G. A. C. et al. Improving steady-state identification. **Proceedings of the 18th European Symposium on Computer Aided Process Engineering – ESCAPE 18**, v. 25, p. 459–464, 2008.

LEER, R. B. **Self-optimizing control structures for active constraint regions of a**

sequence of distillation columns. [s.l.] Norwegian University of Science and Technology, 2012.

LERSBAMRUNGSUK, V. et al. Control structure design for optimal operation of heat exchanger networks. **AIChE Journal**, v. 54, n. 1, p. 150–162, jan. 2008.

LI, R.; HENSON, M. A.; KURTZ, M. J. Selection of Model Parameters for Off-Line Parameter Estimation. **IEEE Transactions on Control Systems Technology**, v. 12, n. 3, p. 402–412, maio 2004.

LUBANSKY, A. S. et al. A general method of computing the derivative of experimental data. **AIChE Journal**, v. 52, n. 1, p. 323–332, jan. 2006.

LUND, B. F.; FOSS, B. A. Parameter ranking by orthogonalization—Applied to nonlinear mechanistic models. **Automatica**, v. 44, n. 1, p. 278–281, jan. 2008.

MAEDER, U.; BORRELLI, F.; MORARI, M. Linear offset-free Model Predictive Control. **Automatica**, v. 45, n. 10, p. 2214–2222, out. 2009.

MANSOUR, M.; ELLIS, J. E. Comparison of methods for estimating real process derivatives in on-line optimization. **Applied Mathematical Modelling**, v. 27, n. 4, p. 275–291, apr. 2003.

MANUM, H.; SKOGESTAD, S. Self-optimizing control with active set changes. **Journal of Process Control**, v. 22, n. 5, p. 873–883, jun. 2012.

MARCHETTI, A. **Modifier-Adaptation Methodology for Real-Time Optimization**. [s.l.] ÉCOLE POLYTECHNIQUE FÉDÉRALE DE LAUSANNE, 2009.

MARCHETTI, A.; CHACHUAT, B.; BONVIN, D. Modifier-Adaptation Methodology for Real-Time Optimization. **Industrial & Engineering Chemistry Research**, v. 48, n. 13, p. 6022–6033, jul. 2009.

MARQUARDT, D. W. An Algorithm for Least-Squares Estimation of Nonlinear Parameters. **Quarterly of Applied Mathematics**, v. 11, n. 2, p. 431–411, 1963.

MARQUARDT, D. W. Generalized Inverses, Ridge Regression, Biased Linear Estimation, and Nonlinear Estimation. **Technometrics**, v. 12, n. 3, p. 591–612, ago. 1970.

MCLEAN, K. A. P.; MCAULEY, K. B. Mathematical modelling of chemical processes-obtaining the best model predictions and parameter estimates using identifiability and estimability procedures. **The Canadian Journal of Chemical Engineering**, v. 90, n. 2, p. 351–366, 17 abr. 2012.

MEIXELL, M. D.; GOCHENOUR, B.; CHEN, C.-C. Chapter 3 – Industrial Applications of Plant-Wide Equation-Oriented Process Modeling—2010. In: SUNDMACHE, K. (Ed.). . **Adv. Chem. Eng.** Burlington: Elsevier, 2010. p. 152.

MIAO, H. et al. On identifiability of nonlinear ode models and applications in viral

dynamics. **SIAM review. Society for Industrial and Applied Mathematics**, v. 53, n. 1, p. 3–39, 1 jan. 2011.

MILETIC, I. P.; MARLIN, T. E. On-line Statistical Results Analysis in Real-Time Operations Optimization. **Industrial & Engineering Chemistry Research**, v. 37, n. 9, p. 3670–3684, set. 1998.

MUHRER, C. A.; COLLURA, M. A.; LUYBEN, W. L. Control of vapor recompression distillation columns. **Ind. Eng. Chem. Res.**, v. 29, n. 1, p. 59, jan. 1990.

NGUYEN, V. V.; WOOD, E. F. Review and Unification of Linear Identifiability Concepts. **SIAM Review**, v. 24, n. 1, p. 34–51, jan. 1982.

NIKEREL, I. E. et al. Model reduction and a priori kinetic parameter identifiability analysis using metabolome time series for metabolic reaction networks with linlog kinetics. **Metabolic engineering**, v. 11, n. 1, p. 20–30, jan. 2009.

NOCEDAL, J.; WRIGHT, S. J. **Numerical optimization**. 1. ed. New York: Elsevier, 1999.

PFAFF, G. C. **Generating Information for Real-Time Optimization**. [s.l.] University of Alberta, 2001.

PRITCHARD, D. J.; BACON, D. W. Prospects for reducing correlations among parameter estimates in kinetic models. **Chemical Engineering Science**, v. 33, n. 11, p. 1539–1543, jan. 1978.

QUAISER, T.; MÖNNIGMANN, M. Systematic identifiability testing for unambiguous mechanistic modeling--application to JAK-STAT, MAP kinase, and NF-kappaB signaling pathway models. **BMC systems biology**, v. 3, p. 50, jan. 2009.

QUELHAS, A. D.; DE JESUS, N. J. C.; PINTO, J. C. Common vulnerabilities of RTO implementations in real chemical processes. **The Canadian Journal of Chemical Engineering**, v. 91, n. 4, p. 652–668, 24 abr. 2013.

RAMDIAL, A. et al. Real-time data, models optimize complex production off Trinidad. **Oil & gas journal**, v. 107, n. 17, 2009.

RAUE, A. et al. Structural and practical identifiability analysis of partially observed dynamical models by exploiting the profile likelihood. **Bioinformatics (Oxford, England)**, v. 25, n. 15, p. 1923–9, 1 ago. 2009.

REN, T. Barriers and drivers for process innovation in the petrochemical industry: A case study. **Journal of Engineering and Technology Management**, v. 26, n. 4, p. 285–304, dez. 2009.

RINCON, F. D.; LIMA, F. V; LE ROUX, G. A. C. **An ARX-based technique for steady-state identification of chemical processes**American Control Conference (ACC), 2015. **Anais**...2015

ROBERTS, P. D. An algorithm for steady-state system optimization and parameter estimation. **International Journal of Systems Science**, v. 10, n. 7, p. 719–734, jul. 1979.

RODGER, E. Dual Modifier Adaptation Methodology For the On-line Optimization of Uncertain Processes. 2010.

RODGER, E. A.; CHACHUAT, B. Design Methodology of Modifier Adaptation for On-Line Optimization of Uncertain Processes. 2011.

RODRIGUES, R.; SOARES, R. P.; SECCHI, A. R. Teaching chemical reaction engineering using EMSO simulator. In: **Comput Aided Chem. Eng.** [s.l: s.n.]. v. 18p. 607.

ROTAVA, O.; ZANIN, A. C. Multivariable control and real-time optimization-An industrial practical view. **Hydrocarbon Processing**, v. 84, n. 6, p. 61, 2005.

SALTELLI, A.; CHAN, K.; SCOTT, E. M. (EDS.). **Sensitivity Analisis**. 1. ed. New York: John Wiley & Sons, 2000.

SECCHI, A. R.; HAYATI, R.; MARVAST, M.A.; AYAZI, M.; GANJI, H. **An algorithm for automatic selection and estimation of model parameters**International Symposium on Advanced Control of Chemical Processes. 2006

SHOKRI, S.; ARKUN, Y. CAKAL, B.; GOKCE, D; KUZU, E. Real time optimization as a tool for increasing petroleum refineries profits. **Petroleum & Coal**, v. 51, n. 2, p. 110–114, 2009.

SILDIR, H.; CARDOZO, N.S.M.; NETO, E.A.; FINKLER, T.F. Plant-wide hierarchical optimization and control of an industrial hydrocracking process. **Journal of Process Control**, v. 23, n. 9, p. 1229–1240, out. 2013.

SKOGESTAD, S. Plantwide control: the search for the self-optimizing control structure. **Journal of Process Control**, v. 10, n. 5, p. 487–507, out. 2000.

SKOGESTAD, S.; MORARI, M. Control configuration selection for distillation columns. **AIChE Journal**, v. 33, n. 10, p. 1620–1635, out. 1987.

SOBOL′, I. . Global sensitivity indices for nonlinear mathematical models and their Monte Carlo estimates. **Mathematics and Computers in Simulation**, v. 55, n. 1-3, p. 271–280, fev. 2001.

SURISETTY, K. et al. Model re-parameterization and output prediction for a bioreactor system. **Chemical Engineering Science**, v. 65, n. 16, p. 4535–4547, ago. 2010.

TJÄRNSTRÖM, F.; LJUNG, L. L2 Model reduction and variance reduction. **Automatica**, v. 38, n. 9, p. 1517–1530, set. 2002.

VAJDA, S. et al. Qualitative and quantitative identifiability analysis of nonlinear

chemical kinetic models. **Chemical Engineering Communications**, v. 83, n. 1, p. 191–219, set. 1989.

WEIJERS, S. R.; VANROLLEGHEM, P. A. A procedure for selecting best identifiable parameters in calibrating actived sludge model no.1 to full-scale plant data. **Water SciencieTechnology**, v. 36, n. 5, p. 69–79, 1997.

YE, L. et al. Approximating Necessary Conditions of Optimality as Controlled Variables. **Industrial & Engineering Chemistry Research**, v. 52, n. 2, p. 798–808, 16 jan. 2013.

YE, L. et al. A Novel Hierarchical Control Structure with Controlled Variable Adaptation. **Industrial & Engineering Chemistry Research**, v. 53, n. 38, p. 14695–14711, 24 set. 2014.

ZHANG, Y.; NADLER, D.; FORBES, J. F. Results analysis for trust constrained real-time optimization. **Journal of Process Control**, v. 11, n. 3, p. 329–341, jun. 2001.

Appendix A

Upper and lower bounds for the parameter initial values used in the first RTO iteration of each Monte Carlo simulation. The set of parameters are uniformly sampled.

Table A1 - Parameter bounds used in the parameter estimation

Parameter bounds used in perfect model simulations						
	$A1$	$Ea1$	$A2$	$Ea2$	$A3$	$Ea3$
Upper	2.7554e12	13333	5.2000e17	16667	3.6099e18	22216
Lower	1.2884e03	3333	2.6853e04	4167	4.3589e04	5554
Parameter bounds used in approximate model simulations						
	$\eta 1$	$\nu 1$	$\eta 2$	$\nu 2$		
Upper	1.7183e09	9289	1.3291e15	14304		
Lower	6.6979e06	6866	1.5076e11	10573		

The measurement noise is simulated by MATLAB® function *randn* with zero mean and standard deviation equal to 0.5% of error:

$$z = m + error.\, m\, .\, \mathrm{randn}() \qquad \text{(A.1)}$$

where z is the measurement contaminated with noise, m is the measurement without noise and error is equal to 0 or 0.005.

Appendix B

This section presents the behavior of the optimization routines implemented using the approximate model and the perfect model. All RTO schemes start with the same parameter values, using noise free measurements and exact derivatives.

Figure.B1 - Algorithms results for ideal conditions (A) RTO path using approximated model and (B) RTO path using perfect model

A B

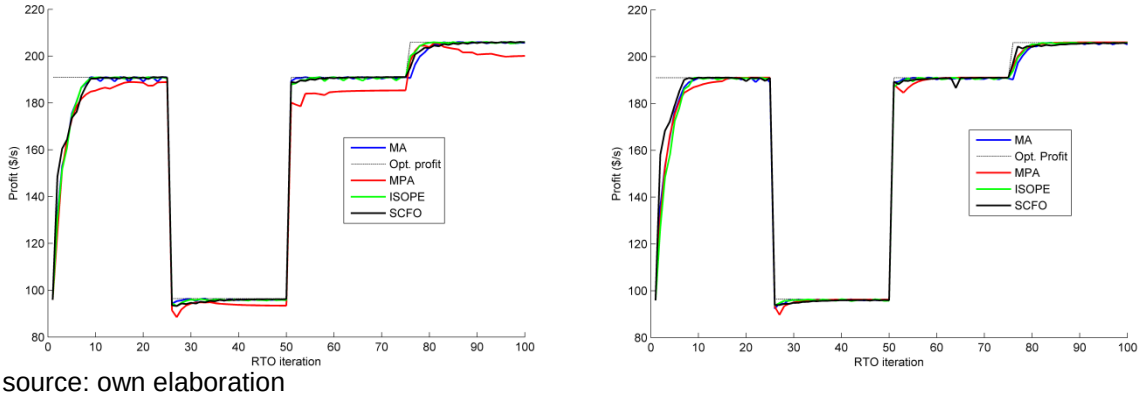

source: own elaboration

According to FigureB1 all RTO methods achieve the true optimum when accurate measurements are available even in presence of model mismatch. The only exception is the MPA that presents offset in the case when it uses the approximate model. This results show the basic behavior of the algorithms assessed in this thesis.

Appendix C

Ben-zvi chooses the net consumption of n_B and production of n_P as the pseudo-outputs $\phi^+ = \left[\phi_1^+, \phi_2^+\right]$.

$$\begin{aligned} \phi_1^+ &= (r_1 + r_2 + r_3 + r_4)V \\ \phi_2^+ &= r_4 V \end{aligned} \tag{C.1}$$

This election was motivated by the fact that, under experimental conditions, only n_B and n_P are measured. The inestimable parameter combinations, $\phi^- = \left[\phi_1^-, \phi_2^-, \phi_3^-\right]$, were calculated using the method of characteristics (Ben-zvi. 2008).

$$\begin{aligned} \phi_1^- &= k_{MT} \\ \phi_2^- &= k_1 - \frac{n_{Al,nom}}{n_{E,nom}} k_3 \\ \phi_3^- &= k_2 - \frac{n_{C,nom}}{n_{E,nom}} k_3 \end{aligned} \tag{C.2}$$

The transformation of the parameters space, $\Phi = \left[\phi^+, \phi^-\right]$, is given by:

$$\Phi = \begin{bmatrix} \frac{n_{B,nom}}{V}(k_1 n_{Al,nom} + k_2 n_{C,nom} + k_3 n_{E,nom} + k_4 n_{F,nom}) \\ \frac{n_{B,nom} n_{F,nom}}{V} k_4 \\ k_{MT} \\ k_1 - \frac{n_{Al,nom}}{n_{E,nom}} k_3 \\ k_2 - \frac{n_{C,nom}}{n_{E,nom}} k_3 \end{bmatrix} \tag{C.3}$$

This transformation fulfills the orthogonality requirement. i.e. $\left\langle d\phi_j^+, d\phi_i^- \right\rangle = 0$ for j = 1, 2 and i = 1, 2, 3.

Appendix D

Complete equation system for the parameter estimation problem of Dow Chemical Co.

$$
\begin{aligned}
\frac{d[HA]}{dt} &= -k_2[A^-][BM] \\
\frac{d[BM]}{dt} &= -k_1[M^-][BM] + k_{-1}[MBM^-] - k_2[A^-][BM] \\
\frac{d[HABM]}{dt} &= +k_2[A^-][BM] + k_3[M^-][AB] - k_{-3}[ABM^-] \\
\frac{d[AB]}{dt} &= -k_3[M^-][AB] + k_{-3}[ABM^-] \\
\frac{d[MBMH]}{dt} &= +k_1[M^-][BM] - k_{-1}[MBM^-] \\
\frac{d[M^-]}{dt} &= -k_1[M^-][BM] + k_{-1}[MBM^-] - k_3[M^-][AB] + k_{-3}[ABM^-] \\
[H^+] &= -[Q^+] + [M^-] + [MBM^-] + [A^-] + [ABM^-] \\
[MBM^-] &= \frac{\exp(K1)[MBMH]}{\exp(K1) + [H^+]} \\
[A^-] &= \frac{\exp(K2)[HA]}{\exp(K2) + [H^+]} \\
[ABM^-] &= \frac{\exp(K3)[HABM]}{\exp(K3) + [H^+]}
\end{aligned}
\qquad \text{(D1)}
$$

where the rate constants are given by the PRITCHARD and BACON (1978) reparametrization:

$$
\begin{aligned}
k1 &= \exp(\varphi_1)\exp\left(\left(\frac{1}{Tref} - \frac{1}{T}\right)\exp(\psi_1)\right) \\
k-1 &= \exp(\varphi_{-1})\exp\left(\left(\frac{1}{Tref} - \frac{1}{T}\right)\exp(\psi_{-1})\right) \\
k2 &= \exp(\varphi_2)\exp\left(\left(\frac{1}{Tref} - \frac{1}{T}\right)\exp(\psi_2)\right) \\
k3 &= \exp(\varphi_3)\exp\left(\left(\frac{1}{Tref} - \frac{1}{T}\right)\exp(\psi_3)\right) \\
k-3 &= \exp(\varphi_{-3})\exp\left(\left(\frac{1}{Tref} - \frac{1}{T}\right)\exp(\psi_{-3})\right)
\end{aligned}
\qquad \text{(D2)}
$$

$$Tref = 342.16K$$

Table D1 - Time vectors (hours) used in the second case study:

40°C	67°C	100°C	120°C
0.00	0.00	0.00	0.00
0.08	0.08	0.08	0.08
0.58	1.08	0.42	0.42
1.58	2.33	0.75	0.75
2.75	3.33	1.17	1.17
3.75	4.33	1.50	1.50
4.75	5.33	2.00	2.00
5.75	12.83	2.50	2.50
8.75	23.33	3.00	3.00
13.05	27.83	3.50	3.50
21.75	30.83	4.00	4.00
28.75	51.67	4.50	4.50
46.25	83.33	5.00	5.00
52.25	93.33	5.50	5.50
76.25	102.42	6.50	6.50
106.25	124.83	7.00	7.00
124.25	148.08	7.50	7.50
147.25	171.83	8.00	8.00
172.25	197.33	8.50	8.50
196.25	228.33	9.00	9.00
219.75	270.33	9.50	9.50
240.25	293.33	10.00	10.00
274.25	-----	10.50	10.50
292.25	-----	11.00	11.00
316.25	-----	11.50	11.50
340.75	-----	12.50	12.50
364.25	-----	13.50	13.50
386.75	-----	14.50	14.50
412.25	-----	16.50	16.50
442.75	-----	21.75	21.75
460.75	-----	29.50	29.50
483.75	-----	53.00	53.00
507.25	-----	-----	-----
553.75	-----	-----	-----
580.75	-----	-----	-----
651.25	-----	-----	-----
673.25	-----	-----	-----
842.75	-----	-----	-----

Table D2 – Initial condition for the other state variables (complement for the Table 1.10)

$[HABM]$	$[M^-]$	$[H^+]$	$[MBM^-]$	$[A^-]$	$[ABM^-]$	Sensitivities
0	0.0131	$0.5(-K2+(K2^2+4K2[HA])^{0.5})$	$[H^+]$	0	0	$0 \in R^{90X1}$

Appendix E

Equations E1 and E2 describe the computation of the output predicted vectors with p predicted intervals and m control actions, where $\bar{c}$ is the predicted vector of artificial SOC variables and $\bar{r}$ is the vector of constrained output variables. Matrices U, V, D and E are given in eq.(4.7).

$$\begin{bmatrix} c(k+1|k) \\ c(k+2|k) \\ \vdots \\ c(k+m|k) \\ c(k+m+1|k) \\ \vdots \\ c(k+p|k) \end{bmatrix} = \begin{bmatrix} UD \\ UD^2 \\ \vdots \\ UD^m \\ UD^{m+1} \\ \vdots \\ UD^p \end{bmatrix} \bar{x}(k) + \begin{bmatrix} UE & 0 & \cdots & 0 \\ UDE & UE & \cdots & 0 \\ \vdots & \vdots & \ddots & \vdots \\ UD^{m-1}E & UD^{m-2}E & \cdots & UE \\ UD^m E & UD^{m-1}E & \cdots & UDE \\ \vdots & \vdots & \ddots & \vdots \\ UD^{p-1}E & UD^{p-2}E & \cdots & UD^{p-m}B \end{bmatrix} \begin{bmatrix} \Delta u(k|k) \\ \Delta u(k+1|k) \\ \vdots \\ \Delta u(k+m-1|k) \end{bmatrix} \qquad \text{(E1)}$$

$$\bar{c}(k) \quad = \quad \Psi \quad \bar{x}(k) + \quad \Theta \quad \Delta\bar{u}_k$$

$$\begin{bmatrix} r(k+1|k) \\ r(k+2|k) \\ \vdots \\ r(k+m|k) \\ r(k+m+1|k) \\ \vdots \\ r(k+p|k) \end{bmatrix} = \begin{bmatrix} VD \\ VD^2 \\ \vdots \\ VD^m \\ VD^{m+1} \\ \vdots \\ VD^p \end{bmatrix} \bar{x}(k) + \begin{bmatrix} VE & 0 & \cdots & 0 \\ VDE & VE & \cdots & 0 \\ \vdots & \vdots & \ddots & \vdots \\ VD^{m-1}E & VD^{m-2}E & \cdots & VE \\ VD^m E & VD^{m-1}E & \cdots & VDE \\ \vdots & \vdots & \ddots & \vdots \\ VD^{p-1}E & VD^{p-2}E & \cdots & VD^{p-m}B \end{bmatrix} \begin{bmatrix} \Delta u(k|k) \\ \Delta u(k+1|k) \\ \vdots \\ \Delta u(k+m-1|k) \end{bmatrix} \qquad \text{(E2)}$$

$$\bar{r}(k) \quad = \quad \Omega \quad \bar{x}(k) + \quad \mathrm{T} \quad \Delta\bar{u}_k$$

where $\Psi \in \mathbb{R}^{(nc\,.\,p)\times(nx+nu)}$, $\Theta \in \mathbb{R}^{(n_c\,.\,p)\times n_u}$, $\Omega \in \mathbb{R}^{(nr\,.\,p)\times(nx+nu)}$ and $\mathrm{T} \in \mathbb{R}^{(nc\,.\,p)\times nu}$

Appendix F

The ammonia production case study is based on conversion of hydrogen and nitrogen in ammonia by the stoichiometric equation given in (F1). This process is composed by 8 equipments, which are modeled as a set of mass and energy balances, and equilibrium equations as follows:

$$3\,H_2 + N_2 \Leftrightarrow 2\,NH_3 \tag{F1}$$

Mixer

$$\begin{aligned} S2 &= S1 + S6 \\ S2\,x2 &= S1\,x1 + S6\,x6 \end{aligned} \tag{F2}$$

where S is the molar flow rate for the respective stream (e.g. stream $S1$, $S2$ and $S6$); x is the vector of molar fractions of the respective stream, sorted by H_2, N_2 and NH_3.

Reactor

$$\begin{aligned} S3\,x3 &= S2\,x2 - \xi E \\ K_{eq} &= \frac{\left(P_{reac} x3_{NH3}\right)^2}{\left(P_{reac} x3_{H2}\right)^3 \left(P_{reac} x3_{N2}\right)} \\ 1 &= x3_{H2} + x3_{N2} + x3_{NH3} \end{aligned} \tag{F3}$$

The reactor is modeled as an equilibrium reactor and its output stream $S3$ is calculated by the extent reaction (ξ). E is a vector of stoichiometric coefficients $[-3,-1,2]^T$. K_{eq} is the equilibrium constant given in Table F1 and P_{reac} is the reactor pressure in bar.

Flash

$$k_{H2} = \frac{H^0_{H2} + H_{H2} T_{flash}}{P_{reac}}$$
$$k_{N2} = \frac{H^0_{N2} + H_{N2} T_{flash}}{P_{reac}} \qquad \text{(F4)}$$
$$k_{NH3} = \frac{10^{A - \frac{B}{(Tflash + C)}}}{P_{reac}}$$

$$x5 = diag([k_{H2}, k_{N2}, k_{NH3}])\, x4$$
$$\sum_{i=\{H2,N2,NH3\}} \frac{x3_i (k_i - 1)}{1 + vf(k_i - 1)} = 0 \qquad \text{(F5)}$$
$$S4 = S3(1 - vf)$$
$$S5 = S3\, vf$$
$$S3\, x3 = S4\ x4 + S5\ x5$$

The constants used to compute the k-values (k_{H2}, k_{N2} and k_{NH3}) are displayed in Table F1, and the vapor fraction vf is calculated by the Rachford-Rice equation.

Splitter

$$S5\ sf = S6$$
$$S5\ (1 - sf) = S7 \qquad \text{(F6)}$$
$$x5 = x6 = x7$$

sf is the splitter fraction used as manipulated variable in Case A of Section 4.4.1.

Feed compressor

$$W_{feed} = S1 R T_0 \log\left(\frac{P_{reac}}{P_0}\right)\frac{1}{\eta_{fc}} \qquad \text{(F7)}$$

W_{feed} is the compressor work used in the feed stream, η_{fc} is the compressor efficiency, R is the gas constant and T_0 and P_0 are the initial conditions of feed stream (see Table F1)

Recycle compressor

$$W_{recy} = S6\,RT_{flash}\log\left(\frac{P_{reac}}{P_{reac}-\Delta P}\right)\frac{1}{\eta_{rc}} \tag{F8}$$

W_{recy} is the compressor work used in the recycle stream $S6$, η_{rc} is the compressor efficiency and ΔP is the system pressure drop.

Cooler

$$Tc = \frac{288 - T_{flash}}{\log\left(\frac{288}{T_{flash}}\right)}$$

$$W_{cool} = \sum_{i=\{H2,N2,NH3\}} S3\; x3_i\, Cp_i \left(288 - Tflash\right)\left(\frac{288}{Tc} - 1\right)\frac{1}{\eta_{cool}} \tag{F9}$$

W_{cool} is the cooler work spent in the system, η_{cool} is the cooler efficiency, Cp_i are the heat capacity of each component. The present cooler model considers only the energy used to bring the temperature down to 288K, for higher temperatures the cooler work is considered zero.

Table F1 - Constant values

Parameter	Value	Unit
K_{eq}	6.36e-5	
H^0_{H2}	210688	
H_{H2}	-656	
H^0_{N2}	110816	
H_{N2}	-342	
A	4.4854	
B	926.132	
C	-32.98	
Cp_{H2}	28.82	J/mol.K
Cp_{N2}	29.13	J/mol.K
Cp_{NH3}	35.06	J/mol.K
T_0	298.15	K
η_{rc}	1	
η_{fc}	1	
η_{cool}	1	
P_0	50	Bar
ΔP	15	Bar

Table F2 - Costs for ammonia production case study

Parameter	Value	Unit
P_{feed}	0.5	$/time
P_{recy}	10	
P_{cool}	1.3	
P_{NH3}	1e4	

Appendix G

This appendix summarizes the equations used to model the Vapor Recompression Distillate process presented in Chapter 5 of this thesis.

Column equilibrium stage

This equipment is modeled by a set of mass, equilibrium, summation and heat equations (G1 – G10). Where F , V , and L denote the molar flow rates of the feed, internal liquid and vapor streams, respectively. x and y are the mole fractions of the liquid and vapor phases, h_V and h_L are the vapor and liquid molar enthalpies, and P_j and ΔP_j are the total pressure and pressure drop in tray j , respectively. C is the set of components, E_j^{MV} is the Murphree efficiency, K_{ij} is the relative volatility and T is the stream temperature.

$$F_j^V y_{iF_j^V} + F_j^L x_{iF_j^L} + V_{j+1} y_{ij+1} + L_{j-1} x_{ij-1} - V_j y_{ij} + L_j x_{ij} = 0 \quad (i = 1,...,C) \tag{G1}$$

$$F_j^V h_{F_j^V}^V + F_j^L h_{F_j^L}^L + V_{j+1} h_{j+1}^V + L_{j-1} h_{j-1}^L - V_j h_j^V + L_j h_j^L = 0 \tag{G2}$$

$$E_j^{MV}(y_{ij}^* - y_{ij+1}) - (y_{ij} - y_{ij+1}) = 0 \quad (i = 1,...,C-1) \tag{G3}$$

$$K_{ij} x_{ij} - y_{ij}^* = 0 \quad (i = 1,...,C) \tag{G4}$$

$$1 - \sum_{i=1}^{C} y_{ij}^* = 0 \tag{G5}$$

$$P_{j-1} + \Delta P_j - P_j^V = 0 \tag{G6}$$

$$1 - \sum_{i=1}^{C} y_{ij} = 0 \tag{G7}$$

$$F_j^V + F_j^L + V_{j+1} + L_{j-1} - V_j + L_j = 0 \tag{G8}$$

$$T_j^L = T_j^V \tag{G9}$$

$$P_j^L = P_j^V \tag{G10}$$

Throttle valve

The expansion valves are modeled as an adiabatic process in which the outlet stream is in vapor−liquid equilibrium (G11 – G17). The nomenclature is the same described in equilibrium stage.

$$Fx_{iF} - Vy_i - Lx_i = 0 \quad (i = 1,...,C) \qquad \text{(G11)}$$

$$Fh_F - Vh^V - Lh^L = 0 \qquad \text{(G12)}$$

$$y_i - K_i x_i = 0 \quad (i = 1,...,C) \qquad \text{(G13)}$$

$$T^L - T^V = 0 \qquad \text{(G14)}$$

$$P^L - P^V = 0 \qquad \text{(G15)}$$

$$1 - \sum_{i=1}^{C} y_i = 0 \qquad \text{(G16)}$$

$$F - V - L = 0 \qquad \text{(G17)}$$

Reboiler

The reboiler is modeled as a thermodynamic equipment (G18 – G28). The cold side of the total reboiler, identified by subscript "C", is the liquid coming from the last tray of the distillation column while the hot side, denoted by subscript "H", is the overheated vapor coming from the compressor.

$$F_C^{in} - F_C^{out} = 0 \qquad \text{(G18)}$$

$$x_{iC}^{in} - y_{iC}^{out} = 0 \quad (i = 1,...,C) \qquad \text{(G19)}$$

$$y_{iC}^{out} - K_{iC}^{out} x_{iC}^{out} = 0 \quad (i = 1,...,C) \qquad \text{(G20)}$$

$$T_C^{L,out} - T_C^{V,out} = 0 \qquad \text{(G18)}$$

$$P_C^{L,out} - P_C^{V,out} = 0 \qquad \text{(G19)}$$

$$1 - \sum_{i=1}^{C} x_{iC}^{out} = 0 \qquad \text{(G20)}$$

$$F_H^{in} - F_H^{out} = 0 \qquad \text{(G21)}$$

$$y_{iH}^{in} - x_{iH}^{out} = 0 \quad (i = 1,...,C) \qquad \text{(G22)}$$

$$y_{iH}^{out} - K_{iH}^{out} x_{iH}^{out} = 0 \quad (i = 1,...,C) \qquad \text{(G23)}$$

$$T_H^{L,eq} - T_H^{V,eq} = 0 \qquad \text{(G24)}$$

$$P_H^{L,out} - P_H^{V,out} = 0 \qquad \text{(G25)}$$

$$1-\sum_{i=1}^{C} y_{iH}^{out} = 0 \qquad \text{(G26)}$$

$$T_H^{out} - T_H^{L,eq} + \Delta T_H^{sub} = 0 \qquad \text{(G27)}$$

$$F_C^{in} h_{F_C}^{L,in} + F_H^{in} h_{F_H}^{V,in} = F_C^{out} h_{F_C}^{V,out} + F_H^{out} h_{F_H}^{L,out} \qquad \text{(G28)}$$

Cooler

The cooler is modeled basically as the reboiler. However, the eq.(G28) is substituted by eq.(G29 - G31). Where Q_{reb} is the total amount of energy changed in this equipment, U is the overall heat transfer coefficient, A is the cooler area, $\mathrm{LMTD}$is the logarithmic mean of temperatures, C_P is the calorific capacity of water, W is the mass flow rate of water and ΔT is the difference of temperatures between the inlet and outlet water streams.

$$Q_{reb} = F_H^{in} h_{F_H}^{V,in} - F_H^{out} h_{F_H}^{L,out} \qquad \text{(G29)}$$

$$Q_{reb} = U.A.\mathrm{LMTD} \qquad \text{(G30)}$$

$$Q_{reb} = C_P W \Delta T \qquad \text{(G31)}$$

Compressor

The compressor model is given by equations G32 to G37. Where s is the entropy, η_{CP} is the isentropic efficiency, Q_{CP} is the compresso mass flow rate and ΔP_{CP} is the difference of pressure between the inlet and outlet streams.

$$F^{in} - F^{in} = 0 \qquad \text{(G32)}$$

$$y_i^{in} - y_i^{out} = 0 \quad (i = 1,...,C) \qquad \text{(G33)}$$

$$P^{out} - P^{in} - \Delta P_{CP} = 0 \qquad \text{(G34)}$$

$$s^{in} - s^{out} = 0 \qquad \text{(G35)}$$

$$\eta_{CP}(h^{out} - h^{in}) - (h^{isen} - h^{in}) = 0 \qquad \text{(G36)}$$

$$\eta_{CP} = 0.5307 + 3.4619e^{-4}\left(Q_{CP}.\Delta P_{CP}\right) \qquad \text{(G37)}$$